Pulsar Searching

A Thesis by

Russell T. Edwards

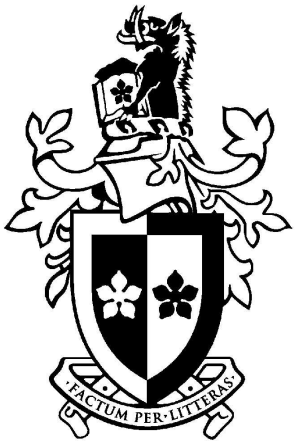

Presented in fulfillment of the requirements
for the degree of
Doctor of Philosphy
at Swinburne University Of Technology

March 2001

There are more things in heaven and earth, Horatio, than are dreamt of in your philosophy.
— **Hamlet, Shakespere**

Abstract

This thesis reports the results of two pulsar survey projects conducted at the Parkes 64-m radio telescope in New South Wales, Australia.

The first, the Swinburne Intermediate Latitude Pulsar Survey, covered a large region of the southern Galaxy ($5^\circ < |b| < 15^\circ$ and $-100^\circ < l < 50^\circ$) flanking that of the ongoing Galactic plane survey ($|b| < 5^\circ$). We used the 13-feed 20 cm "multibeam" receiver package to achieve this broad sky coverage in a short observing campaign with 14 days' total integration time. The survey proved remarkably successful, detecting 170 pulsars, 69 of which were new discoveries.

Eight of the new discoveries possess small periods and period derivatives indicative of "recycling", an hypothesis supported by the fact that six of them are in circular orbits with probable white dwarf companions. Pulse timing measurements have revealed that two of the white dwarfs are massive CO or ONeMg dwarfs. The mass of one of them (the companion to PSR J1157–5112) exceeds 1.14 $M_\odot$, providing the most convincing evidence to date for the production of "ultra-massive" ONeMg white dwarfs as the end result of stellar evolution on the asymptotic giant branch (albeit with mass transfer indicated). PSR J1757–5322 also possesses a heavy (> 0.55 $M_\odot$) white dwarf companion, in a close 11-h orbit. The proximity of the massive companion leads to significant relativistic orbital evolution and the effects of this will be measurable by pulsar timing in the coming decades. Under general relativity, the gravitational wave power radiated from the system is sufficient to cause coalescence in < 9.5 Gyr, an event which will have dramatic and unknown consequences. Such events are possible gamma-ray burst sources, and the remnants could include isolated millisecond pulsars, close eclipsing binaries or pulsar planetary systems. The remaining four pulsar binaries show some discrepancies with the bulk of previously known low mass binary pulsars (LMBPs). PSR J1618-39 is in a 23-d orbit, filling what previously appeared to be a gap in the orbital period distribution. PSR J1745-0952 has a relatively long pulse period (19 ms) and along

with PSR J1618-39 (12 ms) may have experienced a different evolutionary history to the majority of previously LMBPs.

A ninth pulsar discovered in the survey may also be recycled. The mean pulse profile of PSR J1411–7404 is exceedingly narrow ($\sim 2^\circ$) and lies in stark contrast to that of other pulsars of similar pulse period. In the past the only other pulsars known with anomalously narrow profiles were believed (for other reasons) to have been recycled, and this fact in combination with the low period derivative measured in timing analysis of PSR J1411–7404 leads me to suggest that it, too, may have been recycled. If this is the case, it is possible that the recycling took place in a system similar in configuration to the progenitors of the double neutron star systems, but that sudden mass loss or an unfavourably oriented kick in the birth event of the second neutron star disrupted the system, leaving an isolated, mildly recycled pulsar.

The second pulsar survey program conducted for this work was a targeted search of southern globular clusters. We used a baseband recording system to provide unprecedented time resolution (typically 25 μs). The large number of channels and short sampling interval achievable in software filterbanks, in combination with the ability to coherently remove most of the interstellar dispersion from clusters with previously known pulsars, made us the first to achieve a relatively flat sensitivity response to pulsars of $\sim 10^{-3.5}$–10 s. This characteristic is vital if we are constrain the true period distribution of millisecond pulsars, an important task in the evaluation of alternative equations of state for nuclear matter. We detected six millisecond pulsars and produced pulse profiles of higher resolution than were previously available. The basic sensitivity of the search was not high enough to detect any new pulsars, however the work demonstrates that the approach is feasible with the use of currently available high-performance computing resources (such as the Swinburne workstation cluster), and is capable of delivering excellent sensitivity characteristics. It is expected that future searches of this kind, of which this is the first, will achieve the goal of sampling the true pulse period distribution within a few years.

Acknowledgements

As with anything worth doing, undertaking this thesis was a consuming and life-changing endeavour. Several people shared parts of this adventure with me and contributed to the experience in ways for which I'm grateful.

My segue into astronomy from computer science was facilitated by Dick Manchester at the ATNF. Fresh from three mind-numbing years of undergraduate study, my enthusiasm for the indulgence of curiosity that began with my father ("Dad, how come... Why does... What about..."; he, also, should be thanked for this role) was re-kindled through Dick's mentorship after being crushed by an education system that assumes that all students are disinterested future non-scientists learning to regurgitate physics to satisfy course requirements. Dick dumped a bunch of papers and the classic book *Pulsars* (Manchester & Taylor 1977) on my lap for a bit of light after-hours reading, and happily reacted with enthusiasm rather than irritation at my long list of silly questions jotted for discussion each morning.

A year of honours in computer science confirmed my growing thought that academia was a good way to get paid for doing something of intrinsic value, rather than working to make money for someone else like most mugs seemed to be doing, so I followed Dick's advice and applied for candidature in a PhD program with Matthew Bailes. Thank-you Matthew for recognizing my potential despite my lack of a physics degree. Matthew shows a knack for knowing just how much rope to give his students. I'm very grateful for having the opportunity to conduct the projects described herein largely on my own but with just the right level of sanity checks from an old hand.

The Parkes Multibeam Galactic plane survey collaboration must also be thanked for the use of their back-end equipment and online software. The exchange of software and observing time was bi-directional, a laudable state of affairs to be encouraged in the sometimes overly competitive environment of astronomy. My survey would not have been possible without their earlier work, something that cannot be

said the other way 'round, and for this generosity I am indeed grateful.

Mention must be made of the NASA Astrophysics Data System and the arXiv preprint server (astro-ph). These services provide electronic access to the majority of published and to-be-published papers in astronomy today, and are an asset of incalculable value to the astronomical community. The speed with which new results are be reported and the ease with which a thorough literature search can be conducted are the major benefits brought by the services. Through their dedication to free, timely and complete access to scientific communications they have revolutionised the way research is communicated and for this they deserve formal recognition. I hope that in future years we will also see good access to those journals who, whether through fear or greed, do not fully support the schemes at present.

I must also thank the government for maintaining the Australian Postgraduate Award program, which supported me for the last 3 years. That this program persists despite the plethora of crimes against science, society and the environment committed by this government is perplexing but appreciated. Likewise, thanks to my parents who also helped me out from time to time, and didn't even open any new uranium mines in world heritage areas.

Speaking again of sanity, for the fraction of it that remains I must thank my friends. Thanks Willem for sharing my interest in and specific approach to philosophy, art and spirituality as well as an appreciation for aesthetics in software design! Thanks to Chris and Tanya for many stimulating and enjoyable times spent together, for making me realise I'm not alone in my observations about nature, reality and Western society's relationship to them, and for reminding me of the legitimacy of our path. Kara I thank for being my companion and mirror for so long. Now that the binary is disrupted I wish you well in future orbits, however of course our connection and friendship will continue forever. I am grateful to Matthew and Gung Britton, and to Meaghan, for accidentally initiating my interaction with Kim. The orbit is now bound (and comfortably eccentric) indefinitely, hopefully there will even be planets detected some day. As for Kim, my fiancée, I don't know where to start, so I won't; I love you.

Declaration

This thesis contains no material that has been accepted for the award to the candidature of any other degree or diploma. No part of this thesis has been previously published or written by another author. Chapters 3–6 have been published in or submitted to refereed journals, as indicated at the start of their respective texts. All work presented is primarily that of the candidate. Matthew Bailes took part in the planning of observations to be conducted for this thesis, contributed some of the speculations in Chapter 3 regarding the future fate of the J1757–5322 system, collaborated on the achievement in phase connection of new binary pulsar timing observations, and provided suggestions for the content and editing of the manuscripts. Certain parts of the software written by Willem van Straten for pulsar timing with baseband data were also used in the pulsar search described in Chapter 6. Matthew Bailes, Willem van Straten and Matthew Britton helped man the telescope while observations were conducted for Chapters 3–6.

Russell Edwards

Nomenclature

$\odot$	Denotes solar quantity
$\otimes$	Denotes mixing (cross-multiplication) of periodic signals
α	Spectral index, as in $S \propto \nu^{\alpha}$ (see also RA)
ν	Frequency (typically radio, also pulsar spin)
$\tau_{\rm c}$	Characteristic age ($\equiv P/2\dot{P}$)
ω	Longitude of orbital periastron
a	Acceleration; Semi-major axis of orbit
AGB	Asymptotic Giant Branch
B	Unit: byte (as in MB, GB, TB = 2^{20}, 2^{30}, 2^{40} bytes respectively)
B	Magnetic flux density (usually at neutron star surface)
b	Galactic latitude
c	Speed of light ($\sim 3.00 \times 10^{8}$ m s^{-1})
CE	Common Envelope
CO	Carbon/Oxygen (white dwarf composition)
CVS	Concurrent Versions System
d	Unit: days
Dec; δ	Declination
DC	Direct Current ; 0 Hz ; baseband
DLT	Digital Linear Tape
DM	Dispersion measure
e	Eccentricity of orbit
f	Keplerian mass function
FFT	Fast Fourier Transform (algorithm)
FWHM	Full Width at Half-Maximum
G	Unit: Gauss (magnetic flux density; 10^{-4} T)
G	Gravitational constant ($\sim 6.67 \times 10^{-11}$ m^3 kg^{-1} s^2); Telescope gain
h	Unit: hours
i	Inclination angle of orbit
IMBP	Intermediate Mass Binary Pulsar
ISM	Interstellar medium
Jy	Unit: Jansky (electric spectral flux density: 10^{-26} W m^{-2} Hz^{-1})
l	Galactic longitude
LMBP	Low-Mass Binary Pulsar

LMXB	Low-Mass X-ray Binary
lt s	Unit: Light seconds (distance; $c \times 1$ s)
$M_\odot$	Unit: Solar mass (mass; $\sim 1.99 \times 10^{30}$ kg)
$M_{\rm c}, M_{\rm WD}$	Mass of (white dwarf) companion to pulsar
$M_{\rm p}$	Mass of pulsar
MJD	Modified Julian Day (JD - 2,400,000.5)
MPI	Message Passing Interface
MSP	Millisecond pulsar
n	Braking index (where $\dot{P} \propto P^{2-n}$)
P	Pulse period
$\dot{P}$	Pulse period time derivative
$P_{\rm orb}$	Orbital period
pc	Unit: parsec (distance; $\sim 3.09 \times 10^{16}$ m)
PSR	Naming prefix for pulsars
$R_\odot$	Unit: Solar radius (distance; $\sim 6.97 \times 10^8$ m)
RA; α	Right Ascension
RAID	Redundant Array of Inexpensive Disks
S	Flux density ("flux")
s	Unit: seconds
S/N	Signal to noise ratio
sigma; σ	Noise level; standard deviation
T_0	Epoch of orbital periastron
TOA	(Pulse) Time Of Arrival
WD	White Dwarf
yr	Unit: (terrestrial) year

Contents

List of Figures

List of Tables

Chapter 1

Introduction

1.1 Pulsars : An Overview

The discovery of pulsars, like many of the most significant outcomes of scientific research, was the result of serendipity. Jocelyn Bell, a young PhD student at Cambridge was taking part in a study of interplanetary scintillation. The project required high time resolution by the standards of the time, and a large telescope was built to compensate for the resultant loss of signal to noise ratio. Bell soon noticed the reception of a regular train of narrow pulses from a certain part of the sky. This was the discovery of the first pulsar (Hewish et al. 1968), an entirely unexpected phenomenon.

The daily change in transit time of the source quickly indicated that the origin of the pulses was not terrestrial or even within the solar system. It was evident from the short duration of the pulses that the emission region could not be much larger than 10^9 m, ruling out objects of greater than planetary size. It was soon proposed that the object was a rotating, highly magnetised neutron star (Pacini 1968; Gold 1968), objects which until that time existed only in the realms of theory (Baade & Zwicky 1934). Further discoveries and observations have essentially eliminated any doubt of the validity of this model.

It is believed that pulsars are born in the supernova explosions of large stars. In stars of up to about 6–10 $M_\odot$, the usual end result of stellar evolution is a degenerate core composed mainly of carbon and oxygen. In heavier stars core temperatures become high enough to permit further stages of nuclear fusion, eventually resulting in a massive iron core which, unable to produce any further fusion energy (with

its associated radiation pressure), collapses under its own gravity. The density and temperature rapidly rise, fissioning atoms and eventually fusing protons and electrons into neutrons, which form a massive compact object called a **neutron star**. This process results in the copious emission of neutrinos, an event witnessed for the first time from the nearby supernova SN1987A in the Large Magellanic Cloud (Bionta et al. 1987; Hirata et al. 1987). Some of the angular momentum and magnetic dipole moment of the progenitor star is conserved in the proto-neutron star, resulting in rapid rotation and a strong magnetic field which, in general, is not aligned with the spin axis. Through an unknown mechanism beamed radio emission is associated with the magnetic polar regions. If this beam intersects our line of sight at some rotational phases (and not others), the object is observable as a **pulsar**.

The birth spin period of pulsars is believed to be of the order of tens of milliseconds. Due to the emission of magnetic dipole radiation, the spin period increases with time, giving rise to an object which is visible for tens of Myr with a spin period of hundreds of milliseconds, until the pulsar has spun down so much that it no longer produces radio emission. The slowest known radio pulsar has a spin period of 8.5 s (Young, Manchester & Johnston 1999) and challenges previous models of pulsar emission and death, however it is quite possible that pulsar surveys have missed other even slower pulsars.

In 1982, through a capricious increase of time resolution by a promising young PhD student (Shri Kulkarni), a pulsar of unprecedented spin period — 1.6 ms — was discovered in a targeted observation of a previously enigmatic radio source (Backer et al. 1982). Other **millisecond pulsars** (MSPs) were discovered over the following decades, although none was as fast as the original. All have very low spin-down rates, indicating that they may have been shining for billions of years. The distribution of spin periods and spin-down rates of MSPs is clearly separate to the "normal" pulsar population. The most likely scenario for their formation is that the binary companion of a dead pulsar reaches the end stages of its evolution, swelling to such an extent that it transfers matter to the pulsar, spinning it up and reducing its magnetic field strength, giving rise to a long-lived object with a millisecond spin period (Alpar et al. 1982). This process is known as **recycling**. The high proportion of MSPs found in binary orbits with white dwarf or neutron star companions fits this hypothesis well.

1.2 The Nature of Pulsar Signals

1.2.1 Radio Pulsar Emission Mechanism

To this day the exact mechanism for the emission of microwaves from pulsars is still unknown. It is believed that the neutron star is surrounded by a **magnetosphere** containing a relatively high density of charged particles trapped on closed magnetic field lines (Goldreich & Julian 1969). The magnetic field and associated particles corotate with the neutron star out to the **light cylinder** radius, where the corotation velocity equals the speed of light. Within this region the component of the electric field along the magnetic field lines must be nearly zero except where for some reason there is a "gap", or local vacuum. It is suggested in most models (e.g. Sturrock 1971) that (primary) charged particles are accelerated across such a gap, emitting gamma-rays in the process, which in turn decay to (numerous secondary) electron-positron **pairs**. A copious stream of charged particles following the magnetic field lines results. These particles then emit microwave radiation (probably synchrotron, cyclotron or curvature) as they follow helical paths along the field lines. The high luminosity achieved in the relatively small emission region implies a brightness temperature of $\sim 10^{30}$ K, indicating a coherent mechanism is involved, perhaps due to the acceleration of charges in bunches, or by maser amplification.

For pair production to occur the magnetic field strength must be sufficient to cause the decay of gamma-rays at the energy resulting from the available accelerating voltage. This maximum voltage drop possible in a pulsar magnetosphere is proportional to the square of the rotation frequency, so one can define a "**death line**" in P–B space. Since the surface magnetic field strength of a pulsar can be inferred from its measured period and period derivative (see § 1.3) under the assumption of a dipole field, the death line represents an observational test of emission models requiring pair production. As shown in Figure 1.1, this death line essentially divides the pulsar population in half. The model framework can plausibly be salvaged by invoking more complex magnetic field structures (Chen & Ruderman 1993), by assuming a different mechanism for the stimulation of pair production (Zhang, Harding & Muslimov 2000), by using an unusual equation of state for nuclear matter in the calculation of the neutron star mass and radius (Young, Manchester & Johnston 1999) or by assuming that pulsars below the line do not require pair production (Weatherall & Eilek 1997), a division that is apparently supported by the different

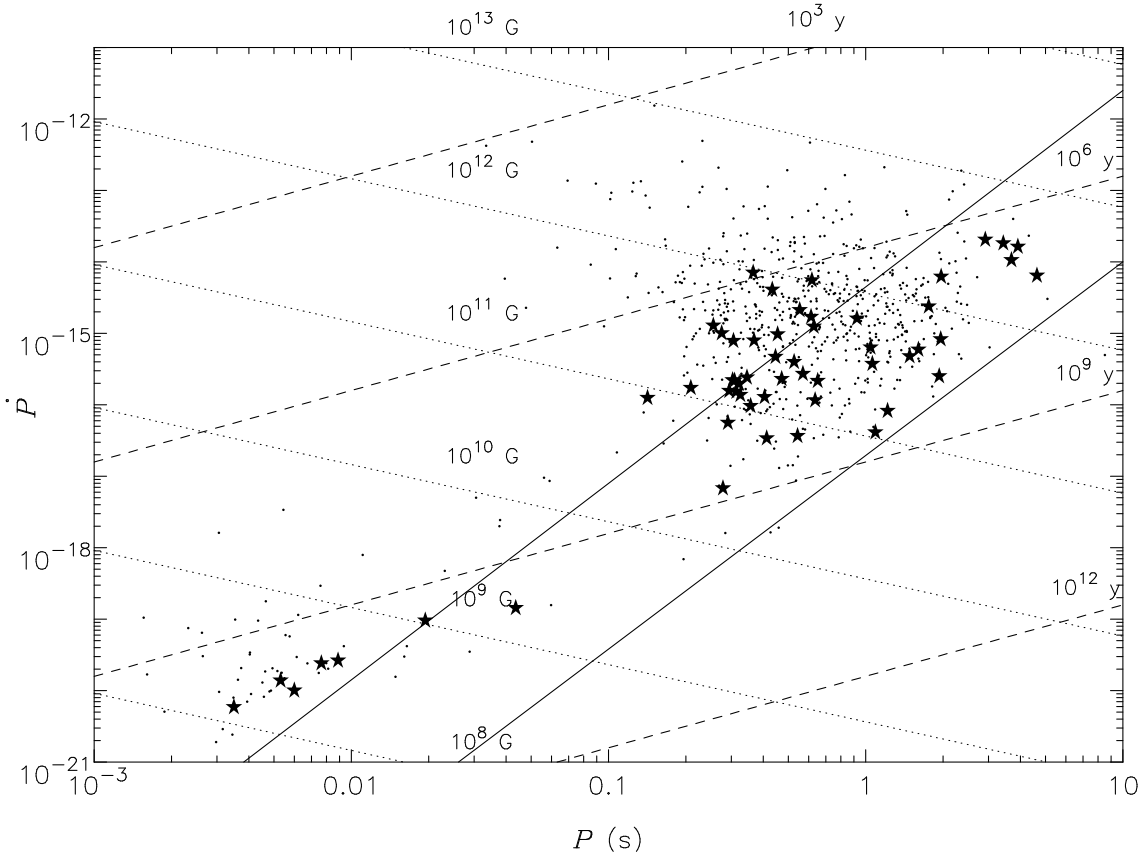

Figure 1.1: Distribution in P-$\dot{P}$ of known pulsars (excluding those in globular clusters, which experience gravitational accelerations corrupting the observed $\dot{P}$). Lines of constant characteristic age (dashed lines) and surface magnetic field (under a dipole assumption; dotted lines) are included : see § 1.3. Upper and lower solid lines represent the death lines of Chen and Ruderman (1993; § 1.2.1) for a simple dipole and for a very warped field structure (case "C") respectively. Pulsars discovered in the Intermediate Latitude Survey (Chapter 5) are drawn as stars.

average pulse morphology of pulsars above and below the line.

1.2.2 Characteristics of Radio Pulsar Emission

Observationally, pulses from radio pulsars appear as short bursts of highly polarised broad band noise. Both the polarisation and the evolution of total intensity is often variable from pulse to pulse, however it is found that the mean pulse shape (known as the pulse **profile**) is highly consistent for most pulsars after integrating several hundred pulses (Helfand, Manchester & Taylor 1975). This property enables the measurement of observed pulse phase at a given epoch to better to than a thousandth of a turn, hence the high precision of measurements obtainable by pulsar timing

(§ 1.3). Some pulsars do exhibit changes of their mean pulse profile shape. The number of different pulse shapes in a given pulsar generally appears to be discrete, hence this effect is called **mode changing**.

For most pulsars, the typical single pulse is narrower than the mean profile and its phase is random, from some distribution which determines the mean pulse shape. For a number of pulsars however there are some non-random phenomena observable in single pulses. Many pulsars exhibit several **sub-pulses** each rotation, and a few of these show **drifting sub-pulses** : that is, individual sub-pulses are persistent for many pulse periods and are observed to gradually drift in phase until they disappear as they reach the end of the "on" part of the integrated profile. These are suggestive of drifting sparks or perhaps standing waves in the magnetosphere. For sufficiently bright pulsars sub-pulses can often be resolved into even shorter spikes of radiation known as **microstructure**, suggesting rapid intensity variability in individual discharge regions. The intensity distribution of single pulses also differs from pulsar to pulsar (Smith 1973). Some pulsars appear to periodically "switch off", showing no detectable pulses at all (Backer 1970). This phenomenon is referred to as **nulling**, and tends to occur on timescales of seconds–minutes, in pulsars that are relatively close to death. Two pulsars occasionally emit "**giant pulses**" with energies thousands of times greater than the mean pulse. These are PSR B0531+21, the pulsar in the Crab nebula (Staelin & Reifenstein 1968), and PSR B1937+21 (Cognard et al. 1996), the first and fastest millisecond pulsar. That this phenomenon should be observed in two pulsars which lie at the opposite extremes of the distribution of observed ages and magnetic field strengths is intriguing.

The morphology of profiles of known pulsars is diverse, however it is possible to make some generalisations. In a series of papers (Rankin 1983a; Rankin 1983b; Rankin 1986; Rankin 1990; Radhakrishnan & Rankin 1990) Rankin develops an empirical theory of pulsar emission in which pulse profiles are classified by their integrated profiles and single pulse behaviour. Aspects of the model are controversial (see e.g. Lyne & Manchester 1988), however it is now generally accepted that there are two types of pulsar emission, referred to as "core" and "conal" after their locations in the proposed polar cap geometry. It is suggested that core emission is responsible for the central component in most profiles with odd numbers of components, and that the rest are conal. Conal and core emission have a different intrinsic beam width which is proportional to $P^{-1/2}$ and, in combination with the (random) viewing geometry this explains the observed distribution of period and pulse width

(Rankin 1990).

1.2.3 Interstellar Dispersion

It was noticed by Hewish et al. (1968) that when "the" pulsating radio source was observed at 80.5 MHz and 81.5 MHz simultaneously, pulses in the lower frequency band arrived approximately 0.2 s later than those in the higher frequency. It was soon realised that this was due to interstellar dispersion. Free electrons in the interstellar medium reduce the electromagentic wave group velocity v_g according to the relation

$$v_g = c\left(1 - \frac{\nu_p^2}{\nu^2}\right)^{\frac{1}{2}} \tag{1.1}$$

where ν is the frequency of the wave, $\nu_p = (n_e e^2/\pi m_e)^{1/2}$ is the "plasma frequency", n_e is the electron number density and e and m_e are the charge and mass of an electron respectively. Typical interstellar electron densities are ~ 0.03 cm^{-3}, yielding $\nu_p \simeq 1.6$ kHz, much lower than the usual pulsar observing frequencies of $0.1 - 10$ GHz, so the above relation can be safely approximated by

$$v_g = c\left(1 - \frac{\nu_p^2}{2\nu^2}\right) \tag{1.2}$$

Defining the **dispersion measure** (DM) as the integrated line of sight electron density, one finds the dispersive time delay of a wave at frequency ν,

$$t = \frac{e^2}{2\pi m_e c}\frac{1}{\nu^2}\mathrm{DM} \tag{1.3}$$

$$\simeq 4.15 \times 10^3 \left(\frac{\nu}{\mathrm{MHz}}\right)^{-2} \frac{\mathrm{DM}}{\mathrm{pc\ cm^{-3}}} \quad \mathrm{(s)} \tag{1.4}$$

In general this leads to a very significant delay from one end of an observing band to the other (see Figure 1.2) which must be taken into account in processing.

By differentiation of equation 1.3 we arrive at a useful approximation of the dispersion delay across a small bandwidth B centred about a frequency ν:

$$\Delta t \simeq 8.3 \frac{B}{\mathrm{MHz}} \frac{\mathrm{DM}}{\mathrm{pc\ cm^{-3}}} \left(\frac{\nu}{\mathrm{GHz}}\right)^{-3} \quad \mu\mathrm{s} \tag{1.5}$$

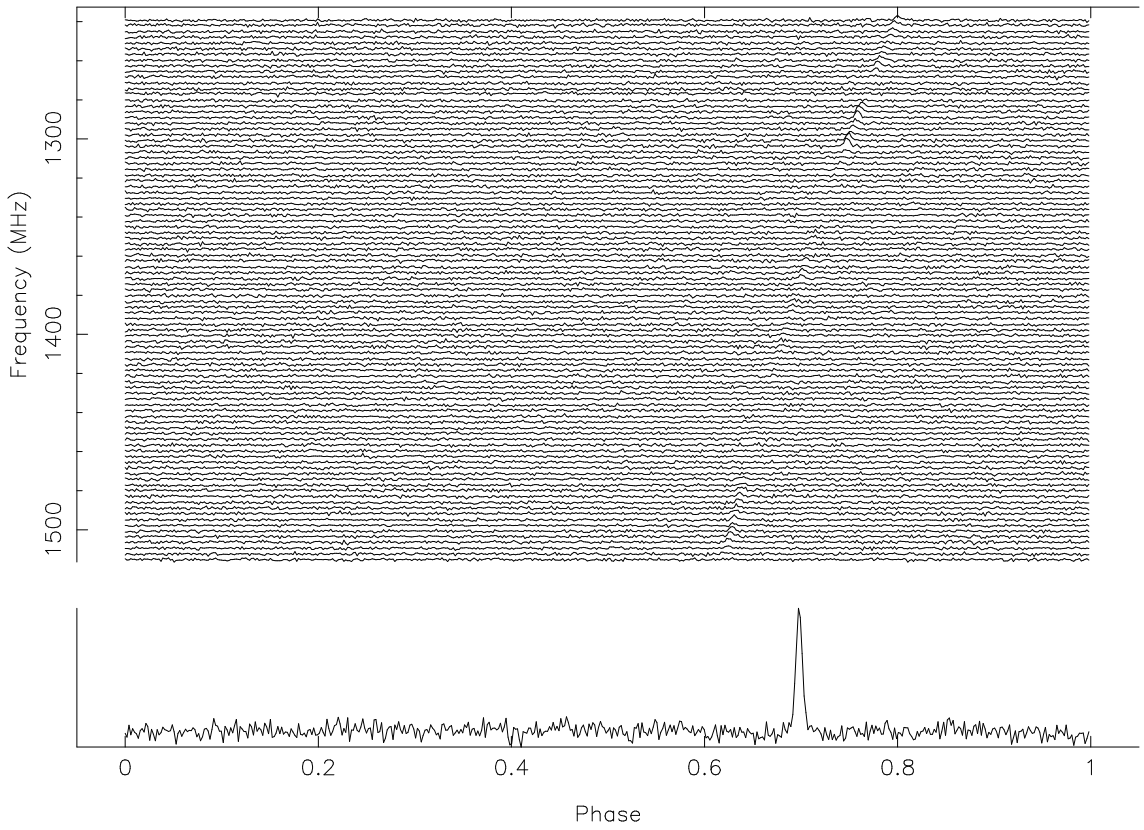

Figure 1.2: Integrated pulse profiles in 96 filterbank channels for the newly discovered pulsar PSR J1410-7404. Clearly visible is the increased dispersion delay in channels of lower frequency. The non-linearity of this delay with frequency is also perceptible. Note also the presence of narrow scintillation bands (§ 1.2.4).

The dispersion measure may be used to obtain an approximate distance to the pulsar. The most recent model of the Galactic electron distribution for this purpose is that of Taylor & Cordes (1993).

1.2.4 Other Effects of the Interstellar Medium

In addition to dispersion (§ 1.2.3), the interstellar medium (ISM) imposes three further pertinent effects on the propagating pulsar signal.

The first is known as **scintillation**, and is the interstellar equivalent to the "twinkling" of stars : it is the variation in observed flux density on timescales of seconds—hours. This is caused by inhomogeneities in the tenuous ionised gas of the ISM with resultant variations in the local refractive index. As a result, observed rays may have taken various paths through the medium, with the difference in distance resulting in constructive or destructive interference. Since the angle of refraction

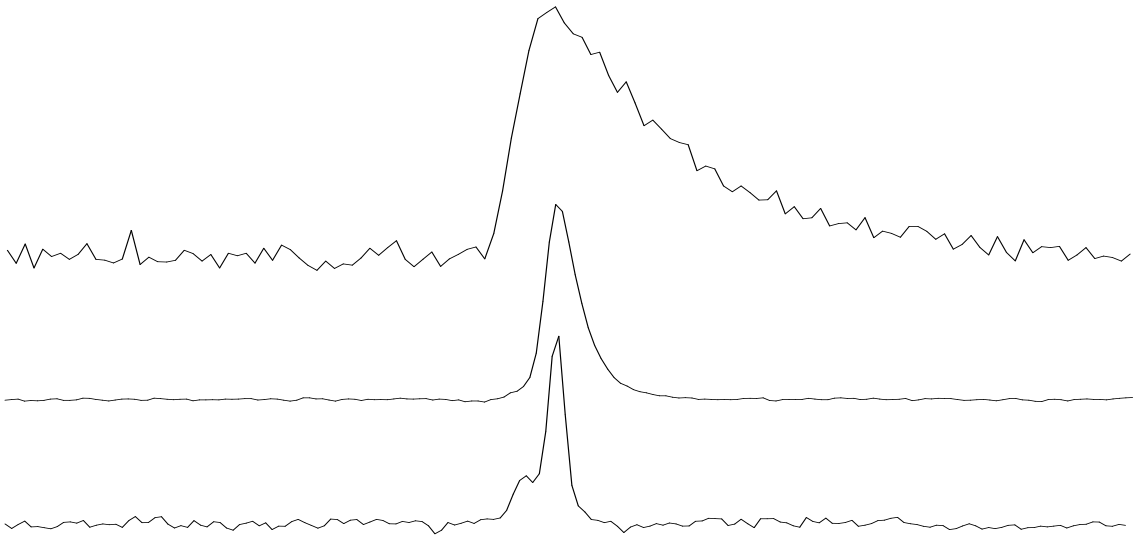

Figure 1.3: Integrated pulse profiles of PSR B1859+03 at (from top to bottom) 400 MHz (Arzoumanian et al. **1994), 606 MHz and 1642 MHz (Gould & Lyne 1998) demonstrating the strong frequency dependence of scatter broadening. Data courtesy of the EPN profile database:** `http://kerr.phys.utas.edu.au/misc/pulsar/data/`

and the interference pattern are both frequency dependent, variation in flux with frequency is often observed, as in Figure 1.2 (§ 1.2.3). Due to the transverse motion of the intervening scattering screen or the pulsar, the flux also varies with time.

Scattering in the ISM also causes a broadening of pulses due to the variations in propagation time among the different propagation paths. The effect of this is approximately to convolve the pulse profile with a decaying exponential tail; see Figure 1.3. The timescale of this **scatter-broadening** varies as ν^{-4} (Ables, Komesaroff & Hamilton 1970), giving high frequency millisecond pulsar surveys a strong advantage. The degree of broadening is also correlated with dispersion measure : $\tau \propto \mathrm{DM}^2$ is expected and fits the data for close pulsars well, however for pulsars with DM > 30 pc cm^{-3} the relation is much steeper : $\tau \propto \mathrm{DM}^{4.4}$ (Lyne & Smith 1998).

Finally, Galactic magnetic fields of the order of 1 μG, whilst tiny compared to that of the neutron star, result in a frequency-dependent alteration of the observed polarization position angle due to Faraday rotation. Since the degree of rotation is proportional to the integral of the product of local electron density and projected magnetic field strength, measurement of the **rotation measure** in combination with the dispersion measure allows one to calculate the average projected Galactic magnetic field strength along the line of sight.

1.3 Pulsar Timing

Observations of pulsars have had diverse implications in astrophysics. Perhaps the most spectacular of these derive from **pulsar timing**. Neutron stars have masses of ~ 1.35 $M_\odot$ (Thorsett & Chakrabarty 1999), and are believed to have radii of approximately 10 km, resulting in a moment of inertia of $\sim 10^{45}$ g cm^2 (see e.g. Shapiro & Teukolsky 1983). This huge moment of inertia provides us with a very stable observable clock and factors affecting the time of arrival of each pulse may be measured to great precision as a result.

Intrinsic to the pulsar is the pulse period, $P(t)$. The evolution of pulse period with time is largely due to the emission of magnetic dipole (or multipole) radiation and generally results in the measurability of the first and, in a few cases, second derivatives, $\dot{P}$ and $\ddot{P}$. Doppler shifts resulting from radial and transverse motion may corrupt the observed P and $\dot{P}$ respectively unless they can be measured independently and taken into account. Should the pulsar have a companion object, the motion of the pulsar around the centre of mass is detectable and may be modelled with the five "**Keplerian**" parameters, $P_{\rm orb}$ (orbital period), T_0 (epoch of periastron), ω (longitude of periastron), e (eccentricity) and $a \sin i$ (projected semi-major axis). In some notable cases, relativistic effects due to a binary companion are also measurable. As the train of pulses propagates through the interstellar medium a radio-frequency-dependent delay is experienced which allows measurement of the density of electrons integrated along the line of sight (i.e. the dispersion measure; see §1.2.3). Finally, with the orbital motion of the Earth, the pulsar's position on the sky (usually specified as right ascension α and declination δ in the $J2000.0$ equinox), and possibly its proper motion (μ_α and μ_δ) and parallax (π) become measurable.

For the majority of "slow" (non-recycled) pulsars, a fit for position, period, period derivative and dispersion measure is sufficient to model the observed pulse times of arrival (TOAs). From the dispersion measure, along with a model of the Galactic electron distribution (Taylor & Cordes 1993) one may derive the distance to the pulsar, typically to an accuracy of around 30% — poor compared to pulsar timing measurements, but reasonably good by general astronomy standards. By assuming a dipole structure to the magnetic field, one may derive a value for the surface magnetic field strength of the pulsar. From classical electrodynamics, the radiated power of a magnetic dipole rotating with angular frequency Ω is $2/3 M_\top^2 \Omega^4 c^{-3}$, where $M_\top$ is the component of the magnetic dipole moment perpendicular to the spin axis.

Equating the radiated power to the rate of change of rotational energy,

$$\frac{\mathrm{d}}{\mathrm{d}t}\frac{1}{2}I\Omega^2 = I\Omega\dot{\Omega} = -\frac{2}{3}M_{\perp}^2\Omega^4 c^{-3} \tag{1.6}$$

Taking $I = 10^{45}$ g cm^2, $R = 10$ km and assuming the spin and magnetic axes are perpendicular, the surface magnetic field strength may be derived,

$$\frac{B}{\mathrm{Gauss}} \simeq 3.3 \times 10^{19}\sqrt{\frac{P}{\mathrm{s}}\dot{P}} \tag{1.7}$$

For most slow pulsars, this leads to an inferred magnetic field strength of $\sim 10^{12}$ Gauss, a very large value indeed (Earth's surface magnetic field strength is ~ 0.4 Gauss)! Such pulsars typically have $P \sim 1$ s and $\dot{P} \sim 10^{-15}$, leading to a useful rule of thumb: $B \simeq \sqrt{P\dot{P}}$, where values are in the commonly used units of $\sim 10^{12}$ Gauss, seconds and 10^{-15}. For millisecond pulsars, typical values are $P \sim 10$ ms and $\dot{P} \sim 10^{-20}$, giving $B \sim 10^{8.5}$ Gauss (see Figure 1.1).

From equation 1.6 one finds that, under the assumption of a constant magnetic field strength and geometry, throughout the spin-down process $\dot{\Omega} \propto \Omega^3$, or equivalently, $\dot{P} \propto P^{-1}$. Relaxing the magnetic dipole assumption, the more general relation

$$\dot{P} \propto P^{2-n} \tag{1.8}$$

may be assumed, where n, the **braking index**, is equal to three in the dipole model. Integrating this expression backward in time therefore gives the age of the pulsar

$$\tau = \frac{P}{(n-1)\dot{P}}\left[1 - \left(\frac{P_0}{P}\right)^2\right] \tag{1.9}$$

where P_0 is the initial spin period. Letting $n = 3$ and taking $P \gg P_0$, one obtains the **characteristic age**, $\tau_c \equiv P/2\dot{P}$. For ordinary observable pulsars the characteristic age is typically 1–100 Myr, whilst millisecond pulsars generally have inferred ages of around 5 Gyr. However, in deriving this age we have noted a number of assumptions above which are not necessarily valid, especially for millisecond pulsars. Recent papers (e.g. Camilo, Thorsett & Kulkarni 1994; Toscano et al. 1999; Arzoumanian, Cordes & Wasserman 1999) address some of these issues, in particular the corruption of the measured $\dot{P}$ by the differential Doppler shift induced by transverse motion (Shklovskii 1970).

The braking index is also a largely unknown value. By differentiating equation 1.8, we find that $n = 2 - P\ddot{P}\dot{P}^{-2}$. Hence, by measuring $\ddot{P}$ one can derive the braking index. However, only very young pulsars have a $\ddot{P}$ sufficiently large to measure and the observed values are very often dominated by rotational instabilities (random "**timing noise**" and almost instantaneous "**glitches**" in P and $\dot{P}$; see Cordes & Helfand 1980 and Shemar & Lyne 1996). Braking indices of four pulsars have been measured, ranging from 1.4 to 2.8, bringing into question the standard dipole braking assumption.

The measurement of the five Keplerian orbital parameters allows constraints to be placed on the component masses of the system. Defining the **mass function**,

$$f(M_p, M_c, i) = \frac{4\pi^2}{G}\frac{a^3 \sin^3 i}{P_{\rm orb}^2} = \frac{M_c^3 \sin^3 i}{(M_p + M_c)^2} \tag{1.10}$$

where M_p is the mass of the pulsar and M_c is the mass of the companion, one may derive a minimum companion mass by taking $\sin i = 1$ and assuming some minimum pulsar mass. Pulsar timing is extraordinarily sensitive to companion objects, as evidenced by the first ever discovery of extra–solar planets, around PSR B1257+12 (Wolszczan & Frail 1992).

Due to the (relativistic) curvature of space around the companion, radiation from the pulsar experiences an extra delay in propagation time, known as the **Shapiro Delay** (Shapiro 1964), which is dependent on the orbital phase, the viewing geometry and the companion mass. The delay–orbital phase relation is parameterised by the "shape", $s \equiv \sin i$ and the "range", $r = GM_c/c^3$. The Shapiro Delay thus gives a direct measurement of the companion mass and, by substituting s and M_c into the mass function (equation 1.10), the pulsar mass.

In systems with sufficiently close orbits and massive companions, other general relativistic effects become measurable. Firstly, due to the emission of gravitational radiation, the orbit decays with time, observable as $\dot{P}_{\rm orb}$. Secondly, due to the non-zero distance between the bodies, the effective position of the gravitating companion lags the "true" position by the light travel time between the objects and the orbit precesses, observable as $\dot{\omega}$. Finally, there is an additional time delay, γ, due to gravitational redshift and time dilation. Since it only takes the measurement of two further parameters to absorb the two degrees of freedom in the mass function, measurement of three or more **post–Keplerian** parameters overdetermines the orbit and permits a test of theories of gravitation. Three post-Keplerian parameters

(the general relativistic terms $\dot{P}$, $\dot{\omega}$ and γ) have been measured for the double neutron star system PSR B1913+16 (Taylor, Fowler & McCulloch 1979; Taylor & Weisberg 1989), providing a confirmation of general relativity to unprecedented precision, for which Joe Taylor and Russell Hulse were awarded the Nobel Prize for Physics in 1993. All five post-Keplerian parameters have been measured for PSR B1534+12 (Stairs et al. 1998) and a number of other pulsars have had two or more post-Keplerian parameters measured: in all cases the pulsar masses (and, for double neutron star systems, companion masses) are very close to the Chandresekhar limit (Chandrasekhar 1931) for the minimum mass of a neutron star. Thorsett & Chakrabarty (1999) estimate that the mass distribution is centred around 1.35 $M_\odot$ with an tight standard deviation of just 0.04 $M_\odot$.

1.4 Pulsar Searching

1.4.1 Search Basics

As we shall see in this thesis, pulsar astronomy and in particular, pulsar searching, is always associated with the cutting edge of data processing technology. In 1967, this consisted of banks of postgraduate students staring at the output of chart recorders. In such systems, the total received power is detected and integrated with some time constant (typically 0.1 – 10 s) and the amplitude of the integrated signal recorded on moving paper with an electrically actuated pen. Charts were fed into the bank of graduate students which produced results to be published (Hewish et al. 1968). For the Cambridge work, which uncovered the first pulsar, the RMS fluctuation in the system noise was 0.5 Jy with a time constant of 0.1 s, implying a minimum detectable mean flux density of the order of 100–200 mJy. In addition to the first pulsar (§ 1.1), three further pulsars were found in the Cambridge data (Pilkington et al. 1968) at a frequency of $\sim$ 80 MHz, and soon thereafter a further 31 pulsars were discovered in similar fashion in a dedicated survey with the Molonglo Cross telescope at 408 MHz which was sensitive to pulsars brighter than about 80 mJy (Turtle & Vaughan 1968; Large, Vaughan & Wielebinski 1968; Large, Vaughan & Wielebinski 1969a; Large, Vaughan & Wielebinski 1969b; Vaughan, Large & Wielebinski 1969; Vaughan & Large 1970).

However, it is fairly obvious that one ought to be able to take advantage of the periodic nature of the signal to improve detection sensitivity. For this, a computer

is required for mathematical analysis of the recorded time series. The Jodrell Bank "A" survey in 1972-73 (Davies, Lyne & Seiradakis 1977) pioneered this approach, using correlation to search for periodicities and discovering 39 new pulsars with flux densities greater than ~ 15 mJy. All further pulsar surveys exclusively used Fourier analysis to detect periodicities. In this technique, the fluctuation power spectrum of the detected time series is computed using the Fast Fourier Transform (FFT) algorithm (see e.g. Press et al. 1986). Since pulsars typically have a narrow duty cycle, their power is spread over a number of harmonics in the power spectrum, sums were made over various number of harmonics. The resultant data was then searched for significant peaks. By extension of Parseval's Theorem, the signal to noise ratio (S/N) of this harmonically summed spectrum approximates the S/N of the resultant integrated pulse profile. Since this is the result of coherently summing N pulses and integrating the incoherent noise N times per bin, the S/N of the integrated profile is $\sqrt{N}$ times greater than that of the individual pulse. Figure 1.4 illustrates this process. In addition, unlike the chart recorder approach, this method is insensitive to the sampling interval as long as it is sufficient to resolve the pulse. Naturally, these advantages resulted in the discovery of large numbers of fainter pulsars by computer-based surveys as high performance computing became more readily available.

To obtain good sensitivity, pulsar surveys generally record the largest practical bandwidth available. However, the differential dispersion delay across the band causes broadening ("**DM smearing**") of pulses if they are detected directly. This reduces the signal to noise ratio (see § 1.4.2), especially for rapidly rotating pulsars. The approach since the 1970s has been to use hardware filters to divide the band into several channels, which proportionately reduces the DM smearing (see Figure 1.2). The detected outputs of each channel are recorded and the computer analysis procedures incorporate a search in DM space by summing channels with delays corresponding to a range of trial DMs before performing a spectral analysis on the time series that result.

1.4.2 Sensitivity

By making several assumptions, it is possible to derive the detection threshold for a pulsar survey. The process is long but educational!

The radio telescope is a device for amplifying and measuring the oscillating elec-

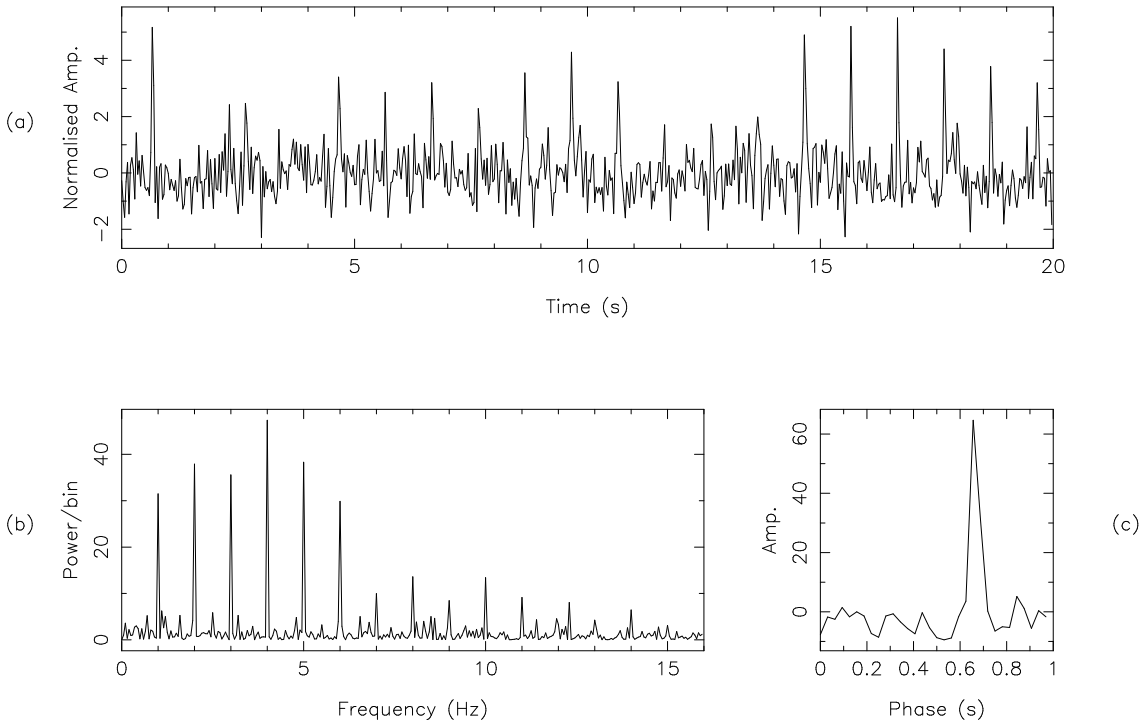

Figure 1.4: Demonstration of computer-based pulsar processing. Part (a) shows simulated pulsar time series. The pulse period is 1 s and most pulses are just visible above the noise (this is the case in reality only for very bright pulsars). Part (b) shows the power spectrum of this time series, with the fundamental (1 Hz) plus approximately 14 visible harmonics. Part (c) shows the integrated pulse profile. The signal-to-noise enhancement due to integration is apparent in parts (b) and (c).

tric field induced by microwave radiation from extra-terrestrial sources. A radio telescope with a single paraboloid reflector (**"dish"**) is sensitive to radiation from an area of sky approximately λ/D radians in diameter, where λ is the observing wavelength and D is the diameter of the dish. This region of sensitivity is called the telescope **beam**, which the dish is said to "illuminate". The receiver itself contains two probes sensitive to orthogonal polarisations of the electric field, limited to a given band of sensitivity. It is generally the case that the detected power from the probes is dominated by noise from the receiver amplifier, and/or background Galactic synchrotron radiation. The power of the detected signal is typically specified in temperature units, corresponding to the temperature at which the thermal electronic Johnson noise of a resistor would have the same power as the apparent voltage fluctuations in the receiver probe. Happily, due to the inverse relationship between telescope gain and beam area this also corresponds to the temperature of a distant extended blackbody that would induce the same voltage fluctuations in the

receiver probes via its radiation.

The ever-present receiver and sky noise induces what is called the **system temperature**, $T_{\rm sys}$. Sensitivity in radio astronomy is achieved by time averaging the detected signal, such that the uncertainty in this average is less than the (generally much smaller) added temperature ($T_{\rm src}$) induced by the source to be observed. Various strategies exist for processing these signals, but losses aside the sensitivity achievable in an integration of a given duration is equivalent in all approaches. Since in modern astronomy one is used to dealing with sampled data series, I will derive the sensitivity of an integration made with a baseband recording system.

In a baseband system, the signals are mixed with a local oscillator to place the band close to DC, and filtered to provide a sharp band-pass. The baseband voltages are then digitally sampled at the Nyquist rate, given by $\nu_{\rm samp} = 2B$ where B is the bandwidth[1], and recorded for processing in software. To measure total power the samples would be squared and summed in polarisation pairs, and I will assume that the squared samples are in known temperature units and hence have a mean of $T_{\rm sys} + T_{\rm src}$, or under the small-signal assumption approximately $T_{\rm sys}$.

Since the system noise is Gaussian in character, the result of summing squared samples follows a χ^2 distribution. For an integration of $N_{\rm samp}$ squared polarisation-summed samples arising from $N_{\rm pol}$ polarisations, the distribution has $N_{\rm samp}N_{\rm pol}$ degrees of freedom and is scaled by the mean of the squared input samples in each polarization, approximately $T_{\rm sys}$. Hence the variance of the integrated signal is $T_{\rm sys}^2 N_{\rm samp}N_{\rm pol}$, and since $N_{\rm samp}$ is large the distribution is approximately Gaussian with standard deviation $T_{\rm sys}\sqrt{N_{\rm samp}N_{\rm pol}}$. Converting the result of the integration to a mean temperature by dividing by $N_{\rm samp}N_{\rm pol}$ gives a standard deviation of $T_{\rm sys}/\sqrt{N_{\rm samp}N_{\rm pol}}$. Since the data are Nyquist sampled we have $N_{\rm samp} = \nu_{\rm samp}t_{\rm obs} = 2Bt_{\rm obs}$ (where $t_{\rm obs}$ is the integration time), and obtain

$$\sigma_T = \frac{T_{\rm sys}}{\sqrt{2N_{\rm pol}Bt_{\rm obs}}} \tag{1.11}$$

where σ_T is the RMS fluctuation in the time series, or the uncertainty with which one can measure the mean temperature across both polarisations in a given integration time.

[1]The resultant samples are real-valued. An alternative is to produce "complex samples" by sampling (at $\nu_{\rm samp} = B$) in-phase and quadrature values derived from two versions of the signal mixed with local oscillator signals offset by 90°, as used later in this thesis.

The signal to be detected induces an added temperature in each receiver probe. Since the instantaneous polarisation vector of electromagnetic radiation is two dimensional and its orientation is stochastic, the mean additional temperature induced in each receiver probe is the product of the telescope gain (G) and the flux density (S), divided by the square root of two. The signal to be detected is $T_{\rm src} = T_{\rm obs} - T_{\rm sys}$ where $T_{\rm obs}$ is the observed mean temperature and is subject to an uncertainty of approximately σ_T (equation 1.11). Under the assumption of a well-calibrated system temperature $T_{\rm sys}$, the signal-to-noise ratio (S/N) of the detection is thus $T_{\rm src}/\sigma_T$. Substituting for the flux density and telescope gain, we obtain

$$S/N = \frac{GS}{\sigma_T\sqrt{2}} = \frac{GS\sqrt{N_{\rm pol}Bt_{\rm obs}}}{T_{\rm sys}} \tag{1.12}$$

Rearrangement of this equation to give the "system noise" or minimum detectable flux density σ_S yields the the well-known **radiometer equation** which applies to the detection of flux relative to a previously calibrated system temperature:

$$\sigma_S = \frac{T_{\rm sys}}{G\sqrt{N_{\rm pol}Bt_{\rm obs}}} \tag{1.13}$$

For the detection of an idealised pulsar with rectangular pulse profile of peak flux density $S_{\rm p}$ and mean flux density $S_{\rm ave} = \delta S_{\rm p}$ where δ is the duty cycle, the signal to noise ratio can be defined in terms of the uncertainty in the measured peak flux. Since there are generally no calibration observations made in pulsar surveys, the "noise" term in the signal to noise ratio calculation has a term for the uncertainty in the "**baseline**" (off-pulse temperature) in addition to the expected term due to uncertainty in the measurement of the on-pulse temperature. From equation 1.11 this uncertainty is given by

$$\sigma = \left[\left(\frac{T_{\rm sys}}{\sqrt{2N_{\rm pol}B\delta t_{\rm obs}}}\right)^2 + \left(\frac{T_{\rm sys}}{\sqrt{2N_{\rm pol}B(1-\delta)t_{\rm obs}}}\right)^2\right]^{1/2} \tag{1.14}$$

$$= \frac{T_{\rm sys}}{\sqrt{2N_{\rm pol}Bt_{\rm obs}}}[1/\delta + 1/(1-\delta)]^{1/2} \tag{1.15}$$

$$= \frac{T_{\rm sys}}{\sqrt{2N_{\rm pol}Bt_{\rm obs}}}[\delta(1-\delta)]^{-1/2} \tag{1.16}$$

From this we may derive the signal to noise ratio in terms of the mean flux density,

$$S/N = \frac{GS_{\rm p}}{\sigma\sqrt{2}} \tag{1.17}$$

$$= \frac{GS_{\rm ave}}{\delta}\frac{\sqrt{N_{\rm pol}Bt_{\rm obs}}}{T_{\rm sys}}[\delta(1-\delta)]^{1/2} \tag{1.18}$$

$$= \frac{GS_{\rm ave}\sqrt{N_{\rm pol}Bt_{\rm obs}}}{T_{\rm sys}}\left[\frac{(1-\delta)}{\delta}\right]^{1/2} \tag{1.19}$$

Including a dimensionless loss factor β and substituting the threshold signal to noise ratio for a positive detection α, the minimum detectable flux density is given by

$$S_{\rm min} = \frac{\alpha\beta T_{\rm sys}}{G\sqrt{N_{\rm pol}Bt_{\rm obs}}}\sqrt{\frac{\delta}{1-\delta}} \tag{1.20}$$

A similar result was derived by Dewey et al. (1985). It must be noted that the observed duty cycle of a pulsar is generally somewhat larger than that emitted by the pulsar due to interstellar and instrumental broadening. These will vary with different search techniques, however a basic analysis would include the broadening due to the finite sampling interval ($\tau_{\rm samp}$), dispersion smearing within each filterbank channel ($\tau_{\rm DM}$; § 1.2.3 and § 1.4.1), and scatter-broadening in the interstellar medium ($\tau_{\rm scat}$; § 1.2.4) to yield

$$\delta = \frac{\sqrt{W_{\rm i}^2 + \tau_{\rm samp}^2 + \tau_{\rm DM}^2 + \tau_{\rm scat}^2}}{P} \tag{1.21}$$

where $W_{\rm i}$ is the intrinsic effective pulse width and P is the pulse period.

Inspection of equation 1.20 reveals the important factors for success of a pulsar survey. For raw sensitivity the telescope gain and system temperatures are the most crucial factors, and (unfortunately) are often beyond direct control of the astronomer due to the considerable cost of improving them. However, all is not as it appears with the telescope gain factor, since the gain and the telescope beam area are inversely related via the square of the diameter of the dish. Hence, for an observing campaign of a given length and sky coverage, the sensitivity achievable scales only as the square

root of the telescope gain. This leaves system temperature as the most important factor, and indeed the excellent noise characteristics of the new multibeam receiver at the Parkes radio telescope are largely responsible for the phenomenal success of recent surveys with this instrument (Chapters 3–5; Lyne et al. 2000a; Camilo et al. 2000b). As discussed above, there is also a contribution to the system temperature by Galactic synchrotron radiation, which has a steep spectrum (Lawson et al. 1987) and strong dependence on Galactic latitude (Haslam et al. 1982), giving the high frequency intermediate latitude survey described in this thesis an advantage over most other surveys. Following the system temperature and receiver gain, the next factors to consider are bandwidth and integration time, with which the sensitivity varies as $\sqrt{Bt_{\rm obs}}$. Integration time is generally limited by the available telescope and computer processing time, and for long integrations the effects of acceleration in pulsar binaries also become important (see next chapter). The available bandwidth is limited by the design of the receiver and the complexity of the backend system, as well as the presence of strong interference signals. Integration time and bandwidth are both usually maximised within the limits of practicability.

In selection of the parameters for a potential pulsar survey, attention must also be given to equation 1.21. Specifically, the sampling interval must be short and the filterbank channels both narrow (to reduce smearing) and numerous (to maintain a large bandwidth in equation 1.20). The effects of scatter-broadening are not removable by any processing technique, however the steep spectrum (§ 1.2.4) and strong Galactic latitude dependence of this phenomenon again favours high frequency surveys off the Galactic plane, such as the one described in this thesis.

1.5 Pulsar Surveys: Past, Present and Future

The topic of this thesis is Pulsar Searching, and as such it is helpful to explore the kinds of pulsars that exist, and the best ways to find them. For this reason, in this section I review the techniques and findings of past and present major pulsar surveys and suggest some ways that we might expand our sample of interesting objects.

1.5.1 Past

We have already discussed the first three surveys in § 1.4.1. After examining the data in the Cambridge scintillation survey, three pulsars were found (Hewish et al.

1968; Pilkington et al. 1968). Following this the first Molonglo survey took the technique of searching using chart recorders as far as was practical, discovering 31 pulsars in the process (Vaughan & Large 1970 and references therein). Next came the Jodrell Bank "A" survey which used computer-based auto-correlation analysis to find a further 39 pulsars (Davies, Lyne & Seiradakis 1977).

All subsequent pulsar surveys used computer-based Fourier analysis to achieve essentially optimal sensitivity, in the process discovering a large number of pulsars. Exploiting the impressive collecting area of the 305-m Arecibo radio telescope, the UMass-Arecibo survey (Hulse & Taylor 1974; Hulse & Taylor 1975b) covered a small region of sky to unprecedented depth ($S > 1$ mJy at 430 MHz), discovering 40 pulsars. The most interesting pulsar discovered in this survey was PSR B1913+16 (Hulse & Taylor 1975a), the first binary pulsar. As noted in § 1.3, this system appears to have a neutron star companion, and relativistic effects on the orbital evolution of the system are measurable to high precision (Taylor & Weisberg 1982; Taylor & Weisberg 1989). These measurements are thus an important confirmation of relativity theory, and Hulse and Taylor were awarded the Nobel Prize for Physics in 1993[2].

The next major pulsar survey was the second Molonglo survey (Manchester et al. 1978), which searched most of the sky visible to the instrument to moderate sensitivity at 408 MHz, discovering 155 new pulsars. Among the considerable spoils of this survey was another binary pulsar, PSR B0820+02 (Manchester et al. 1980). This system is in a very wide orbit making it uninteresting in terms of tests of gravitation, however to this day its evolutionary history remains enigmatic compared to other pulsar binaries.

Contemporaneous with the second Molonglo survey was a pulsar survey employing the 92-m NRAO Green Bank radio telescope (Damashek, Taylor & Hulse 1978). This survey complemented the Molonglo work by covering the whole sky north of $\delta = +20°$ at 408 MHz with comparable sensitivity. A total of 23 pulsars were discovered, including the third known binary pulsar, B0655+64 (Damashek et al. 1982), which is in a close 1-d orbit around what appears to be a massive CO white dwarf. As with the two binary pulsars known before it, PSR B0655+64 remains anomalous compared to others which followed it. Whilst it bears similarities to other systems with massive white dwarf companions (referred to as the intermediate mass binary

[2]The pulsar itself was discovered much earlier, in 1974: the same year for which Hewish was awarded the Nobel Prize for the discovery of the first pulsar!

pulsars, or IMBPs; Camilo et al. 1996), its long spin period ($P = 196$ ms) is unique among them, probably reflecting a difference in the nature and degree of spin-up it received during recycling.

Throughout the history of pulsar astronomy, targeted observations of likely candidates have yielded important discoveries, including the Crab pulsar (Staelin & Reifenstein 1968), which is the youngest known pulsar and is believed to be the remnant of the historical supernova of AD 1054. High time resolution observations conducted in 1982 of the enigmatic steep-spectrum radio source 4C21.53 yielded the discovery of the first millisecond pulsar (Backer et al. 1982) and heralded the beginning of a new era in pulsar astronomy. The revolution was slow, however, with subsequent searches detecting only a handful of further millisecond pulsars in the next few years. The second known MSP, PSR B1953+29 was discovered in a targeted observation of a gamma-ray source (Boriakoff, Buccheri & Fauci 1983), although the gamma-ray source and the pulsar are not believed to be associated : the discovery was fortuitous! Three further MSPs were found in the field in years up to 1990 (see below).

A second survey took place at Green Bank in 1982-3 at 390 MHz (Dewey et al. 1985), resulting in the discovery of a further 34 pulsars. Among the discoveries was a new binary pulsar, PSR B2303+46, in a wide eccentric orbit around a massive companion. It was suggested that the companion was a neutron star, however unlike B1913+16 it did not appear to be recycled and hence must have been the second-born system. Later observations (van Kerkwijk & Kulkarni 1999) suggested that the companion was in fact a massive white dwarf that formed from a star initially more massive than the pulsar progenitor. After the discovery of the first millisecond pulsar, it became obvious that high time resolution was advantageous for discovering interesting new objects, and a second phase of the survey was initiated to detect pulsars down to 4 ms (Stokes et al. 1985). This survey discovered 20 new pulsars, but the fastest spin period among them was 101 ms.

In 1983-4 a new survey at Jodrell Bank was conducted at 1400 MHz , the first to go to a relatively high frequency (the Jodrell Bank "B" survey; Clifton & Lyne 1986; Clifton et al. 1992). As has been noted earlier, there are several advantages to searching for pulsars at high frequency. Whilst pulsars tend to be intrinsically less luminous at high frequencies ($S \propto \nu^{-1.6}$; Lorimer et al. 1995), the greatly reduced sky temperature ($T \propto \nu^{-2.6}$; Lawson et al. 1987) offsets this loss, especially near the Galactic plane where the sky noise dominates the system temperature

at low frequencies. Scatter-broadening is also greatly reduced at high frequencies (§ 1.2.4), facilitating detection of short-period pulsars such as MSPs and young pulsars. However the telescope beam area is much smaller at high frequencies ($\propto \nu^{-2}$), limiting the practicality of large scale high-frequency surveys. The Clifton & Lyne survey concentrated on the northern Galactic plane and discovered 40 new pulsars, including a high proportion of young pulsars and a slow pulsar (B1820–11) in a wide eccentric orbit around a probable main sequence companion (Lyne & McKenna 1989; Phinney & Verbunt 1991). No millisecond pulsars were discovered due to the marginal sensitivity provided by the 2-ms sampling interval and 5-MHz channels. A similar region of sky was later covered with 0.3-ms sampling (the "C" survey; Biggs & Lyne 1992), however no new pulsars were found.

A third survey to adopt high time resolution in the search for millisecond pulsars was the Princeton-Arecibo survey (Stokes et al. 1986). The survey covered the region of the Galactic plane visible from Arecibo at 430 MHz with 0.3-ms sampling. Due to the modest 1 MHz bandwidth available, the survey only discovered 5 new pulsars, including the third known millisecond pulsar, B1855+09 (Segelstein et al. 1986), which was later the first binary pulsar for which the relativistic Shapiro delay of its companion was measured (Ryba & Taylor 1991). In the late 1980s the Arecibo Galactic plane was revisited at 430 MHz with an improved system temperature and bandwidth, and a time resolution of 517 μs (Nice, Fruchter & Taylor 1995). A total of 24 new pulsars were discovered, including the binary millisecond pulsar B1957+20 (Fruchter, Stinebring & Taylor 1988). The companion to this pulsar is very light (~ 0.025 $M_\odot$) and its close orbit results in eclipses in the radio and strong heating of the companion which is detectable optically (Fruchter et al. 1988).

The late 1980s also saw the beginning of searches for pulsars in globular clusters. Under the recycling hypothesis of millisecond pulsar formation (Alpar et al. 1982), a large number of MSPs were expected in Globular clusters, where stellar densities are high and binary interactions commonplace, leading also to a high density of low-mass X-ray binaries. Nevertheless, the announcement of the discovery of a 3 ms pulsar in M28 (Lyne et al. 1987) had considerable dramatic impact! Globular clusters soon proved to be rich hunting grounds for millisecond pulsars, with observations at 610 and 1400 MHz on the Jodrell Bank telescope finding a further four pulsars in three clusters: M4 (Lyne et al. 1988), NGC 6342 (Lyne et al. 1993) and NGC 6624 (Biggs et al. 1994), two of which possessed millisecond spin periods. Contemporaneous with these discoveries were similarly successful searches

at Arecibo, which found 14 pulsars (mainly MSPs) in 5 clusters: M5 (Wolszczan et al. 1989a), M13 (Anderson et al. 1989a), M15 (Wolszczan et al. 1989b; Anderson et al. 1990b; Anderson 1992), M53 (Anderson et al. 1989b) and NGC 6760 (Anderson et al. 1990a). The most prolific cluster searched at Arecibo was M15, with an amazing eight pulsars discovered, all within $1'$ of the cluster core. The southern globular cluster 47 Tucanae proved even more fertile, with observations at the Parkes 64-m radio telescope yielding 11 pulsars (Manchester et al. 1991), all with millisecond spin periods. Searches at Parkes also discovered pulsars in NGC 6440 (Manchester et al. 1989), Terzan 5 (Lyne et al. 1990; Lyne et al. 2000b) and NGC 6539 (D'Amico et al. 1993). The discoveries in 47 Tucanae and M15 highlighted the biggest advantage of globular clusters in the search for fast pulsars: the possibility of discovering numerous pulsars in a single telescope beam area, even at high frequencies on large telescopes. For this reason globular cluster surveys used high observing frequencies just as often as low ones. By 1990 the capabilites of the available instruments had largely been exhausted and $\sim$30 pulsars had been discovered in globular clusters, many of which had millisecond periods, comprising the vast majority of known MSPs at the time.

In 1988-9 the first large scale pulsar survey to use the Parkes radio telescope was conducted by Johnston et al. (1992a). Like the Jodrell Bank "B" survey, this survey was conducted along the Galactic plane at the high frequency of 1400 MHz, and was highly successful, discovering 46 new pulsars including a number of young pulsars. Perhaps the most interesting discovery of this survey was the binary pulsar B1259–63, which is in an eccentric orbit around a Be star (Johnston et al. 1992b).

In February 1990 an impromptu 430 MHz millisecond pulsar survey was conducted at Arecibo at high Galactic latitudes. The small 150 sq. deg. survey proved astoundingly successful, discovering the second-known relativistic double neutron star system, B1534+12 (Wolszczan 1991) and B1257+12, with the first ever detection of planets outside the solar system (Wolszczan & Frail 1992). This led to the commencement of several further surveys at high latitudes (Thorsett et al. 1993; Foster et al. 1995; Ray et al. 1995; Camilo, Nice & Taylor 1996). In late 1993 the Arecibo telescope entered an extended period of construction during which movement of the feed was limited. Interest in high-latitude millisecond pulsar surveys remained high, and the accessible portion of the sky was divided by the scheduling committee into declination strips for drift-scan searching by competing collaborations (Ray et al. 1995; Foster et al. 1995; Camilo et al. 1996; Lommen et al. 2000).

The resultant non-uniformity in sensitivity and scattering of discoveries amongst numerous publications was regrettable, but nevertheless the surveys made some important discoveries, finding $\sim$ 70 pulsars, $\sim$ 10 of which possess millisecond spin periods, but none is as spectacular as B1534+12 or B1257+12. Perhaps the most interesting discoveries were the intermediate mass binary pulsars J0621+1002 and J1022+1001 (Camilo et al. 1996).

The second large survey to be conducted at Parkes was the Parkes Southern Pulsar Survey (Manchester et al. 1996; Lyne et al. 1998; D'Amico et al. 1998), with the ambitious goal of surveying the entire southern sky at 436 MHz for millisecond pulsars. The survey discovered 101 new pulsars, of which 17 possessed millisecond spin periods, making this the most successful survey ever in terms of MSP discoveries. Most of the millisecond pulsars possessed He white dwarf companions in circular orbits, being members of the swelling class of low mass binary pulsars. Highlights included J2051–0827, a millisecond pulsar in a close orbit with a ~ 0.03 $M_\odot$ companion (Stappers et al. 1996) being visibly heated by the pulsar radiation (Stappers, Bessell & Bailes 1996), and J0437–4715 (Johnston et al. 1993), the closest and brightest known millisecond pulsar, of which timing to exquisite precision is achievable (Sandhu et al. 1997; van Straten et al. in preparation).

1.5.2 Present

It is conceivable that the author is biased, however I shall assert here that the most important work in pulsar surveys at present is all being conducted at Parkes.

In 1997 the Australia Telescope National Facility commissioned a new 1400 MHz front-end, primarily for use in two large scale surveys for HI galaxies (Henning et al. 2000; Barnes et al. 2001). This system offers excellent noise characteristics, a wide bandwidth and, most significantly, 13 independent dual linear polarization receivers distributed across the focal plane. The potential of this instrument for deep, large-scale pulsar surveys was immediately realised and in 1997 August observations commenced for a highly sensitive survey of the Galactic plane (Camilo et al. 2000b; Manchester et al. 2001), conducted by a collaboration of workers from several institutions. The survey is proving phenomenally successful, having discovered $\sim$580 pulsars at the time of writing (March 2001). A number of interesting individual objects have been found, including a double neutron star system (J1811–1736; Lyne et al. 2000a), a non-recycled pulsar in an eccentric orbit around a

probable ultra-massive white dwarf (J1141–6545; Kaspi et al. 2000b), a pulsar with an 11 $M_\odot$ probable K supergiant star (J1740–3052; Manchester et al. 2000), and several young pulsars with extremely strong magnetic fields (Camilo et al. 2000c; R. N. Manchester, personal communication). Five apparently recycled pulsars in circular binaries have been discovered (Camilo et al. 2000b), with most possessing longer spin periods ($9 < P < 90$ ms) than is typical of low mass binary pulsars. So far only two pulsars have been discovered with periods less than 10 ms (Camilo et al. 2000b; R. N. Manchester, personal communication), a somewhat surprising result (cf. Toscano et al. 1998), however future population modelling may be able to explain the result in light of the degree of scatter-broadening experienced or the scale-height of MSPs.

A second, shallower survey has recently been conducted by myself and colleagues at Swinburne, with the same system used for the Galactic plane survey. Our survey flanked the Galactic plane survey region with 10°-wide strips above and below the latitude region of the deeper survey, using shorter pointings to quickly cover the entire region in 14 days of integration time. A total of 69 pulsars, including 8 recycled and six binary systems were discovered. The survey and its discoveries are the topics of later chapters of this thesis.

The centre beam of the new 21-cm system provides such high gain with so little receiver noise that it has proved an excellent instrument for renewed efforts at Globular cluster searching. Camilo et al. (2000a) report the discovery of a further 9 pulsars in 47 Tucanae using this instrument, and of the 20 pulsars now known in the cluster, 15 now have timing solutions (Freire et al. 2001), yielding parameters with broad and interesting implications for cluster dynamics and binary pulsar evolution. In addition, the instrument has been used to discover new millisecond pulsars in four clusters which previously were not known to contain pulsars (D'Amico et al. 2001a).

1.5.3 Prospects for Novel New Developments

What is the future of radio pulsar astronomy? By the early 1980s an extensive and largely homogenous population of pulsars was known, with the characteristics of the Galactic population as a whole largely well constrained (e.g. Vivekanand & Narayan 1981). Little in the way of unexpected discoveries seemed to be on the horizon, until the discovery of the millisecond pulsar initiated something of a renaissance in pulsar

astronomy. This was perhaps the most dramatic instance of a continual stream of interesting and unanticipated discoveries, all of which tended to derive from the exploring of new parameter spaces and/or the use of newly available equipment.

At the time of the discovery of the first millisecond pulsar, the low end of the observed period distribution was more a result of survey selection effects than the underlying distribution of the population, and so it remains today even after the extension of survey parameter spaces to include some sensitivity to MSPs (Lorimer et al. 1996). One can continue to build ever more populous filter banks to minimise dispersion smearing and indeed this approach has recently seen some success in the new Parkes Globular cluster discoveries (D'Amico et al. 2001a), which exploited the newly-available $2 \times 512 \times 0.5$ MHz filter system. An alternative with numerous advantages is now reaching the stage of feasibility due to continual advances in the affordability of mass data storage and processing: this is baseband searching.

Through the Nyquist-sampled recording of the raw (pre-detection) receiver voltages, baseband processing allows the construction of an optimal filterbank in software, giving the highest possible time resolution for a given dispersion measure range. In addition, if the search is directed at objects for which DM estimates are available (e.g. globular clusters), the dispersion can be coherently removed (Hankins & Rickett 1975), leaving only the (typically negligible) smearing due to divergence from the estimated DM. In this manner targets can be searched to essentially arbitrary time resolution (limited only by the available offline computing power), regardless of dispersion measure. This approach was recently used in a survey of Globular clusters at 50 cm, described in this thesis. Whilst my efforts in this direction failed to discover any new pulsars, they do indicate that the technique is capable of delivering consistent sensitivity to pulsars with normal, millisecond and sub-millisecond periods, a characteristic that is vital if we are to resolve the true pulse period distribution of pulsars.

The discovery of just one sub-millisecond pulsar would have profound implications for theories of nuclear matter (e.g. Cook, Shapiro & Teukolsky 1994). If such objects are reasonably common, I expect that it is only a matter of a few years before baseband surveys with improved basic sensitivity discover some. A rigorous null result would be almost as important, if less spectacular.

A more subtle selection effect in past surveys has been against objects of very long pulse period, due to the use of short time constants in digitiser high-pass filters, and due to software period cut-offs. This was dramatically illustrated with the realisation

that PSR J2144–3933, originally thought to have a period of 2.84 s (Manchester et al. 1996), actually only spins once every 8.5 s (Young, Manchester & Johnston 1999)! A great deal of interest rests at present on the so called Anomalous X-Ray Pulsars (AXPs) and Soft Gamma-ray Repeaters (SGRs), which emit high-energy radiation pulsed with periods of 5–12 s (Mereghetti 2000 and references therein). The detection of radio counterparts to such sources would represent a discovery of great importance, and if radio surveys or targeted searches are to reliably find them this sensitivity issue must be addressed.

In the future the construction of extensive arrays of radio telescopes such as the proposed Square Kilometre Array will dramatically change the face of pulsar astronomy. The sensitivity of such instruments will be sufficient to make a fairly complete sample of the full Galactic population (beamed in our direction), and perhaps even to detect bright pulsars in nearby galaxies. The distribution of all pulsar parameters will be well-known and much less affected by selection effects than they are today. The large numbers of potentially detectable MSPs in globular clusters will present an unprecedented probe into cluster dynamics. The precision available to pulsar timing will facilitate the measurement of large numbers of parallax distances, proper motions, and post-Keplerian orbital effects and will make possible the use of MSPs as use as gravitational wave detectors (Kopeikin 1997). The unprecedented sensitivity of such instruments will no doubt result in the discovery of rare examples of classes of objects previously undreamt of, with interesting and unpredictable implications. We hope.

1.6 Thesis Overview

This thesis describes two campaigns undertaken at the Parkes radio telescope to search for pulsars, and the attendant timing program for the new discoveries. Following this introductory chapter, Chapter 2 describes the techniques employed in the analysis of search data.

Three chapters describe results from a large scale survey of intermediate Galactic latitudes. Chapter 3 announces the discovery of two recycled pulsars with massive white dwarf companions and discusses the implications of the existence of these unique objects. Chapter 4 discusses the full sample of recycled pulsars discovered in the survey. The search procedure, sensitivity and discovery of slow pulsars is

described in detail in Chapter 5.

The penultimate chapter of the thesis describes a baseband survey of Globular clusters for ultra-fast pulsars. This is followed by a chapter of Conclusions.

The software written for this thesis was designed for maximum flexibility and should be of use in the future to those wishing to conduct pulsar searches. The appendix of this thesis serves as a reference manual for this software, which is freely distributed.

Chapter 2

The Search Procedure

2.1 Overview of the Process

This thesis describes two separate pulsar surveys carried out recently : one involving a great many short observations (chapter 5), the other a handful of very long observations (chapter 6). The software development for these projects was carried out in such a way as to produce a uniform and parameterised set of tools for pulsar searching. In this chapter the methods used by the software are described in detail. Appendix A acts as a reference manual for the software, with technical information regarding the use and development of the programs.

A schematic outline of the processing schemes is presented in Figure 2.1. The basic stages are data recording, filterbank formation (for baseband data), interference mitigation, partial-dedispersion, repeated spectral analysis of time series at trial dispersion measures and acceleration, time-domain fine-tuning of pulsar suspects, and suspect scrutiny by human viewing. We now consider each in turn.

2.2 Data Recording

2.2.1 Hardware Filterbanks

Recent pulsar surveys have without exception relied on the use of radio spectrometers or "filterbanks" to allow for offline searching of a range of dispersion measures, subject to the dispersion measure smearing within each filterbank channel. Such a system was used for the Intermediate Latitude Survey (chapter 5). In this scheme,

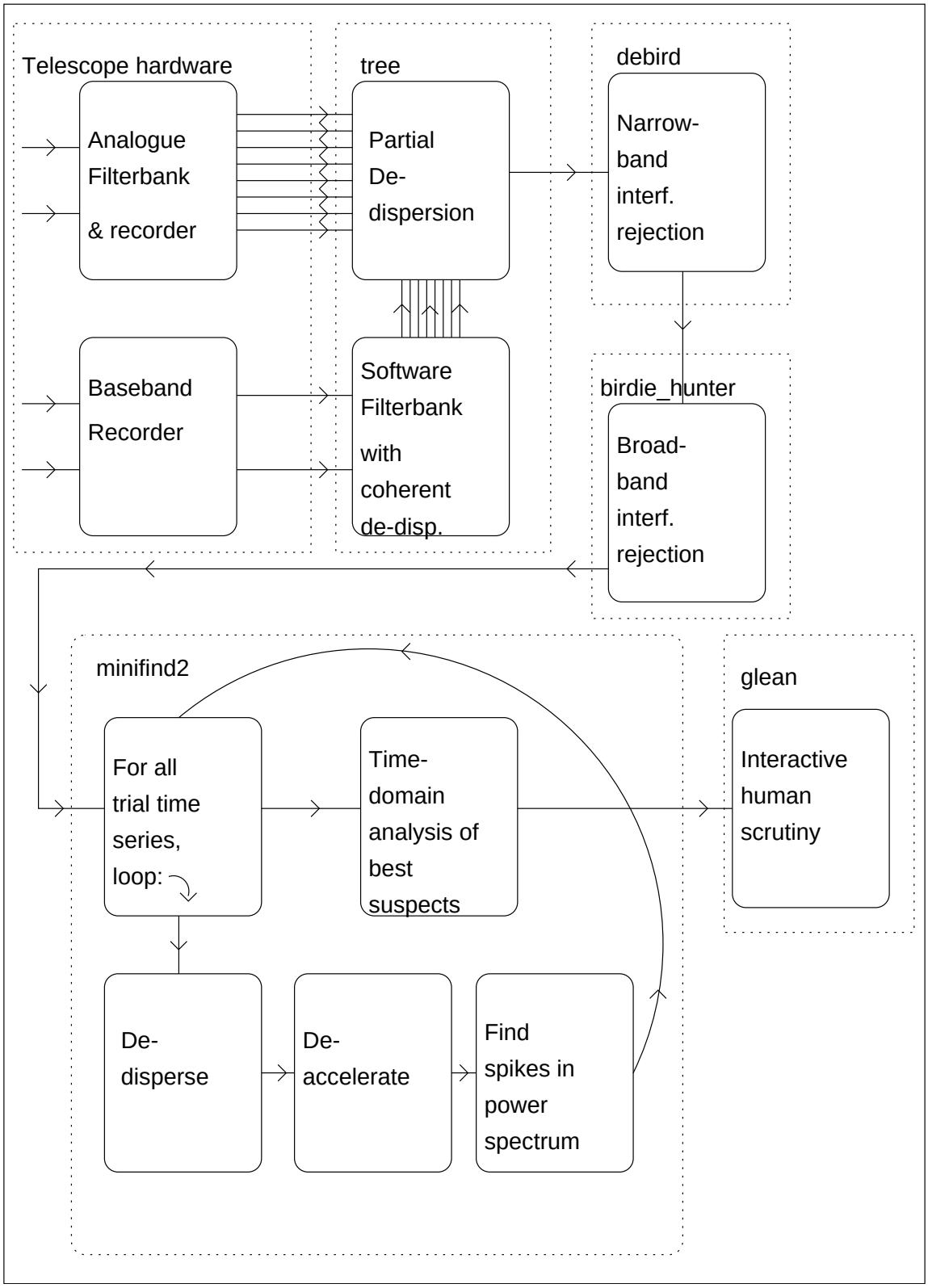

Figure 2.1: Schematic view of search strategy

the detected outputs of the corresponding filters from each polarisation are summed and sampled, typically with one bit of precision by comparison to a smoothed average of the last few seconds of signal.

2.2.2 Baseband Recording

Hardware filterbanks or autocorrelation spectrometers are limited by the number of channels and/or output sample rate they can provide. When searching for millisecond or sub-millisecond pulsars at moderate–high unknown dispersion measure, narrow channels are essential to limit smearing. Likewise, fast sampling is necessary to fully resolve the pulse and maximise the signal-to-noise ratio.

If on the other hand, the received band is mixed to DC (**"baseband"**) and sampled at their Nyquist rate, within the limitations of sampling quantization, the full information content of the data is recorded. Any other hardware backend can be simulated in software, or the data can be processed in ways not possible with hardware. In the simplest case for searching, one can form a "software filterbank". To form a software filterbank one takes N complex samples[1], performs an FFT on them and divides the complex spectrum into n segments. These segments are then individually inverse transformed and square-law detected to give a time series in a channel corresponding to that segment of the spectrum. Thus one produces data in n channels, sampled at $1/n$ times the rate of the baseband data. Since the channel bands are $1/n$ times the width of the entire band, they appear at half the Nyquist rate; the factor of two could be avoided by performing a complex–real inverse transform as the last step, however in most cases this time resolution is sufficient.

Possessing a coherent recording of the electric field vector at the telescope also allows for de-dispersion of the data without any smearing. In this process, known as **coherent de-dispersion**[2], segments of the data are convolved by spectrum multiplication with the inverse of the interstellar dispersion impulse response (Hankins & Rickett 1975). The relative computational burden of this approach combined

[1] I assume that the data is sampled in-phase and quadrature, as in Chapter 6. Factors of two appear if the calculations are made for data real-sampled at the rate $2B$.

[2] Whilst it is coherent in the sense of applying the filter to the raw voltages, it should be remembered that the pulsar signal is believed to be modulated (incoherent) noise, so there is no need to preserve coherence. This would require the DM delay to be known to within one phase turn across the band, a feat that is impractical due to uncertainties in aligning pulses at different frequencies, with different pulse morphologies.

with the need to use thousands of trial dispersion measures still necessitates the use of a software filterbank for searching, however it is possible to apply de-dispersion filters to the data for each individual channel, thus removing any DM smearing for a pulsar at the chosen (**"nominal"**) dispersion measure. Since dispersion delay is proportional to dispersion measure, the smearing in each channel now becomes proportional to the difference between the pulsar DM and nominal DM. This is a distinct advantage in searches in globular clusters of known dispersion measure, for one may use relatively broad coherent filters centered on the cluster DM and expect to experience in-channel smearing only from a DM range of $\sim \pm 1$ pc cm^{-3}. This allows a correspondingly higher sampling time in each channel, commensurate with the DM smearing at the edges of the selected DM range. In practice (e.g. Chapter 6), this provides a surfeit of time resolution which must be reduced through the use of more channels, or by summing adjacent samples.

The number of channels in the synthesised filterbank is a matter for consideration. As with hardware filterbanks, smearing arises from the differential dispersion delay across each channel, although as noted above this can be reduced if an estimate of the dispersion measure is available. Increasing the number of channels proportionately reduces the amount of dispersion smearing, however it also results in a longer sampling interval in each channel. It is therefore sensible to choose a number of channels such that the sampling interval is approximately equal to the dispersion smearing for most pulsars to be detected. The resultant sampling interval is given by n/B whilst the dispersion smearing can be derived from equation 1.5 to yield

$$n/B \simeq 8.3B/n\mathrm{DM}\nu^{-3} \quad (2.1)$$

$$\Rightarrow n \simeq 2.9B\sqrt{\mathrm{DM}}\nu^{-3/2} \quad (2.2)$$

using the units assumed in equation 1.5. The dispersion measure in this relation is often referred to as the **"diagonal DM"** since at this DM the slope of the dispersion trail is 1, in terms of channel number versus sample number. Since the number of channels is generally a power of two to maximise the efficiency of later de-dispersion, the choice of dispersion measure is effectively limited to a set of values spaced at intervals of two octaves. In the search described in Chapter 6 the usual synthesised filterbank had 512 channels, providing a diagonal DM of $\sim$ 22.7 pc cm^{-3} with a sampling interval of 25.6 μs at a centre frequency of 660 MHz.

2.3 De-Dispersion

As already discussed, pulsar searching involves using numerous trial DMs for de-dispersion of possible pulsars. The spacing of these DMs is chosen such that the maximum smearing experienced by a pulsar with a DM half-way between two trial DMs is comparable to the sampling interval. This means using DMs that induce delays across the band spaced by two samples. For large DMs, the smearing in each filterbank channel may correspond to several sample intervals. For this reason, at higher DMs samples are summed to increase the sample interval to a more appropriate value, and the spacing of trial DMs is correspondingly increased.

Since the data are discretely sampled, forming sums across channels on a variety of similar paths involves a great deal of redundant arithmetic, adding the same sets of samples over and over again for closely spaced DM trails. One may take advantage of this redundancy in ways analogous to FFT algorithms by repeatedly summing in pairs to obtain a speedup of $n/\log n$ for n channels. Such an algorithm is described by Taylor (1974), and is often referred to as the "tree" algorithm.

The software written for this project de-disperses only to a certain extent, summing groups of d channels to produce $s = n/d$ "sub-bands" in d "DM groups". Later software then chooses the DM group which best approximates the average slope of the dispersion delay across the band at a chosen DM and sums this DM group, with appropriate delays, across all sub-bands. Whilst the latter uses the correct dispersion delays, the the first step of de-dispersion assumes a linear delay with frequency. This causes some smearing in itself, however the smearing due to the later use of a single DM group is in general greater and limits the number of channels that can be summed in the earlier stage. The worst-case smearing can be approximated using equation 1.5:

$$\tau_{\mathrm{SDM}} \simeq 8.3Bd/n\mathrm{DM}(\nu_0^{-3} - \nu_c^{-3}) \tag{2.3}$$

where ν_0 is the frequency of the lower edge of the band and ν_c is the centre frequency.

In order to keep this smearing smaller than or comparable to the dispersion smearing within each filterbank channel, the number of channels summed must be limited. Taking the filterbank smearing at the centre of the band, we have

$$8.3Bd/n\mathrm{DM}(\nu_0^{-3} - \nu_c^{-3}) \;<\; 8.3B/n\mathrm{DM}\nu_c^{-3} \tag{2.4}$$

$$\Rightarrow d \;<\; \frac{1}{\left(\frac{\nu_c}{\nu_0}\right)^3 - 1} \tag{2.5}$$

This yields an upper limit on the number of channels to be summed into each sub-band, indepedent of the actual total number of channels present.

The baseband survey described in Chapter 6 used 20 MHz of bandwidth at a centre frequency of 660 MHz. From equation 2.3 the resulting maximum number of channels to be summed is 14. Given the restriction of the algorithm to operate on powers of two channels, I chose to sum 16 channels using the linear algorithm, resulting in smearing comparable to that induced by the software filterbank.

For the intermediate latitude survey (Chapter 5) the fractional bandwidth was so large that little linear de-dispersion was possible without smearing. Application of equation 2.3 with 288 MHz of bandwidth centred at 1374 MHz yields $d < 2.5$, indicating that linear de-dispersion was essentially inapplicable to these data at any level. To allow the fast linear algorithm to be applied to multibeam data, samples from its 96 channels were distributed along with "dummy" channels in an array of 128 channels, in such a way as to produce a dispersion relation that was linear with channel number.

2.4 Acceleration

Pulsars with binary companions are subject to acceleration which can be strong enough to cause a noticeable smearing in the course of an observation if the search software expects a constant apparent pulse period. PSR J1757-5322 (§ 3.3), for example, was discovered while it was experiencing a line-of-sight acceleration of 7.5 m s^{-2}. In this case the observation was sufficiently short to allow acceptable sensitivity when folded as a signal of constant period. For long integrations such as those described in Chapter 6, however, acceleration becomes a problem.

The velocity of the pulsar relative to the observatory is a function of the proper motion of the pulsar and of the solar system, of the orbits of the pulsar and the earth and also of the earth's rotation, however for integrations of a few hours or less the only appreciable change in this velocity arises from the orbital motion of the pulsar. Modelling this motion fully requires the use of five orbital parameters and as such expands the dimensionality of the search space to a prohibitive degree. Ransom (2000) developed a method which is capable of detecting pulsars in orbits of

shorter duration than the observation via the sidebands induced in the fluctuation spectrum, effectively removing four dimensions from this search at the expense of some sensitivity. However for the majority of the expected population of pulsar binaries the orbital period is longer than the observations undertaken in Chapter 6 (∼900–1800s) and such pulsars would remain undetected by the scheme. For pulsars with orbits longer than the observation by a factor of ~ 2 or more, one may make the approximation of constant acceleration and perform a search instead in period and period derivative space.

Considering the effect of acceleration as causing a smearing of the fluctuation spectrum, one can calculate the number of spectral bins over which a signal will be smeared. The differential Doppler shift experienced is at/c, resulting in smearing over a frequency range $\nu at/c$, where a is the line of sight acceleration, t is the integration time and c is the speed of light. The size of a spectral bin is $1/t$, so the number of bins of smearing is $\nu at^2/c$. This results in loss of signal to noise ratio, especially for higher harmonics of the pulsar signal.

The approach taken in the globular cluster searching (Chapter 6) was to re-bin each de-dispersed time series in such a way as to remove the effect of a given acceleration. This process was repeated for numerous trial accelerations in such a way as to provide good sensitivity over a range of accelerations. Radiation received at time t experienced an additional propagation delay $t - t' = 2c/at^2$ due to acceleration relative to a given velocity at time $t = 0$, which in this analysis I take as zero since it is inseparable from the unknown intrinsic pulsar period. Hence, the rate of passage of time in the pulsar frame with respect to the observer frame is given by

$$\frac{\mathrm{d}}{\mathrm{d}t} t[1 - 2c/at^2] = 1 - at/c \tag{2.6}$$

Placing $t = 0$ at the centre of the observation and assigning sample indices i in the range of 0 to $N - 1$, the algorithm for traversing the vector of input samples and computing equivalent indices (i') for re-binning (or interpolation) into an output vector is simple:

$i \leftarrow 0$
$i' \leftarrow 0$
while $i < N$ **do**
  $t \leftarrow \tau_{\mathrm{s}}(i + 0.5 - N/2)$
  re-bin sample i to index i'

$i \leftarrow i + 1$

$i' \leftarrow i' + 1 - at/c$

end while

where τ_s is the sampling interval. It should be noted that this effectively performs a piecewise numerical integration of equation 2.6, and that the step size is so small that the errors induced are negligible. This algorithm preserves the total number of samples and maintains the same effective sampling rate in both frames. In this regard the scheme is equivalent to that described by Camilo et al. (2000a).

2.5 Periodicity Search

The periodicity search software of the Southern 70-cm Survey (Manchester et al. 1996) was used as a starting point since it incorporated a thorough search with good handling of interference. The process was extensively modified to handle the requirements of the searches described in later chapters.

The task was divided into sub-cubes in acceleration–DM space and processed (if necessary) in parallel on $\sim$ dozens of Compaq Alpha 500 MHz EV6 supercomputer nodes. For each trial acceleration–DM pair a time series was produced by the slave from a DM group it was sent. A running average of $\sim$ 1 s was subtracted from the data to remove the effects of gain variations and interference. The time series was Fourier transformed using an FFT and a power spectrum formed.

In the case of a periodic signal with a frequency on the boundary between two FFT bins, the result is the spreading of the power across both bins with half a turn of phase difference between the complex co-efficients. Such signals were searched for by computing the complex difference between each bin and each of its neighbours and using half the squared values of the results as alternative estimates of the spectral power in the bin. The maximum of the these values and the power of the bin on its own was used to compute the value in the "power" spectrum that resulted. This power spectrum was then smoothed through division by a running average to remove the large bias towards red noise that is generally observed. This normalised the spectrum to a "floor" at unity, with higher values representing signal-to-noise ratios.

The spectrum at zero dispersion measure and acceleration was searched first for spikes within a pre-defined set of interference (**"birdie"**) frequencies. Some of these

may have come from a pre-processing search for signals occurring across many parts of the sky (see below). All subsequent spectra were zeroed in the bins corresponding to the occurrence of the birdies at zero DM.

All spectra were then repeatedly "folded" in such a way as to store in each bin the sum of values in lower-frequency bins for which the present bin comprises the 2nd, 4th, 8th, or 16th harmonic. In this manner sensitivity was maintained to signals with narrow duty cycles and correspondingly large numbers of harmonics. All peaks in the resulting spectra above a certain threshold were saved and returned to the master process. After all DMs and accelerations were processed, the detections were collated into "suspects" of similar pulse period (occurring at multiple DMs and accelerations). The suspects were then subject to a fine search in period and DM space and information about the suspects was saved to disk for later scrutiny.

2.6 Interference Mitigation

2.6.1 Narrow-band Signals

In modern radio astronomy it is virtually impossible to record pure, clean astrophysical radio noise: it is always contaminated with terrestrial interference. For pulsar searching, modulated interference is the most troublesome for it gives rise to scores of potential pulsar candidates. Hence it is vital to reject as many spurious signals as possible without harming sensitivity to real pulsars.

The first step used in the searches described in this thesis was to independently Fourier analyse each filter channel for modulated signals. Channels were then repeatedly summed in pairs to detect signals of a range of bandwidths. This was performed after filterbank formation but before de-dispersion. Figure 2.2 shows a beam contaminated with a number of strongly modulated narrow-band signals. When such signals are strong enough to produce strong periodicities in the de-dispersed time series, removing them by zeroing ("zapping") the few channels in which they appear is the best course of action. Since sensitivity to pulsars is proportional only to the square root of the bandwidth, zapping a few channels barely hurts sensitivity while strongly rejecting interference before it can cause problems further in the processing chain. Since pulsars are generally observed as broad-band sources, selecting only very strong and narrow signals at this step prevents the spurious rejection of pulsars. Automated software detected the strongest narrow signals and zeroed the

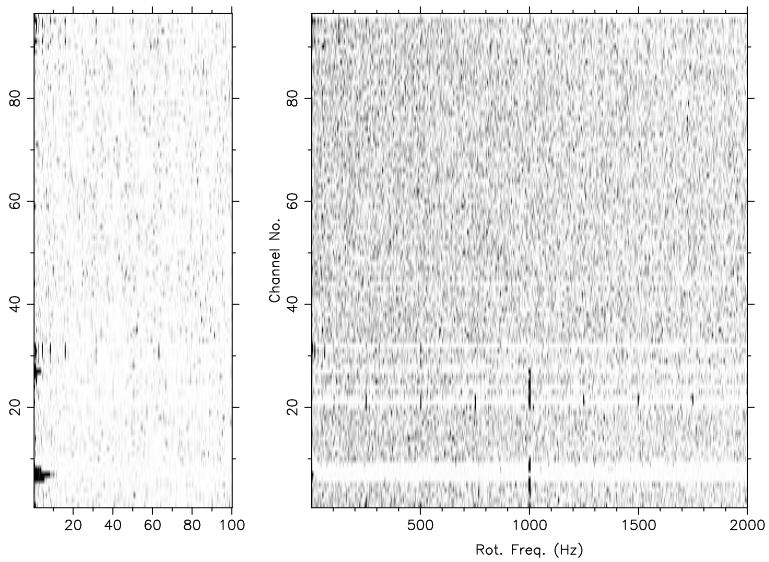

Figure 2.2: Power modulation spectra of filterbank channels for a sample data file from the multibeam system. Several channels are contaminated with strong low frequency noise, channel 21 contains a 250 Hz signal with harmonics and channels 29–32 suffer from the "sampler birdie" (§ 2.6.2).

corresponding channels. For the multibeam survey, local digital telecommunications services always produced strong quasi-periodic modulation in channels 6–8 so the zapping of these channels was hard-coded.

2.6.2 Persistent Broad-Band Signals

For broad band signals it is more difficult to separate pulsars from interference. One strategy is to rely on the fact that interference signals generally persist for minutes to hours, whilst pulsars should only be detectable in a handful of beams around the pulsar position. For this reason, the processing of the Southern 70-cm Survey (Manchester et al. 1996) incorporated a search for persistent periodicities in few-hour segments of data. I adapted this approach for the multibeam survey (Chapter 5) by examining the data in sets of six pointings, treated as $6 \times 13 = 78$ independent beams spanning around 30 minutes of telescope time.

Filterbank channels in each beam were summed (at zero dispersion measure) across the band, and the power spectrum of the time series was searched for harmonic signals as in § 2.5. Figure 2.3 shows the result of this procedure on some survey data containing, among other things, the ubiquitous "sampler birdie" of the multibeam system. This signal is induced by a counter in the sampler, producing

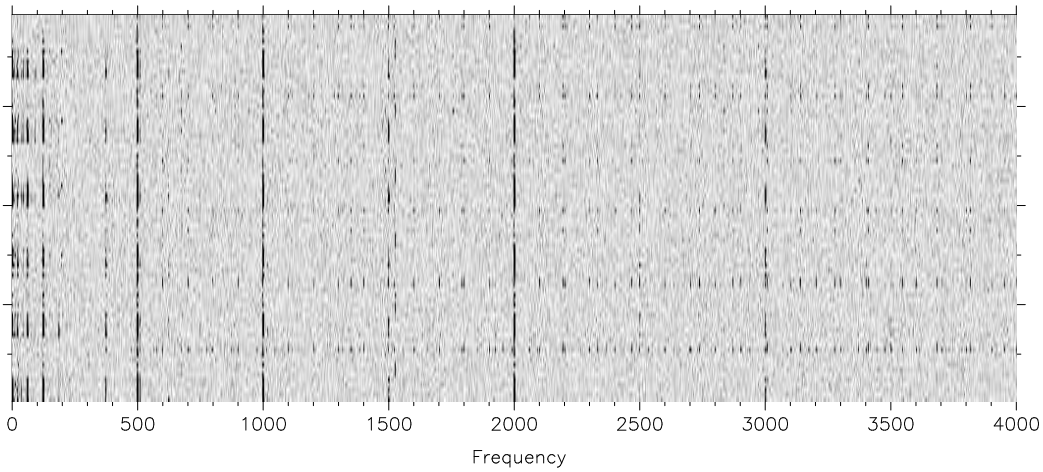

Figure 2.3: Power modulation spectra of full-band time series for six pointings (78 beams) of the multibeam system. Each horizontal line in the greyscale plot represents a spectrum from one beam of one pointing. Most prevalent is the "sampler birdie" at 2^{-n} multiples of the sampling frequency (8000 Hz).

self-similar saw-tooth shaped waveform with Fourier components with a 2^n frequency dependence where n is an integer harmonic index. Periodicities that appeared in a large number of beams in a small frequency range were logged in a file which was consulted by the periodicity search software when beams from this group were searched. These signals, if present in the zero-DM time series, were then excised from the power spectrum before other spikes were detected. The output "filters" from the interference analysis can be rather wide in order to accommodate interference signals with slowly varying frequency. To prevent the loss of pulsars in a potentially significant proportion of the spectrum to be zapped, in each beam only spectral channels which actually contained a strong signal were zeroed.

Certain modulations are ubiquitous in any search data. Most common is the 50 Hz mains power modulation. Also very common in multibeam data is the "sampler birdie" (above), and inter-modulation products from the mixing of unidentified 100 Hz and harmonically rich 135 Hz site-generated interference also cause large numbers of spurious periodicities. For the 50 Hz signal a relatively broad window was searched for the spike corresponding to the actual mains frequency at observing time, and only the narrow range of frequency bins actually traversed in each observation was ignored by the search software. Other signals such as the sampler birdie and the $100 \otimes 135$ Hz encompassed a large number of harmonics however the coherence of the signals generally meant only a single bin for each harmonic needed to be zapped at this stage. Filters for these common birdies were hard-coded to

ensure that they were always ignored.

2.7 Suspect Scrutiny

The final factor in the sensitivity of a survey is the scrutiny exercised by the person viewing the suspects produced by the search code. When large numbers of suspects are to be scrutinised, as is the case in a large scale survey, ample diagnostic information aids rapid discrimination between pulsars and interference signals. Interference signals may outnumber pulsar signals by factors of thousands or more. Pulsar signals can be determined by their characteristic signatures in plots of pulse profiles, DM vs S/N, acceleration vs S/N and in greyscales of S/N in time/phase, sub-band/phase and P/DM space. Sample output pages for a pulsar and an interference signal are shown in Figures 2.4 & 2.5. For globular cluster searching the number of suspects is small enough that all can by scrutinised by eye. For large scale surveys such as the intermediate latitude survey efforts must be made to reduce the number of spurious interference signals to be viewed.

My first approach was to use the scheme employed in the 70 cm survey of Manchester et al. (1996), whereby suspects from $\sim$8 h of observing were viewed at once, after the removal of suspects of similar periods occurring over many beams. This method must be used with care when large numbers of spurious signals are present, since large portions of the fluctuation spectrum can be censored in this case. I therefore required that any signals to be excluded must be present hundreds of times, rather than six times as used in earlier surveys. This provided some measure of viewer relief and only cost a small portion of the spectrum. All remaining suspects with signal-to-noise ratios greater than 8 were scrutinised by eye, a process prone to human error due to the huge numbers ($\sim 300,000$) of suspects to be viewed.

To provide a more complete sample whilst quantifying selection effects and reducing the scope for human error, new software for "gleaning" pulsars from large sets of candidates was developed. This allowed graphical exploration of the distributions of various parameters of the candidates by means of scatter plots, and group selection and deletion by boolean parameter conditions. Figure 2.6 shows a typical scatter plot of candidates from the intermediate latitude survey (Chapter 5), indicating the clustering of suspects around interference periods, and the large number of suspects with S/N < 9. Large sets of macros were built to filter out interference

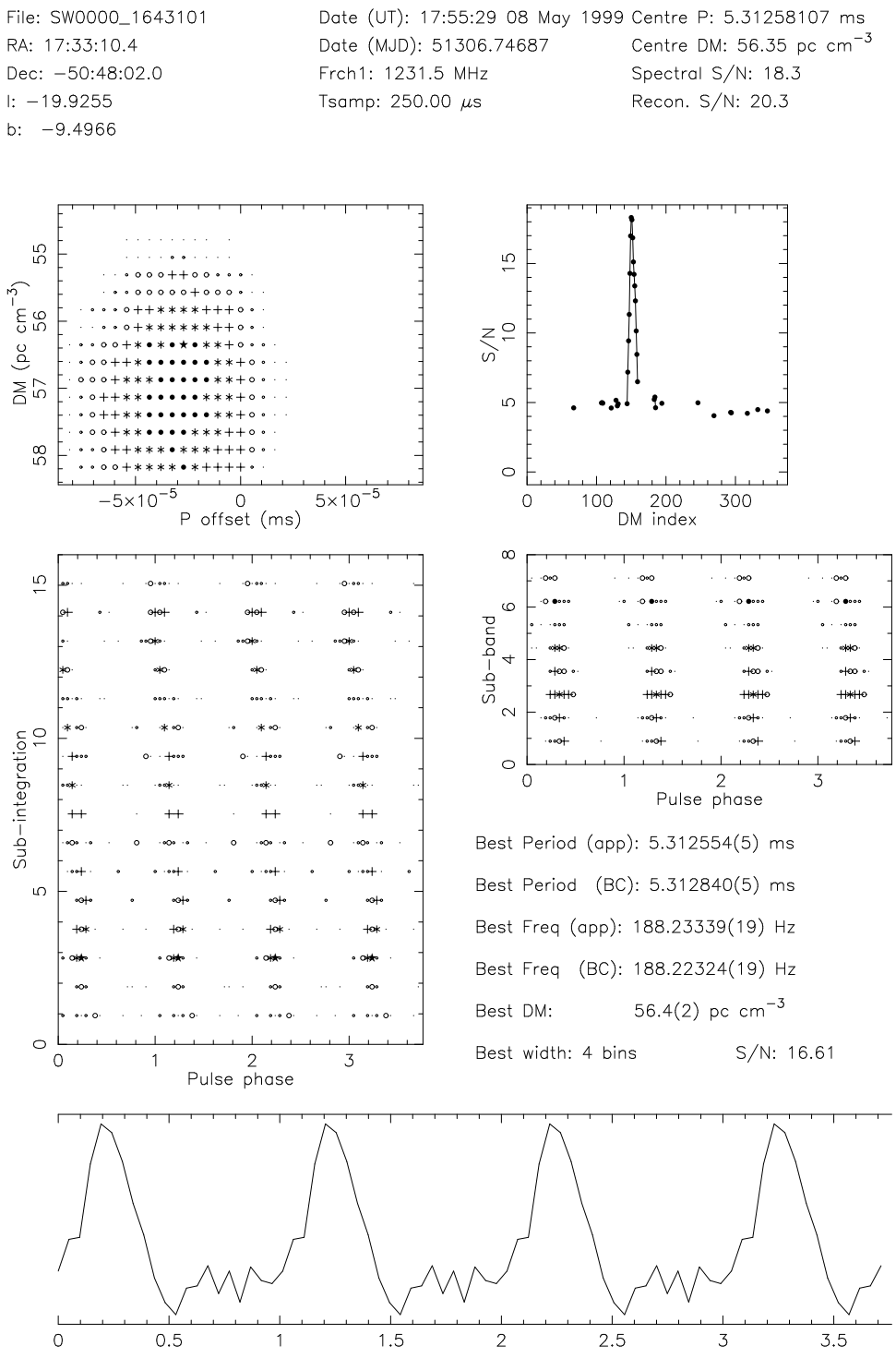

Figure 2.4: Suspect scrutiny plot showing discovery observation of J1732–5049.

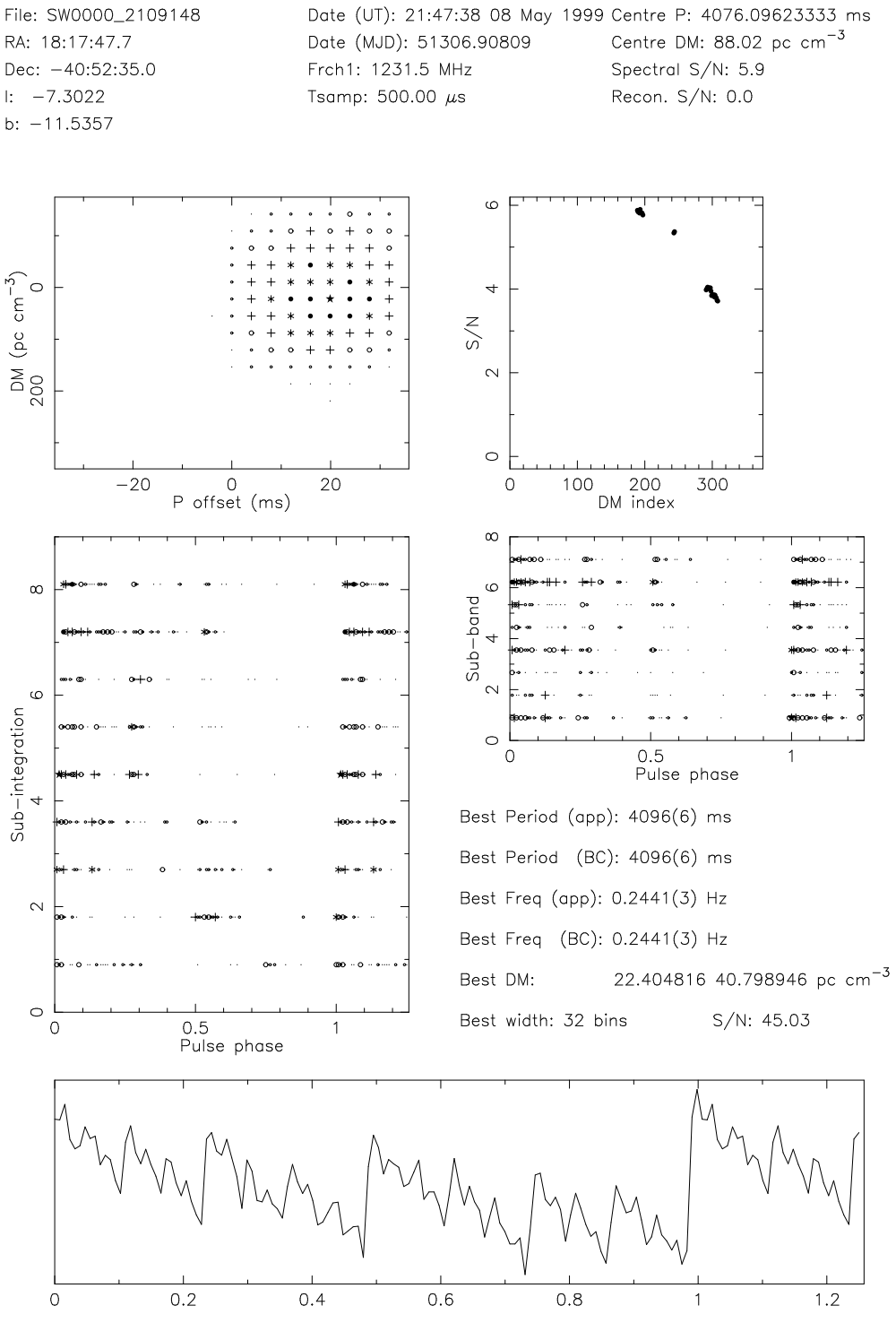

Figure 2.5: Suspect scrutiny plot of "sampler birdie" signal as candidate pulsar.

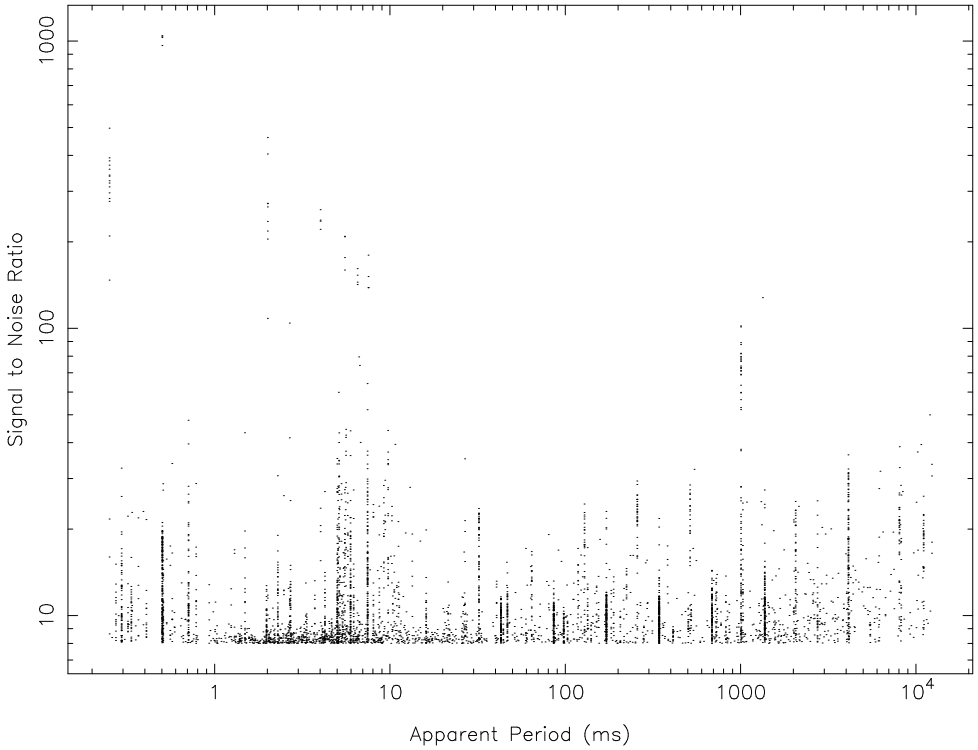

Figure 2.6: Example scatter-plot from the glean software package. The axes are apparent period and S/N. Apparent is the strong clustering around interference periods, and the large number of candidates with S/N < 9.

suspects when possible based on the presence of a period in a given narrow range, and on other criteria such as pulse width when applicable. Large numbers of candidates have best fit dispersion measures near zero since they are of terrestrial origin. Based on their distribution in a scatter plot of pulse period versus fractional error in dispersion measure, large numbers of such candidates were excluded. On the remaining suspects global signal-to-noise ratio cuttoffs were placed at 9 or 9.5 for signals with $P < 20$ ms. These three techniques in relatively equal measure resulted in a huge reduction in the number of candidates, in many cases by a factor of 30 or more from the raw 8-sigma sample. The revised scrutiny scheme was applied to the suspects from the intermediate latitude survey and resulted in the discovery of 11 additional pulsars (in addition to re-discovering the 58 pulsars originally found).

Suspect pulsars which survived through all phases of interference excision and passed human scrutiny were selected for re-observation with the telescope. If the

signal was detected again, usually months after the first detection, and was not detected in data taken "off-source", the object was likely a pulsar and a program of pulse timing was undertaken.

Chapter 3

Intermediate Latitude Survey: Relativistic Neutron Star–White Dwarf Binaries

This Chapter was published in The Astrophysical Journal *Letters* as Edwards & Bailes 2001, "Discovery of Two Relativistic Neutron Star–White Dwarf Binaries", ApJ, 547, L37 (Edwards & Bailes 2001b). Minor alterations for consistency of style have been made.

Abstract

We have discovered two recycled pulsars in relativistic orbits as part of the first high-frequency survey of intermediate Galactic latitudes. PSR J1157–5112 is a 44 ms pulsar and the first recycled pulsar with an ultra-massive ($M > 1.14$ M$_\odot$) white dwarf companion. Millisecond pulsar J1757–5322 is a relativistic circular-orbit system which will coalesce due to the emission of gravitational radiation in less than 9.5 Gyr. Of the ∼40 known circular orbit pulsars, J1757–5322 and J1157–5112 have the highest projected orbital velocities. There are now three local neutron-star/white-dwarf binaries that will coalesce in less than a Hubble time, implying a large coalescence rate for these objects in the local Universe. Systems such as J1141–6545 (Kaspi et al. 2000b) are potential gamma-ray burst progenitors and dominate the coalescence rate, whilst lighter systems make excellent progenitors of millisecond pulsars with planetary or ultra-low mass companions.

3.1 Introduction

The first surveys of the Galactic plane at high frequencies for radio pulsars (Clifton & Lyne 1986; Johnston et al. 1992a) uncovered a much younger and more distant population than the traditional 400 MHz surveys. High frequency surveys are much less affected by the deleterious effects of scatter-broadening and dispersion smearing which make short period pulsars impossible to detect at large dispersion measures. Unfortunately, the sampling rates employed in these early surveys limited their sensitivity to millisecond pulsars (MSPs) (Johnston & Bailes 1991), and the spatial coverage was limited by the small beam of a radio telescope at high frequencies. No millisecond pulsars were discovered in these early high-frequency surveys. It was widely believed (Foster, Fairhead & Backer 1991) that MSPs were steep-spectrum objects, and that there was little point in searching for them at high frequencies. As the population of MSPs became larger however, a series of spectral studies (Lorimer et al. 1995; Toscano et al. 1998) provided evidence that spectra of millisecond pulsars were not too dissimilar from that of normal pulsars. In a simulation of the Galactic millisecond pulsar population, Toscano et al. (1998) predicted that high frequency surveys undertaken with the Parkes multibeam system (Staveley-Smith et al. 1996) should detect a large number of millisecond pulsars. Motivated by this study we have conducted the first large-scale survey for millisecond pulsars at intermediate Galactic latitudes.

Our survey covered the region enclosed by $5^\circ < |b| < 15^\circ$ and $-100^\circ < l < 50^\circ$. Pointed observations of 265 seconds were made with the 64-m Parkes radiotelescope using the 21-cm multibeam receiver. The receiver consists of thirteen dual linear polarization feeds arranged in a sparse focal-plane pattern which allows full sky coverage with beams overlapping at the half-power points. This increases the rate of sky coverage by a factor of thirteen over a single-beam receiver and enabled us to conduct a large-scale survey in only 14 days of integration time. The system is sensitive to frequencies from 1230 MHz to 1530 MHz, with an average total system noise temperature of 24 K. The backend system was built at Jodrell Bank for the ongoing deep Galactic plane multibeam pulsar survey (Lyne et al. 2000a). It includes twenty-six filterbanks, each with ninety-six channels and total bandwidth of 288 MHz, centred at a sky frequency of 1374 MHz. Filterbank outputs were summed in polarisation pairs and one-bit digitised with an integration time of 125 μs. The large bandwidth, narrow channels, fast sampling, low system temperature

and multiple beams facilitiated the discovery of a large number of pulsars, including millisecond pulsars, with greater time efficiency than any previous large survey. Data were recorded on magnetic tape for offline processing on the Swinburne supercluster, a network of 64 Compaq Alpha workstations, using standard techniques (Manchester et al. 1996).

The survey is now complete. Full details of the survey are available in Chapter 5. In all, we have discovered 58 new pulsars, of which one has a period of 44 ms and seven others have periods less than 20 milliseconds. In this *Letter* we will discuss the two recycled pulsars for which we have phase-connected solutions, PSRs J1157–5112 and J1757–5322.

3.2 PSR J1157–5112 — Ultramassive Companion

PSR J1157–5112 is a 44 ms pulsar in a 3.5 d circular orbit, discovered in an observation made on 1999 Jan 19th. Its parameters, derived from pulse time-of-arrival analysis, are listed in Table 3.1. The pulsar's relatively short pulse period, small spin-down rate and circular orbit indicate recycling in a binary from an evolved companion (van den Heuvel 1984). If the companion formed a neutron star after recycling the pulsar, we would expect an eccentric orbit due to the sudden mass loss associated with the neutron star's production. The circularity of the orbit implies that the companion is a white dwarf. Since observed neutron star masses are consistent with a Gaussian distribution with a standard deviation of just 0.04 $M_\odot$ around the mean of 1.35 $M_\odot$ (Thorsett & Chakrabarty 1999), a conservative lower limit on the mass of the companion white dwarf can be obtained by assuming a 1.27 $M_\odot$ pulsar and an edge-on orbit. This means that $M_{\rm WD} > 1.14$ $M_\odot$, indicating an "ultra-massive" ONeMg degenerate, and could easily be near the Chandrasekhar limit if the orbit is near the median inclination angle of binaries. By similar reasoning, if the white dwarf mass is less than 1.35 $M_\odot$, the pulsar mass is at most 1.75 $M_\odot$.

A number of ultra-massive white dwarf systems are now known. The largest sample are those that have been discovered in recent X-ray and extreme ultraviolet observations (Bergeron, Saffer & Liebert 1992; Vennes et al. 1997), the masses of which are estimated from model-dependent spectroscopic measurements. The companion to PSR J1157–5112 is the first ultra-massive white dwarf to have a

Table 3.1: Astrometric, Spin, Binary and Derived Parameters

	J1157–5114	J1756–5322
Right ascension, α (J2000.0).....	$11^h57^m08^s.166(1)$	$17^h57^m15^s.1618(4)$
Declination, δ (J2000.0)	-51°12′56″.14(3)	-53°22′26″.38(1)
Pulse period, P (ms)	43.58922706284(12)	8.86961227275(4)
P epoch (MJD)	51400.000000	51570.000000
Period derivative, $\dot{P}$ (10^{-20})	14.6(16)	2.78(15)
Dispersion Measure (pc cm^{-3}).....	39.67(3)	30.793(4)
Orbital Period, $P_{\rm orb}$ (d)	3.50738639(3)	0.4533112382(7)
Projected semi-major axis, $a \sin i$ (lt-s) .	14.28634(3)	2.086526(5)
Epoch of Ascending Node, $T_{\rm asc}$ (MJD)..	51216.4442642(14)	51394.1080692(3)
$e \cos\omega$ [a]	-0.000322(4)	$-1.0(40)\times10^{-6}$
$e \sin\omega$	0.000240(4)	$4.3(45)\times10^{-6}$
Derived Parameters		
Longitude of periastron, ω (°)	306.7(6)	347(58)
Orbital eccentricity, e	$4.02(4)\times10^{-4}$	$4.4(45)\times10^{-6}$
Companion mass, $M_{\rm WD}$ ($M_\odot$)	>1.14	>0.55
Characteristic age, τ_c (Gyr)	4.70	5.04
Surface magnetic field, $B_{\rm surf}$ (10^8 Gauss)	25.55	5.02

[a] – We used the ELL1 binary timing model of TEMPO (Wex, unpublished). To avoid the large covariance between the time of periastron (T_0) and ω for $e \ll 1$, the time of ascending node ($T_{\rm asc}$) and the Laplace parameters $e\cos\omega$ and $e\sin\omega$ are used instead.

Values in parentheses apply to the final digit of the value and represent twice the formal uncertainties produced by TEMPO after scaling TOA uncertainties to achieve a reduced χ^2 of unity.

firm lower mass limit which relies only on the narrow band of observed neutron star masses and Newtonian physics. Steller mergers have been suggested for the formation of ultra-massive white dwarfs, however it is clear from the maintenance of a binary association that this is not the case with the companion of PSR J1157–5112, which must have resulted from largely standard stellar evolution.

PSR J1157–5112 is the latest example of a pulsar system that possesses a very massive white dwarf companion. Recent optical observations of the eccentric binary pulsar B2303+46 have indicated that a faint object consistent with a white dwarf is coincident with the position of the pulsar (van Kerkwijk & Kulkarni 1999). If this proves to be a genuine association, the periastron advance and mass function limit the companion mass to greater than 1.2 $M_\odot$. The newly discovered pulsar binary J1141–6545 (Kaspi et al. 2000b), with a minimum companion mass of 0.95 $M_\odot$

is probably also a white dwarf (Kaspi et al. 2000b; Tauris & Sennels 2000). The orbits of these systems are highly eccentric and thus it is believed that the neutron stars were born *after* their white dwarf companions. Since the pulsar in the PSR J1157–5112 binary is recycled, it is the first example of an ultra-massive white dwarf that was formed after the neutron star.

The high mass ratio between any possible progenitor to the white dwarf and the pulsar must have resulted in a phase of unstable mass transfer. The system probably passed through a common envelope phase when the white dwarf progenitor was on the asymptotic giant branch (AGB), as suggested by van den Heuvel (1994) for the PSR J2145–0750 system. Recent models (Ritossa, García-Berro & Iben 1999) indicate that main sequence stars as massive as 11 $M_\odot$ can avoid core collapse on the AGB to produce ultra-massive white dwarfs ($M_{\rm WD} = 1.37$ $M_\odot$ in the above case). Given that envelope loss in the common envelope phase reduces the resultant remnant mass from a donor star of given mass (Iben & Tutukov 1993), we expect that the progenitor to the white dwarf companion of PSR J1157–5112 weighed in excess of 10 $M_\odot$. This would mean that the companion's radius (Ritossa, García-Berro & Iben 1996; García-Berro, Ritossa & Iben 1997; Iben, Ritossa & García-Berro 1997; Ritossa, García-Berro & Iben 1999) was < 800 $R_\odot$ at the time of Roche lobe overflow. The orbital energy lost during spiral-in to the current orbit was insufficient to expel the envelope of the companion, without an additional energy source such as an accreting neutron star. Future proper motion measurements will help constrain models for its evolution. For an 11 $M_\odot$ companion with a pre-CE Roche lobe radius > 500 $R_\odot$ (requiring that at most 7/8 of the envelope ejection energy comes from non-orbital sources), the kick velocity of the pulsar birth event must have been < 120 km s^{-1} for the system to have remained bound. On the other hand, if the system was much closer at the time of explosion much greater kicks could be accommodated and we might expect the system to have a very large runaway velocity (Bailes 1989).

Along with J1757–5322 (below), J1157–5112 brings the total number of intermediate mass binary pulsars (those with white dwarf companions heavier than 0.6 $M_\odot$) (Arzoumanian, Cordes & Wasserman 1999; Tauris & Savonije 1999; Camilo et al. 1996) to seven. The companion of PSR J1157–5112 is by far the most massive of the class. That the neutron star survived what seems to have been a common envelope phase with a massive AGB star strongly supports the case against black hole formation via hypercritical accretion (Armitage & Livio 2000).

3.3 PSR J1757–5322 – Coalescing Binary

PSR J1757–5322 is an 8.9 ms pulsar which was discovered in an observation made on 1999 May 8th, at an epoch where the orbital acceleration experienced by the pulsar ($\sim$7.5 km s^{-2} in the line-of-sight) resulted in noticable period evolution in the 265-s integration. Subsequent observations revealed the pulsar to be in a nearly circular 11-h orbit with a companion of at least 0.55 $M_\odot$. A phase coherent timing solution has been obtained, the parameters of which are listed in Table 3.1. From similar reasoning to that invoked above for J1157–5112, we expect that the companion is a white dwarf. Its parameters are compatible with the common envelope model discussed above for the intermediate mass binary pulsars.

The J1757–5322 system is highly relativistic, having the highest orbital velocity of all circular orbit binaries (followed by J1157–5112). The near-circularity of the orbit reduces the measurability of relativistic effects, however some effects could be measurable in the coming decades with long timing baselines. Specifically, assuming an inclination angle $i = 60°$ (the median value for randomly oriented orbits), General Relativity predicts that the periastron of J1757–5322 is advancing at a rate of $\sim 1\overset{\circ}{.}2$ yr^{-1}, that its orbital period is decreasing by 1.8 μs yr^{-1}, that the pulsar's spin axis is precessing an entire turn every 1700 yr and that the system will coalesce in at most 9.5 Gyr due to the emission of gravitational waves. The Shapiro delays due to space-time curvature around the companion (for $i = 60°$) are 29 μs and 13 μs peak-to-peak respectively for PSR J1157–5112 and PSR J1757–5322, and may be considerably longer if the systems are nearly edge-on to the line of sight.

After about 7.6 Gyr the orbital period of J1757–5322 will have decreased to one-third its current value, resulting in four times the orbital acceleration. Such a system, if observed in our survey would have experienced significant signal-to-noise ratio loss, limiting the chance of detection. However, such a system will only live for $\sim$400 Myr, as compared to $\sim$8 Gyr for the preceding less accelerated post-CE evolution phase in which J1757–5322 was detected. Such highly accelerated systems are thus likely to be an order of magnitude lower in detectable population.

The companion of J1757–5322 will fill its shrinking Roche lobe when it has an orbital period of $\sim$50 s. The range of potential outcomes of this is diverse and interesting. Models suggest that after a period of mass transfer, the white dwarf will tidally disrupt and form an accretion disk around the pulsar in just a few seconds if the companion mass is greater than about 0.7 $M_\odot$ (van den Heuvel & Bonsema 1984).

The rapid mass transfer will result in an enormous release of energy, potentially in the form of a gamma-ray burst. However, it is not clear whether or not the accretion luminosity would be self-limiting due to the outward radiation pressure inhibiting mass transfer (Fryer et al. 1999). If there is no remnant of the white dwarf we might expect a solitary millisecond pulsar with a very rapid rotation rate (van den Heuvel & Bonsema 1984) (possibly like PSR B1937+21) and bigger than average mass. Alternatively it may be that the mass of the pulsar is driven over the critical limit for neutron stars and becomes a black hole. If the disk surrounding the neutron star is not completely destroyed the formation of a planetary system around a millisecond pulsar is not unreasonable, similar to PSR B1257+12. On the other hand if just 5% of the mass of the white dwarf is retained intact, a short-period eclipsing pulsar system such as PSR J2051–0827 may result. The measurement of the proper motion of the system is therefore vital in addressing these issues. A large velocity would provide a good match to the planet pulsar PSR B1257+12. A very small velocity is probably less conclusive.

The observed rate of gamma-ray bursts in the local Universe (Phinney 1991) is now broadly compatible with the expected coalescence rate of pulsar-white dwarf binary systems. There are now three such systems known that will coalesce in the lifetime of the universe. PSR J0751+1807 will coalesce in $\sim$7 Gyr. It is only 2 kpc away but has a light 0.15 $M_\odot$ companion that upon reaching its critical Roche lobe will undergo stable mass transfer to its much heavier pulsar companion, resulting in an ultra-compact X-ray binary (Ergma, Lundgren & Cordes 1977). PSR J1141–6545, as mentioned above, has a white dwarf companion of at least 0.95 $M_\odot$ in an eccentric orbit that will coalesce in only $\sim$1.3 Gyr, and is $\sim$3.2 kpc distant. It is a prime candidate for rapid mass transfer after the onset of Roche lobe overflow and a potential gamma-ray burst progenitor due to its high mass. The alarming thing about this pulsar is its youth. Its characteristic age is just 1 Myr and it may not pulse for much more than 10 Myr due to magnetic dipole breaking pushing it past the rotation limit for the emission of radio pulses. If we take the standard pulsar beaming fraction of $\sim$5, and the short lifetime of the binary in an observable state ($\sim$10 Myr) compared to the coalescence time (1.3 Gyr), the extrapolated Galactic coalescence rate for such objects is enormous! We could reasonably expect there to be $5 \times 1300/10 = 850$ dead white dwarf neutron star binaries within a few kpc of the Sun that will coalesce in less than a Hubble time. The total Galactic population would then be 1-2 orders of magnitude greater than this, and the coalescence rate

near 10^{-5} yr^{-1} per Galaxy, similar to that expected of double neutron star binaries, another candidate for gamma-ray bursts (Phinney 1991; Narayan, Paczyński & Piran 1992).

The contribution of PSR J1757–5322 to the inferred deathrate of white dwarf-neutron star binaries is much smaller. With the relative proximity ($\sim$2 kpc) but enormous characteristic age ($\sim$5 Gyr) of PSR J1757–5322, we might expect $\sim$250 similar coalescing systems in the Galaxy, with a coalescence rate of 5×10^{-8}yr^{-1} if we assume an evenly distributed disk population 15 kpc in radius. Hence there should be $\sim$500 systems in the Galaxy which have already coalesced, compatible with the observed population of Galactic disk pulsars with planetary or evaporating white dwarf remnant companions (three within 1.5 kpc).

The white dwarf companions of PSR J1157–5112 and PSR J1757–5322 are possibly observable with 10m class telescopes or HST. PSR B0655+64 ($M_{\rm WD} > 0.64$ M$_\odot$) has a timing age of 3.6 Gyr and a 22nd R-magnitude companion (Kulkarni 1986) at a distance of about 500 pc. The pulsars described here are probably 2-4 times as distant and of comparable timing ages so we might expect their companions to have R-magnitudes of 24-26. Detections of the companions to PSR J1757–5322 and PSR J1157–5112 will provide invaluable information about the cooling times of massive white dwarfs as the pulsars give an independent estimate of their age.

Chapter 4

Intermediate Latitude Survey: Recycled Pulsars

This Chapter has been accepted for publication in The Astrophysical Journal as Edwards & Bailes 2001, "Recycled Pulsars Discovered at High Radio Frequency", ApJ, in press astro-ph/0102026 (Edwards & Bailes 2001a). Minor alterations for consistency of style have been made.

Abstract

We present the timing parameters of nine pulsars discovered in a survey of intermediate Galactic latitudes at 1400 MHz with the Parkes radio telescope. Eight of these pulsars possess small pulse periods and period derivatives thought to be indicative of "recycling". Six of the pulsars are in circular binary systems, including two with relatively massive white dwarf companions. We discuss the implications of these new systems for theories of binary formation and evolution. One long-period pulsar (J1410–7404) has a moderately weak magnetic field and an exceedingly narrow average pulse profile, similar to other recycled pulsars.

4.1 Introduction

Since the early days of pulsar astronomy it has been known that radio pulsars are steep-spectrum objects (Comella et al. 1969). The majority of pulsar surveys were conducted at low frequency to exploit the higher flux and increased telescope beam

size made available. By the mid 1990s 70-cm surveys had resulted in the discovery of ∼700 pulsars, approximately 60 of which belonged to the class of "millisecond pulsars" (MSPs; $P \lesssim 25$ ms). However the elevated sky temperature and effects of interstellar dispersion, scatter-broadening and terrestrial interference present significant barriers to the discovery of pulsars, particularly MSPs, at low frequency. Early efforts at 20-cm surveys (Stokes et al. 1985; Clifton & Lyne 1986; Johnston et al. 1992a) were surprisingly successful in discovering large numbers of pulsars, however the time resolution afforded by the backend systems did not provide sufficient sensitivity to discover any MSPs. We have conducted a high frequency survey of intermediate Galactic latitudes with the new multibeam 21-cm receiver and pulsar backend at the Parkes radio telescope. The rapid sky coverage afforded by the multiple beams combined with improved backend hardware has enabled us to overcome the limitations of previous surveys and succeed in discovering a large number of millisecond pulsars. In this paper we discuss nine new low-magnetic-field pulsars found in this survey.

4.2 The Swinburne Intermediate Latitude Pulsar Survey

Over a period of 12 months from 1998 August - 1999 August, we conducted a pulsar survey with the 13-beam 21-cm "multibeam" receiver at the Parkes radio telescope (Staveley-Smith et al. 1996). The rapid sky coverage and high sensitivity of this system makes for a formidable survey instrument. Coupled with the thirteen 2×96-channel filterbanks covering 288 MHz each centred at a frequency of 1374 MHz, pulsars are being discovered at a rapid rate. The pulsar backend was originally built for an ongoing deep survey of the Galactic plane which is expected to almost double the known pulsar population (Lyne et al. 2000a; Camilo et al. 2000b). Based on Monte Carlo simulations similar to those discussed by Toscano et al. (1998), we found that 5–10 previously unknown millisecond pulsars ought to be detectable with unprecedented time efficiency in a shallower survey flanking the region of the Galactic plane survey. With the surfeit of computational power made available with the upgrade of the Swinburne supercomputer to 64 Compaq Alpha workstations, we chose to use half the sampling interval of the Galactic plane survey (that is, 125 μs vs. 250 μs) in the hope of discovering any nearby sub-millisecond pulsars. With 265-

s integrations covering the region enclosed by $5^\circ < |b| < 15^\circ$ and $-100^\circ < l < 50^\circ$ we completed the survey in 14 days of integration time and discovered ~ 70 pulsars[1] pulsars of which 8 show spin-down behavior consistent with recycling, confirming the predictions of the simulations. The survey was sensitive to slow and most millisecond pulsars with flux densities greater than approximately 0.3–1 mJy. Full details of the survey are available in Chapter 5.

4.3 New Recycled Pulsars

Pulsars discovered in the intermediate latitude survey were subjected to a campaign of pulsar timing observations to determine their astrometric, spin and orbital parameters. The center beam of the multibeam system was used to make observations of typically 250 seconds in length. The raw filterbank samples were folded offline at the topocentric pulse period to form integrated pulse profiles that were subsequently fitted to a "standard" profile to produce a nominal pulse time-of-arrival (TOA). These TOAs were then used to fit for the parameters of a standard timing model using the TEMPO software package[2] with the DE200 solar system ephemeris (Standish 1982). To avoid the high degree of covariance between the time of periastron and the longitude of periastron experienced with nearly circular binaries, we used the ELL1 binary timing model (Lange et al. 2001) which fits for the time of ascending node and the Laplace parameters $e\cos\omega$ and $e\sin\omega$ instead. In the absence of such covariance the uncertainty estimates of the ELL1 model are more reliable, however its result is subject to the assumption of a very small eccentricity. To check the validity of this assumption, particularly in the case of PSR J1157–5112 which has a large eccentricity compared to most white dwarf pulsar binaries, we have also fitted for the BT model (Blandford & Teukolsky 1976) and find the parameters consistent to better than 0.1σ. Due to its long orbital period, we have not yet been able to obtain a phase-connected solution for PSR J1618–39[3]; the parameters presented derive from analysis of secular variations in barycentric pulse period.

The parameters of nine newly discovered pulsars with small pulse periods and/or spin-down rates are listed in Table 4.1. Values in parentheses represent the error in the last quoted digit, calculated from twice the formal uncertainty produced by

[1]Some candidates are yet to be confirmed
[2]http://pulsar.princeton.edu/tempo
[3]The name of this pulsar may change when a better position measurement becomes available.

Table 4.1: Astrometric, Spin, Binary and Derived Parameters

	J1157–5112	J1410–7404	J1618–39
Right ascension, α (J2000.0)	$11^h57^m08\overset{s}{.}166(1)$	$14^h10^m07\overset{s}{.}370(5)$	$16^h18^m30(50)^s$
Declination, δ (J2000.0)	$-51°12'56\overset{''}{.}14(3)$	$-74°04'53\overset{''}{.}32(2)$	$-39°19(10)'$
Pulse period, P (ms)	43.58922706284(12)	278.7294436271(15)	11.987313(5)
P epoch (MJD)	51400.0	51460.0	...
Period derivative, $\dot{P}$ (10^{-20})	14.3(10)	674(9)	...
Dispersion Measure (pc cm^{-3})	39.67(4)	54.24(6)	117.5(4)
Orbital Period, $P_{\rm orb}$ (d)	3.50738640(3)	...	22.8(2)
Projected semi-major axis, $a \sin i$ (lt-s)	14.28634(3)	...	10.24(17)
Epoch of Ascending Node, $T_{\rm asc}$ (MJD)	51216.4442640(13)	...	51577.37(8)
$e \cos\omega$	$-0.000323(4)$	...	...
$e \sin\omega$	0.000240(4)	...	...
Span of timing data (MJD)	51197–51888	51309–51889	...
Weighted RMS timing residual (μs)	73	60	...
Pulse width at FWHM, w_{50} (°)	18	2.3	43
Pulse width at 10% peak, w_{10} (°)	33	4.5	...
Derived Parameters			
Longitude of periastron, ω (°)	306.6(6)	...	...
Orbital eccentricity, e	0.000402(4)	...	...
Minimum Companion mass, m_c ($M_\odot$)	1.18	...	0.18
Characteristic age, τ_c (Gyr)	4.8	0.65	...
Surface magnetic field, $B_{\rm surf}$ (10^8 Gauss)	25	440	...
Galactic longitude, l (°)	294.3	308.3	340.8
Galactic latitude, b (°)	10.75	-12.04	7.88
Distance, d (kpc)	1.9	2.1	4.8
Distance from Galactic plane, $\lvert z \rvert$ (kpc)	0.35	0.45	0.65

TEMPO. Dispersion measures were fit for with the inclusion of one or more TOAs produced from 660 MHz data, which in the absence of adequate signal to noise ratio were obtained by cross-correlation with the same template profile used for the high frequency TOAs. For this reason the errors quoted are probably underestimated. Also presented in the table are several derived quantities of interest, including the minimum companion mass for binary systems assuming a 1.35 $M_\odot$ companion (Thorsett & Chakrabarty 1999), the surface magnetic field strength assuming a dipole geometry (given by $B_{\rm surf} \simeq 3.2 \times 10^{19}$ Gauss $s^{-1/2}\sqrt{P\dot{P}}$), the "characteristic age" assuming magnetic dipole spin-down (with a braking index of 3) from a very fast initial rotation and the distance and Galactic z-height derived from the electron density model of Taylor & Cordes (1993) (accurate on average to around 30%). Average pulse profiles from these pulsars are provided in Figure 4.1. As is visible in the plot, PSR J1918–0642 possesses an interpulse which follows the main pulse by $\sim 190°$ with $\sim 15\%$ of its peak intensity. Apparent in the profile of PSR J1618–39 is a weak component leading the main pulse by $\sim 120°$ with $\sim 10\%$ of the peak intensity.

These systems are of particular interest because they most likely belong to the class of so-called "recycled" pulsars. In the standard model, the origin of the short spin period and low inferred magnetic field strength of these pulsars lies in an earlier

Table 4.1: *continued* — **Astrometric, Spin, Binary and Derived Parameters**

	J1629–6902	J1721–2457	J1745–0952
Right ascension, α (J2000.0)	$16^{\rm h}29^{\rm m}08\overset{\rm s}{.}7706(4)$	$17^{\rm h}21^{\rm m}05\overset{\rm s}{.}496(2)$	$17^{\rm h}45^{\rm m}09\overset{\rm s}{.}1400(9)$
Declination, δ (J2000.0)	$-69°02'45\overset{''}{.}294(3)$	$-24°57'06\overset{''}{.}1(4)$	$-09°52'39\overset{''}{.}67(5)$
Pulse period, P (ms)	6.0006034432179(19)	3.496633727625(7)	19.37630312709(3)
P epoch (MJD)	51600.0	51600.0	51500.0
Period derivative, $\dot{P}$ (10^{-20})	1.00(3)	0.59(10)	9.5(4)
Dispersion Measure (pc cm^{-3})	29.490(3)	47.758(19)	64.474(14)
Orbital Period, $P_{\rm orb}$ (d)	...	...	4.9434534(2)
Projected semi-major axis, $a \sin i$ (lt-s)	...	...	2.378615(17)
Epoch of Ascending Node, $T_{\rm asc}$ (MJD)	...	...	51270.674499(8)
$e \cos\omega$	...	...	$10.0(148)\times10^{-6}$
$e \sin\omega$	...	...	$1.5(16)\times10^{-5}$
Span of timing data (MJD)	51395–51889	51395–51889	51254–51889
Weighted RMS timing residual (μs)	7.3	56	72
Pulse width at FWHM, w_{50} (°)	24	95	33
Pulse width at 10% peak, w_{10} (°)	60	...	186
Derived Parameters			
Longitude of periastron, ω (°)	...	...	34(49)
Orbital eccentricity, e	...	...	$1.8(16)\times10^{-5}$
Minimum Companion mass, m_c ($M_\odot$)	...	...	0.11
Characteristic age, τ_c (Gyr)	9.5	9.4	3.2
Surface magnetic field, $B_{\rm surf}$ (10^8 Gauss)	2.5	1.5	13.8
Galactic longitude, l (°)	320.4	0.4	16.4
Galactic latitude, b (°)	−13.93	6.75	9.90
Distance, d (kpc)	1.4	1.6	2.4
Distance from Galactic plane, $\lvert z \rvert$ (kpc)	0.33	0.18	0.41

epoch of binary interaction (e.g. (Bhattacharya & van den Heuvel 1991)). Matter accreted from the companion simultaneously spins up the pulsar and dramatically attenuates its magnetic field. The resultant rapid rotation rate provides the required conditions for pair production (even with a "weak" magnetic field) and the pulsar, which had previously ceased to emit after spinning down below the critical rate, is recycled into a radio-loud short-period pulsar.

Of the pulsars listed in Table 4.1, three are isolated and six are members of binary systems. Of the six binaries, four are members of a large class of millisecond pulsars with low mass white dwarf companions (§ 4.4). The remaining two are orbiting massive white dwarfs (§ 4.5) in orbits sufficiently close that relativistic perturbations to the timing behavior should be measurable in a few years. PSR J1757–5322 in particular emits sufficient gravitational radiation that its orbit will decay to the point of coalescence within a Hubble time, with dramatic and unknown consequences (Edwards & Bailes 2001b). The systems were discovered with signal to noise ratios in the range of 12–45, implying flux densities of approximately 0.4–8 mJy and luminosities of 0.8–60 mJy kpc^2, comparable to those of previously known MSPs in the Galactic disk, although a thorough treatment must await calibrated flux density measurements.

Table 4.1: *continued* — **Astrometric, Spin, Binary and Derived Parameters**

	J1732–5049	J1757–5322	J1918–0642
Right ascension, α (J2000.0)	$17^h32^m47^s.7671(4)$	$17^h57^m15^s.1615(3)$	$19^h18^m48^s.0363(8)$
Declination, δ (J2000.0)	$-50°49'00''.11(1)$	$-53°22'26''.387(5)$	$-06°42'34''.80(5)$
Pulse period, P (ms)	5.312550204595(6)	8.869961227277(4)	7.645872761379(18)
P epoch (MJD)	51575.0	51570.0	51600.0
Period derivative, $\dot{P}$ (10^{-20})	1.38(9)	2.63(4)	2.4(3)
Dispersion Measure (pc cm^{-3})	56.839(9)	30.817(7)	26.595(17)
Orbital Period, $P_{\rm orb}$ (d)	5.26299721(6)	0.4533112381(5)	10.9131774(5)
Projected semi-major axis, $a \sin i$ (lt-s)	3.982868(5)	2.086527(5)	8.350489(16)
Epoch of Ascending Node, $T_{\rm asc}$ (MJD)	51396.3659935(12)	51394.1080693(3)	51569.117366(4)
$e \cos\omega$	$2.9(19)\times10^{-6}$	$-1.3(42)\times10^{-6}$	$-1.3(4)\times10^{-5}$
$e \sin\omega$	$-9.4(20)\times10^{-6}$	$3.8(44)\times10^{-6}$	$-1.8(4)\times10^{-5}$
Span of timing data (MJD)	51306–51889	51306–51889	51395–51889
Weighted RMS timing residual (μs)	17	21	40
Pulse width at FWHM, w_{50} (°)	58	17	35
Pulse width at 10% peak, w_{10} (°)	136	81	...
Derived Parameters			
Longitude of periastron, ω (°)	163(12)	341(61)	216(11)
Orbital eccentricity, e	$9.8(20)\times10^{-6}$	$4.0(44)\times10^{-6}$	$2.2(4)\times10^{-5}$
Minimum Companion mass, m_c ($M_\odot$)	0.18	0.56	0.24
Characteristic age, τ_c (Gyr)	6.1	5.3	5.0
Surface magnetic field, $B_{\rm surf}$ (10^8 Gauss)	2.8	4.9	4.3
Galactic longitude, l (°)	340.0	339.6	30.0
Galactic latitude, b (°)	−9.45	−13.98	−9.12
Distance, d (kpc)	1.8	1.4	1.4
Distance from Galactic plane, $\|z\|$ (kpc)	0.30	0.33	0.22

There does not seem to be any particular preference for high or low Galactic latitudes in the pulsars presented here. A Kolmogorov-Smirnov test on the seven new "millisecond" pulsars ($P < 20$ ms) indicates that the observed values of $|b|$ differ from a uniform distribution at a significance level of only 18%. Clearly a campaign to survey higher Galactic latitudes with the multibeam system would also be worthwhile in terms of millisecond pulsar discoveries. The dearth of MSPs found so far in the Galactic plane survey (Manchester et al. 2000) is puzzling in light of the lack of any indication of diminishing returns from our survey at smaller latitudes with the same observing system. Although we employ a higher sampling rate, the dispersion smearing induced by the filterbank channels is greater than two sample intervals for all new MSPs. In addition, it was discovered (after completion of the survey!) that the strength of a ubiquitous and problematic signal generated by the sampler is much reduced at slower sample rates.

4.4 The Formation of Low Mass Binary Pulsars

The newly discovered pulsar PSR J1618–39 lies in the middle of what previously appeared to be a "gap" (Camilo 1995) in the distribution of binary pulsar orbital

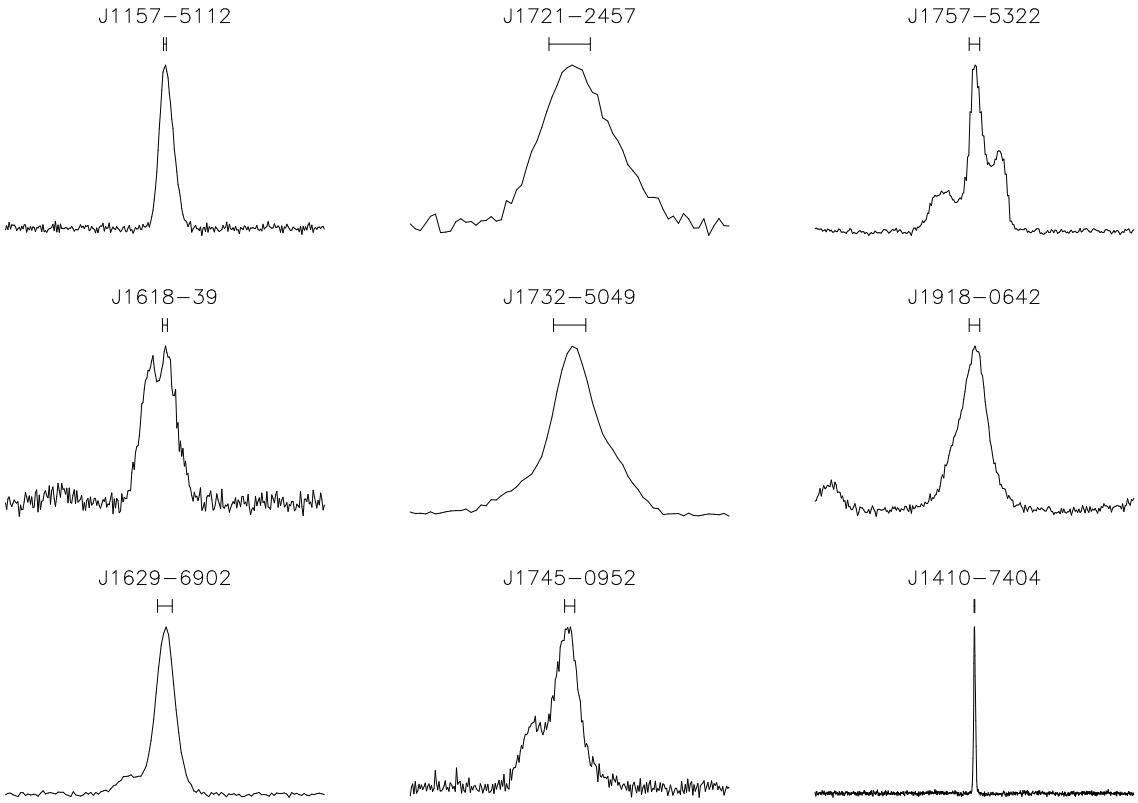

Figure 4.1: Average pulse profiles for the pulsars presented in this paper. These result from the summation of several observations using the system described in § 4.2 (except for the J1618–39 profile which arises from data taken with a $2 \times 512 \times 0.5$ MHz channel system at a center frequency of 1390 MHz). The vertical flux scale is arbitrary and normalised between pulsars. Horizontal bars represent the degree of time smearing induced by the differential dispersion delay within individual filterbank channels.

periods (see Figure 4.2). Whilst its spin-down rate has not been measured, only a recycled pulsar or a very young pulsar could exhibit such rapid rotation, and its large displacement from the Galactic plane (∼650 pc) rules out the latter option. Since it is recycled and its orbital parameters other than orbital period are typical of the low mass binary pulsars (LMBPs), we contend that the physics of the formation of LMBPs do not exclude such orbital periods. With the discovery of this pulsar and two (J1732–5049, J1918–0642), perhaps three (J1745–0952 appears to have an anomalously long rotation period; see § 4.5.1) other LMBPs, it is timely to reassess the standard model of their formation.

Briefly, the standard evolutionary scenario for LMBPs (see e.g. Phinney & Kulkarni 1994) is as follows: a pair of main-sequence stars (∼10 $M_\odot$ and ∼1 $M_\odot$ in mass respectively) are in a binary system. The (more massive) primary evolves to

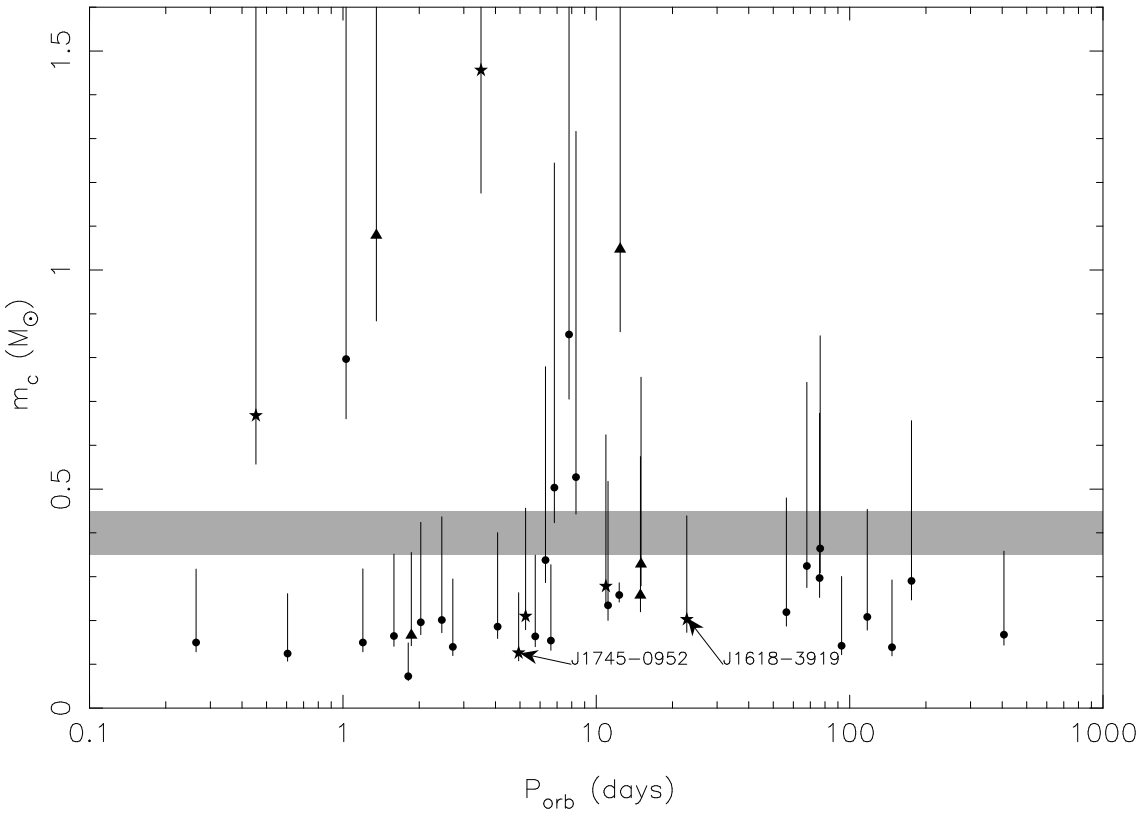

Figure 4.2: Distribution in orbital period and companion mass of known circular-orbit pulsars in the Galactic disk (excluding those with planets or evaporating companions). Points and upper and lower ends of error bars represent median, 90% upper limit and minimum companion masses assuming randomly inclined orbits and a 1.35 $M_\odot$ pulsar, with the exception of PSR B1855+09 which has much smaller errors resulting from a Shapiro delay measurement (Kaspi, Taylor & Ryba 1994). Stars, triangles and circles represent pulsars discovered in the intermediate latitude survey (this work), the Galactic plane survey (Camilo et al. 2001), and previously known systems respectively. The gray bar between 0.35–0.45 $M_\odot$ represents the transition from He to CO white dwarf companions.

fill its Roche lobe and begins unstable mass transfer in a common envelope (CE) phase. The envelope is eventually expelled, the remaining core of the primary collapses in a supernova and a pulsar is formed. The pulsar shines for several Myr, after which the pulsar has spun-down to the extent that radio emission ceases. The secondary eventually evolves to fill its Roche lobe, transferring matter (with angular momentum) to the neutron star, "recycling" it by spinning it up to millisecond periods where emission is once again possible (despite the accompanying large reduction in magnetic field strength). It is believed that the low mass X-ray binaries are in fact systems in this phase. For systems with orbital periods greater than 1–2

d at the beginning of this phase the orbit is expected to expand to a final period $\gtrsim$ 50 d due to the transfer of mass from a lighter secondary to a heavier primary. However, for closer initial orbits, angular momentum losses due to magnetic braking and gravitational radiation become important and the orbit will shrink during the mass transfer stage. Hence a "gap" in the orbital period distribution is expected from around this critical "bifurcation" period, $P_{\rm bif} \simeq 2$ d (e.g. Pylyser & Savonije 1988) to $\sim$50 d.

Figure 4.2 shows the distribution of orbital periods and companion masses for all known circular orbit pulsar binaries in the Galactic disk. There is arguably still an under-density of pulsars between 12 d $< P_{\rm orb} <$ 56 d, even including the newly discovered PSR J1618–39 and the 22.7-d low-mass binary PSR J1709+23 (Cadwell 1997) which is not depicted in Figure 4.2 due to the lack of a published mass function. We note that the discovery of just one system with $P_{\rm orb} \simeq 45$ d would be sufficient to remove the suggestion of an under-density, especially if the massive systems around $P_{\rm orb} = 10$ d are disregarded due to their probable different origin. Even if the under-density is real, the presence of significant numbers of systems between the bifurcation period and $P_{\rm orb} = 12$ d requires explanation. Tauris (1996) argues that systems with initial orbital periods only slightly longer than $P_{\rm bif}$ may experience moderate angular momentum losses that are sufficient to reduce the degree of spiral-out. To preserve the observed underdensity in this case one must require that the significance of the magnetised stellar wind is a sharp function of orbital separation, with the transition from moderate to insignificant magnetic braking occuring at some orbital period greater than $P_{\rm bif}$.

Two further models predict the presence of pulsars in the range 1 d $< P_{\rm orb} <$ 12 d. The first begins with a binary system consisting of a pulsar and a star on the red (or asymptotic) giant branch, and produces a recycled pulsar in a close binary via a common envelope spiral-in phase. The remnant companion is either a helium dwarf or, in the case of Roche lobe overflow on the asymptotic giant branch, a CO dwarf with $m_{\rm c} > 0.45$ M$_\odot$. Doubt has been cast over the plausibility of this model for many binary pulsars due to energy considerations (Taam, King & Ritter 2000), however for several pulsars such as the newly discovered PSR J1157–5112 it is the only feasible scenario (see § 4.5). An alternative model that may produce systems in the required orbital period range is that of "massive case A" or "early case B" mass transfer (Taam, King & Ritter 2000; Tauris, van den Heuvel & Savonije 2000). In this scenario a massive star on the late main sequence or early red giant branch

loses much of its envelope in a phase of highly super-Eddington mass transfer, and a common envelope phase is avoided due to the radiative envelope of the companion, which responds to mass loss by contracting. The end result is a CO white dwarf in excess of 0.35 $M_\odot$[4] in an orbit shorter than ∼70 d. This is the model favored by Taam, King & Ritter (2000), however it is clear from Figure 4.2 that most of the systems with 1 d $< P_{\rm orb} <$ 12 d must be lighter He dwarfs. We expect that to account for this high proportion of He dwarfs the standard LMBP model must be capable of producing some systems in this orbital period range, perhaps via the curtailment of spiral-out by moderate angular momentum losses (Tauris 1996).

4.5 Intermediate Mass Binary Pulsars

With the discovery of PSRs J1157–5112, J1757–5322 (Edwards & Bailes 2001b; this paper), J1435–6100 and J1454–5846 (Camilo et al. 2001), there are now eight recycled pulsars known to have heavy (CO or ONeMg) white dwarf companions (see Table 4.2). As mentioned in the previous section, there are two plausible scenarios for the formation of heavy white dwarfs in close orbits: massive late case A/early case B mass transfer (Tauris, van den Heuvel & Savonije 2000; Taam, King & Ritter 2000) or common envelope evolution on the first (Tauris 1996) or second (van den Heuvel 1994) ascent of the red giant branch. The first scenario is limited to systems with orbital periods greater than a few days (thus excluding J1757–5322, B0655+64, J1435–6100 and perhaps J1232–6501) and companions lighter than ∼0.9 $M_\odot$(thus excluding J1157–5112 and perhaps J1454–5846). The common envelope scenario is able to produce the systems excluded from the first scenario, albeit with some difficulty for J1157–5112. In the common envelope formalism of Webbink (1984), one requires $\eta\lambda > 2$ to reproduce the present orbital separation of the J1157–5112 system (where $\lambda \approx 0.5$ depends on the stellar density distribution and affects the estimate of its binding energy and η is the efficiency of use of orbital energy in envelope expulsion). In the absence of other plausible models, we must conclude for now that the system did evolve through a CE phase and that either additional energy sources are available ($\eta > 1$) or the binding energy of the stellar envelope is lower than is generally assumed. The latter option has some support from recent numerical studies (Dewi & Tauris 2000).

[4]In the work of Tauris, van den Heuvel & Savonije (2000) the scenario occasionally produces a ligher He dwarf.

Table 4.2: Possible Intermediate Mass Binary Pulsars

Name	P (ms)	$\dot{P}$	P_{orb} (d)	m_c^1 ($M_\odot$)	Ref
J0621+1002	28.85	3.5×10^{-20}	8.32	0.53	4
B0655+64	195.7	6.9×10^{-19}	1.03	0.78	1
J1022+1001	16.45	4.2×10^{-20}	7.81	0.85	4
J1157–5112	43.59	1.5×10^{-19}	3.51	1.47	6
J1232–6501	88.28	7.9×10^{-19}	1.86	0.17	5
J1435–6100	9.348	2.3×10^{-20}	1.35	1.08	5
J1454–5846	45.25	8.0×10^{-19}	12.42	1.05	5
J1603–7202	14.84	1.6×10^{-20}	6.31	0.34	3
J1745–0952	19.38	9.2×10^{-20}	4.94	0.126	7
J1757–5322	8.87	2.8×10^{-20}	0.45	0.67	6
J1810–2005	32.82	1.3×10^{-19}	15.01	0.33	5
J1904+0412	71.09	1.0×10^{-19}	14.93	0.26	5
J2145–0750	16.05	3.0×10^{-20}	6.84	0.50	2

[1] — Assuming an orbit inclined at 60° and a 1.35 $M_\odot$ pulsar

References: (1) Damashek, Taylor & Hulse 1978; (2) Bailes et al. 1994; (3) Lorimer et al. 1996 (4) Camilo et al. 1996; (5) Camilo et al. 2001; (6) Edwards & Bailes 2001b; (7) this work

Figure 4.3 shows a region of the P–$\dot{P}$ diagram for all presently known disk pulsars. With the recent discoveries made at Parkes the region between 10 and 100 ms is now well populated. We note that the positive correlation visible in the plot is simply a result of magnetic spin down over time scales necessarily shorter than the age of the Galaxy. It is clear that the standard assumption of relatively short initial spin period and magnetic dipole spindown with constant magnetic field strength is in error for the millisecond pulsars due to the anomalously large ages inferred, especially when kinematic contributions to the observed $\dot{P}$ are taken into account (e.g. Camilo, Thorsett & Kulkarni 1994). Indeed, even when the initial spin frequency is limited to that allowed in the standard spin-up scenario, little impact is made on the inferred ages. In Figure 4.3 we adopt a spin-up line defined by $\dot{P}_0 = 1.1 \times 10^{-15} \mathrm{s}^{-4/3} P_0^{4/3}$ (Arzoumanian, Cordes & Wasserman 1999) and show the predicted positions of pulsars immediately after spin-up, at 1 Gyr and at 20 Gyr. Also shown is a dashed line representing a "characteristic age" of 1 Gyr assuming $P_0 \ll P$, tracing virtually the same locus in the P–$\dot{P}$ diagram.

In the work of Arzoumanian, Cordes & Wasserman (1999), massive pulsar binaries were divided into two groups, the "B1913+16-like" systems and the "J0621+1002-

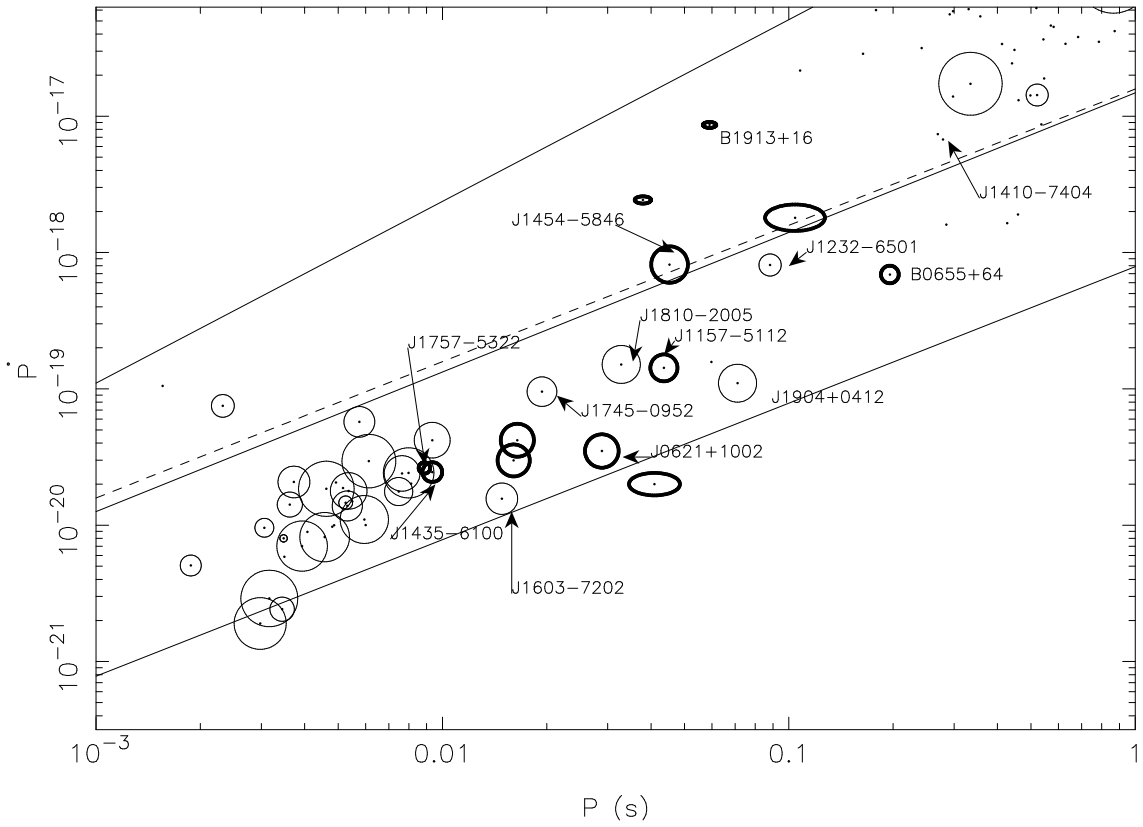

Figure 4.3: Distribution of known disk pulsars in the recycled region of the P-$\dot{P}$ plane (excluding systems with planets or evaporating companions). Solid lines represent (from top to bottom) the expected positions of pulsars at $t = 0$, 1 and 20 Gyr after spin-up to equilibrium with an Alfvén-terminated accretion disk. The dashed line depicts a line of constant "characteristic age" (i.e. assuming infinite initial spin frequency) at $\tau_c = 1$ Gyr. After Arzoumanian, Cordes & Wasserman (1999), points representing binary pulsars are enclosed by a circle with a radius proportional to $1+\log P_{orb}$ (d). Lines are bold in the case of massive companions, and elliptical in the case of eccentric binaries.

like" systems. These were distinguished by a tendency in the 0621 group for wider orbits and more complete recycling (i.e. smaller periods and particularly period derivatives). In the context of this scheme the newly discovered systems J1435–6100 and (especially) J1757–5322 are anomalous by virtue of their strongly recycled nature and close orbits.

4.5.1 Systems with Intermediate Spin Periods

In the past it seemed that nearly all LMBPs had $P < 10$ ms whilst all IMBPs had longer spin periods. It has been argued mainly on this basis (Tauris & Savonije 1999;

Arzoumanian, Cordes & Wasserman 1999) that PSR J1603–7202 ($P = 15$ ms) also possesses a CO companion in a relatively face-on orbit, hence its low mass function. The newly discovered moderately recycled pulsars J1810–2005, J1904+0412 and especially J1745–0952 and J1232–6501 also have small mass functions despite their relatively long spin periods, suggesting perhaps a similar interpretation. However with the discovery of IMBPs J1435–6100 and J1757–5322, both with $P \sim 9$ ms, it is clear that there is some overlap between LMBPs and IMBPs in P-$\dot{P}$ space and that assignments to either class based on these parameters are subject to significant uncertainty. In addition, it is quite unlikely *a priori* for this many systems to be as face on as is required to make them IMBPs: only around one in 20 pulsar binaries with 0.45 $M_\odot$ companions would be expected to have mass functions as low as those of J1745–0952 or J1232–6501.

If the newly discovered recycled systems with $P > 10$ ms and small mass functions are ordinary LMBPs that have evolved from LMXBs, it is difficult to see why only one of the previously known LMBPs rotated so slowly. The relative insensitivity of the multibeam backend to pulsars with $P \lesssim 10$ ms at dispersion measures typical of recycled pulsars discovered in the deep Galactic plane survey (~ 200 cm^{-3} kpc; Camilo et al. 2001) can account for some but probably not all of the high proportion of recent recycled discoveries with $P > 10$ ms. Indeed, it could be argued that the pulse periods of the four new low mass systems reported here are also anomalous, and for this sample dispersion smearing imposes no more of a selection effect than in the previous surveys that detected the known population. A Kolmogorov-Smirnov test finds their distribution different to that of previously known LMBPs with 91% significance, however with a sample size of four this conclusion should be taken with caution.

One possibility is that the long period systems evolved instead from massive late case A / early case B mass transfer (Tauris, van den Heuvel & Savonije 2000) resulting in a low mass He companion. Camilo et al. (2001) favor this interpretation and suggest that such systems were preferentially detected in the Galactic plane and intermediate latitude surveys due to the low scale height of this population in the Galactic disk. Whilst no conclusions should be drawn without full population modelling, in the work of Tauris, van den Heuvel & Savonije (2000) it seems that most systems produced by this channel ought to possess heavy CO companions. Since there are five known systems with $P > 10$ ms and small mass functions that one may suggest evolved through this channel, one would expect to have discovered

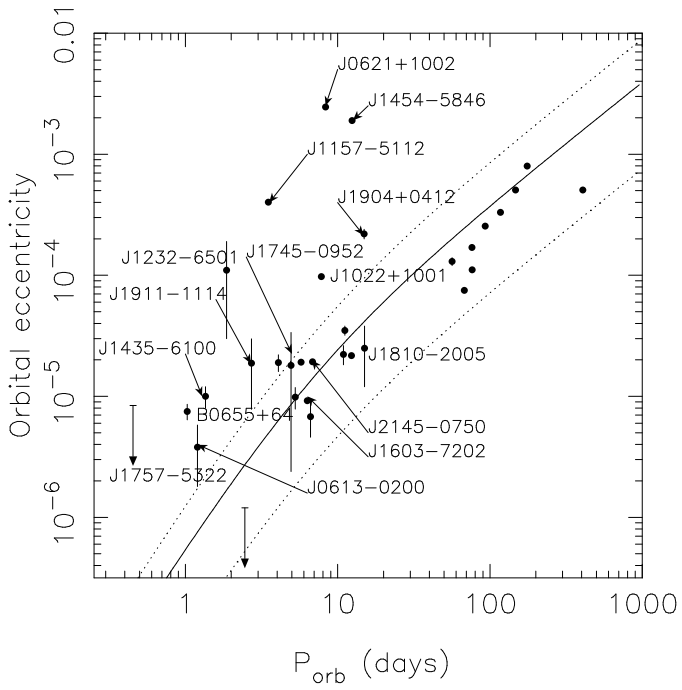

Figure 4.4: Orbital periods and eccentricities of circular pulsar binaries in the Galatic disk. The solid and upper and lower dashed curves represent the median and 95% upper and lower bounds respectively of an orbital period – eccentricity relation based on that of Phinney (1992), modified for applicability to all orbital periods (S. Phinney 2000 pers. comm.). Error bars in general represent twice the nominal uncertainty produced by TEMPO. It should be noted that the ordinate has a logarithmic scale and that larger error bounds would make some measurements consistent with zero.

many more than the four remaining known CO systems that are allowed by this scenario.

One may look to orbital eccentricities to resolve questions of evolutionary history, since in the absence of a final stage of stable mass transfer IMBPs are not expected to obey the LMBP orbital period – eccentricity relation of Phinney (1992) (Camilo et al. 1996). The situation has become more complicated (Figure 4.4) with updated measurements of previously known pulsars (Toscano et al. 1999) and newly discovered pulsars (this work; Camilo et al. 2001). Since PSR J2145–0750 has a minimum companion mass consistent with a CO companion in an orbit as circular as most LMBPs, we cannot take the similar eccentricities of PSRs J1603–7202, J1745–0952 and J1810–2005 as evidence against a massive companion. Likewise the probable high eccentricities (relative to the relation) of J0613–0200 and J1911–1114, pulsars which we have no reason to doubt are LMBPs, mean that we must be conservative in our interpretation of candidate IMBPs on the basis of large eccentricities, partic-

ularly at short orbital periods — a connection one might be tempted to make in the case of J1904+0412 and especially J1232–6501 due to their positions in Figures 4.3 and 4.4.

Optical identifications of large numbers of recycled pulsar companions would provide useful information about the statistical correlation between observable pulsar parameters and companion mass by means of temperature measurements in the context of white dwarf cooling models. The newly discovered systems add significantly to the sample potentially detectable with 8-m class telescopes.

4.6 PSR J1410–7404: Disrupted Binary?

As shown in Figure 4.1, the mean pulse profile of the newly discovered isolated pulsar J1410–7404 is extraordinarily narrow. Given its period of 279 ms, the pulse width – period relation of Rankin (1990) predicts a minimum width of 4.6° (FWHM), double the measured value of 2.3°. Rankin's model fits normal pulsars well and the only exceptions to it (more than a factor of few percent smaller than the predicted minimum) in the 688 published pulse widths recorded in our local pulsar catalogue are the recycled pulsars for which there appears to be no correlation between period and duty cycle (see also Kramer et al. 1998). The period derivative of J1410–7404 is 6.8×10^{-18}, again a very small value relative to other pulsars with slow spin periods. This leads us to suggest that the pulsar may in fact be recycled. From the period and period derivative we infer a magnetic field strength of 4.4×10^{10} G, lower than all but five apparently un-recycled pulsars and comparable to the double neutron star systems B1913+16 (at 2.3×10^{10} G) and B1534+12 (at 1.0×10^{10} G). A wider orbit and/or unfavorably oriented kick could easily result in the disruption of the orbit of a system similar to the progenitors of B1913+16 or B1534+12 at the time of the companion's supernova (Bailes 1989), leading to an isolated mildly recycled pulsar similar to J1410–7404. Unlike the double neutron star systems that coalesce due to gravitational radiation while still possessing pulsars with relatively fast spin periods, such systems would continue to be observable as "slow" pulsars with weak magnetic fields throughout their spin-down to the pair production death line.

Of the five slow pulsars now known with weaker inferred magnetic fields, PSRs J1320–3512 (D'Amico et al. 1998), B1952+29 and B1848+04 (Gould & Lyne 1998) do not possess narrow profiles. Should either of the remaining two slow pulsars

(J1355–6206 and J1650–4341, reported at the web site of the Galactic plane survey collaboration[5]) with weak magnetic fields possess narrow average profiles we suggest a similar possible interpretation to J1410–7404. It is possible that other weakly magnetised pulsars with long spin periods are also recycled but possess broader pulse profiles, due to the dependence of pulse width on α, the angle between the pulsar spin and magnetic axes. This dependence could be removed through polarimetric measurements of α, as in Kramer et al. (1998).

[5]http://www.atnf.csiro.au/~pulsar/psr/pmsurv/pmwww/

Chapter 5

Intermediate Latitude Survey: Slow Pulsars & Analysis

This Chapter has been accepted for publication in the Monthly Notices of the Royal Astronomical Society as Edwards, Bailes, van Straten & Britton 2001, "The Swinburne Intermediate Latitude Pulsar Survey".

Abstract

We have conducted a survey of intermediate Galactic latitudes using the 13-beam 21-cm multibeam receiver of the Parkes 64-m radio telescope. The survey covered the region enclosed by $5^\circ < |b| < 15^\circ$ and $-100^\circ < l < 50^\circ$ with 4,702 processed pointings of 265 s each, for a total of 14.5 days of integration time. Thirteen 2×96-channel filterbanks provided 288 MHz of bandwidth at a centre frequency of 1374 MHz, one-bit sampled every 125 μs and incurring $\sim$DM/13.4 cm^{-3} pc samples of dispersion smearing. The system was sensitive to slow and most millisecond pulsars in the region with flux densities greater than approximately 0.3–1.1 mJy. Offline analysis on the 64-node Swinburne workstation cluster resulted in the detection of 170 pulsars of which 69 were new discoveries. Eight of the new pulsars, by virtue of their small spin periods and period derivatives, may be recycled and have been reported elsewhere. The slow pulsars discovered are typical of those already known in the volume searched, being of intermediate to old age. Several pulsars experience pulse nulling and two display very regular drifting sub-pulses. We discuss the new discoveries and provide timing parameters for the 48 slow pulsars for which we have a

phase-connnected solution.

5.1 Introduction

By the late 1990s radio pulsar surveys had resulted in the discovery of ∼700 pulsars, spawning numerous studies with wide ranging implications for astrophysics and physics in general. Despite having been first discovered over a quarter of a century earlier, pulsars with unique and interesting properties (e.g. Wolszczan & Frail 1992; Johnston et al. 1992b; Johnston et al. 1993; Bell et al. 1995; Stappers et al. 1996) continued to be uncovered by surveys which also served the purpose of providing a larger sample for statistical analyses of classes of pulsars and pulsar binaries (e.g. Lyne et al. 1998).

Nearly all early surveys were conducted at low frequencies ($\nu \simeq 400$ MHz) due to the steep spectrum ($\alpha \simeq -1.6$, where $S \propto \nu^{\alpha}$; Lorimer et al. 1995) characteristic of microwave radiation from pulsars and the faster sky coverage afforded by the larger telescope beam at these frequencies. However, two effects that hamper the detection of certain pulsars at low frequencies can be avoided by using a higher frequency. Firstly, for small Galactic latitudes the background of Galactic synchrotron emission comprises the main contribution to the system temperature at these frequencies. The spectrum of this radiation is steep ($\alpha \simeq -2.6$; Lawson et al. 1987) and at high frequencies generally represents an insignificant contribution compared to the thermal receiver noise. Since they share the low Galactic z-height of their progenitor population, young pulsars in particular are selected against in low frequency surveys due to the elevated sky background temperature. Secondly, radiation propagating through the interstellar medium is subject to "scattering" due to multi-path propagation, effectively convolving the light curve with an exponential of a time constant that scales as ν^{-4} (Ables, Komesaroff & Hamilton 1970). Since the minimum detectable mean flux density in pulsar observations is proportional to $[\delta/(1-\delta)]^{1/2}$ where δ is the effective pulse duty cycle, scatter-broadening of the received pulses hampers the detection of pulsars at low frequencies, especially those with short spin period such as the interesting and important class of "millisecond" pulsars, and (again) young pulsars. Moreover, by conducting a survey at high frequencies one is sensitive to pulsars with flatter spectra that were missed in earlier surveys.

With the rise in availability of affordable computing power in the 1980s it became feasible to process surveys with fast sampling rates and large numbers of pointings, as required for large scale high frequency surveys for millisecond pulsars. Clifton et al. (1992) and Johnston et al. (1992a) conducted highly successful 20-cm pulsar surveys near the Galactic plane, discovering 86 pulsars between them, including a high fraction of young pulsars. However, the surveys did not have sufficient sensitivity at high time resolution to discover any millisecond pulsars. In addition, for the reasons mentioned above the surveys concentrated on the Galactic plane and hence the samples of detected pulsars were of reduced value in modelling the Galactic pulsar population compared to larger surveys.

In 1997 the Australia Telescope National Facility commissioned a new 21-cm 13-feed multibeam receiver, primarily for HI surveys (Henning et al. 2000; Barnes et al. 2001). The large instantaneous sky coverage and excellent sensitivity also makes the system a powerful pulsar survey instrument and this led to the commencement of a long-running deep survey of the southern Galactic plane ($|b| < 5°$) which is expected to almost double the known population (Lyne et al. 2000a; Camilo et al. 2000b). We conducted Monte Carlo simulations similar to those discussed by Toscano et al. (1998) and found that a shallower "flanking" survey should discover a sizeable population of pulsars with unprecedented time efficiency in an area of sky not previously sampled at high frequencies. Based on this result we conducted such a survey between 1998 August and 1999 August. The survey proved highly successful, discovering 69 pulsars including two pulsar binaries containing heavy CO white dwarfs, one of which will coalesce in less than a Hubble time with dramatic and unknown consequences (Edwards & Bailes 2001b), and a further four binary and two (perhaps three) isolated recycled pulsars with important implications for theories of binary evolution (Edwards & Bailes 2001a). In this paper we report in detail on the observing system, analysis procedures, sensitivity and completeness. We discuss detections of previously known pulsars and present the new sample of slow pulsars, including timing results for those with solutions.

5.2 Observations and Analysis

5.2.1 Hardware Configuration and Survey Observations

The 64-m Parkes radio telescope was used with the 13-beam 21-cm receiver (Staveley-Smith et al. 1996) which provides 300 MHz of bandwidth and a system temperature of ∼21 K. Signals from the two orthogonal polarisations of each beam were mixed with a local oscillator before being fed to an array of 26 96-channel filterbanks. Each filterbank channel was 3 MHz wide and the band was centred at a frequency of 1374 MHz. The detected signals from corresponding polarisation pairs in each channel were summed and high pass filtered (with a time constant of ∼0.9 s; Manchester et al. 2000) before being integrated and one-bit sampled every 125 μs. The data stream was written to magnetic tape (DLT 7000) for offline processing, as well as being made available to online interference monitoring software in near-real-time via the computer network. With the exception of the sampling interval, the system was identical to that used for the Galactic plane survey (Manchester et al. 2001).

The receiver feeds are arranged in such a way as to allow coverage of the sky in a hexagonal grid, with beams overlapping at their approximate half-power points ($7'$ from the beam centre). A group of four pointings results in the uniform coverage of a roughly circular shape ~ 1 degree in radius which in turn can be efficiently tessellated (see Figure 5.1). The region enclosed by $5^\circ < |b| < 15^\circ$ and $-100^\circ < l < 50^\circ$ was covered in 4,764 265-s proposed pointings, amounting to only 14.6 days of integration time. Most of these pointings were observed in several week-long observing runs between August 1998 and August 1999.

5.2.2 Search Analysis Procedure

The processing of the 64-tape $\sim$ 1.6 terabyte data set was performed on the Swinburne Supercluster, a network of 64 Compaq Alpha workstations. Before searching for pulsars, each beam was analysed for the presence of powerful signals that appeared in only a few filterbank channels, a common type of interference signal. When such signals were present, samples in the culprit channels were zeroed, a process that does not incur too much loss of sensitivity since this varies as the square root of the effective bandwidth. In addition, broad-band periodic signals that appear in large numbers of beams in any given 30-minute period were detected and logged to a file for later reference.

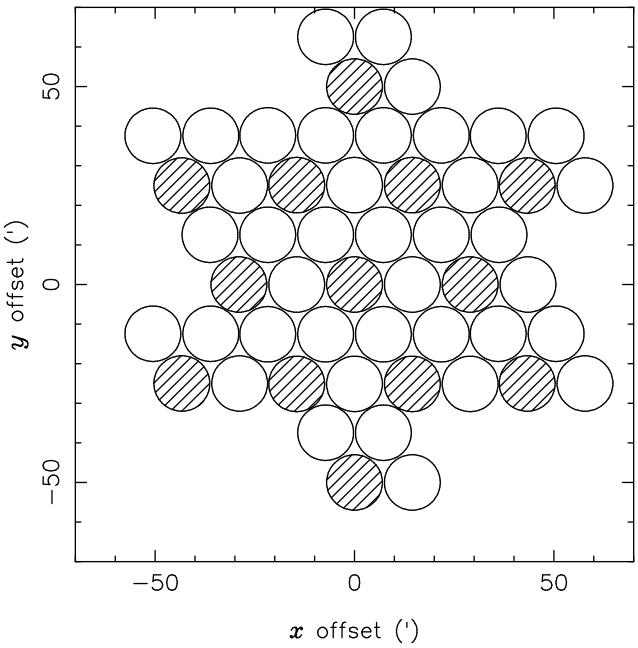

Figure 5.1: The multibeam tessellation unit shown with circles depicting the half-power points of beams. A unit is observed with four offset pointings, one of which is hatched in the above for clarity. The shape made by the 52 beams can be seamlessly self-tessellated.

To correct for the effects of non-linearity in the dispersion relation, data from the 96 filterbank channels were padded with 32 dummy channels in such a way as to allow linear de-dispersion of the resulting 128 channels, as used by the Galactic plane survey collaboration. This enabled the use of the fast "tree" algorithm of Taylor (1974) to partially de-disperse the data into eight trial dispersion measures in each of sixteen sub-bands. Whilst the linearity of dispersion with respect to channel number would enable full de-dispersion (that is, 128 trial DMs with no sub-band divisions), in order to limit storage requirements and to allow the recording of frequency-resolved pulse profiles to aid in suspect scrutiny, application of the algorithm was stopped after the production of eight DMs.

The tree algorithm produces trial DMs up to the "diagonal" DM of 17.0 cm^{-3} pc, where the dispersion delay across one sub-band in units of samples is equal to the number of channels used to form it. It should be noted that in previous surveys where the linear dispersion approximation was acceptable for the tree stage, this parameter was approximately equal to the DM at which the smearing induced in each channel was one sample interval. The latter parameter is commonly quoted in conjunction with the sampling interval to give an indication of the time resolution

available to pulsars of various DMs in a pulsar survey. For the present survey this value varies from 9.4 to 17.5 cm^{-3} pc depending on the centre frequency of the channel, and for evaluation purposes one should use the geometric mean of 13.4 cm^{-3} pc. The tree algorithm was extended to also produce time series for 1–2 times the diagonal DM, and beyond this value the sample interval was doubled by summing of samples before re-application of the algorithm, and the process repeated to produce time series with 2–4, 4–8, 8–16 and 16–32 times the diagonal DM.

The periodicity search itself was based on that of the Parkes Southern Pulsar Survey (Manchester et al. 1996), generalised and modified to handle the large number of spurious interference signals present in the multibeam data. Time series were constructed at 375 trial values of dispersion measure from 0 to 562.5 cm^{-3} pc by summing partially de-dispersed sub-bands in the nearest DM with the appropriate time offsets. The trial DMs were spaced in such a way that the effective smearing induced due to the difference between the DM of a pulsar and the nearest trial DM was no more than twice that induced by the finite width of individual filterbank channels. The time series were filtered with a boxcar of width 2048 ms to remove the effects of receiver noise and gain variations during the course of the observation, before being Fourier transformed and detected to form the fluctuation power spectrum.

For signals with frequencies lying on the boundary between two spectral bins the result is two components of equal magnitude and opposite sign in the adjacent bins. To maintain sensitivity to such signals we also computed the difference of each bin and its neighbours and used half the squared magnitude of the results as alternative estimates of spectral power. For each bin the highest of the three power values computed was chosen for use in the final power spectrum. In the case of the zero-DM time series, this spectrum was checked for the occurrence of any signal with a frequency close to one earlier logged as a broad band interference signal contemporaneous with this observation. Should such a signal be present, its exact extent in the spectrum was assessed and the corresponding bins zeroed in this and all other power spectra searched in this beam. The spectrum above a frequency of 1/12 Hz was then searched for significant spikes compared to a local mean (to compensate for the overall redness of the spectrum). Harmonics were summed and the process repeated for up to 16 harmonics to maintain sensitivity to signals with short duty cycles. Significant signals at any level of harmonic summing were recorded and after all trial dispersion measures had been searched the set of

signals was collated into a number of candidates, each covering signals of similar pulse period occurring at multiple trial DMs. The top 99 candidates in each beam were subject to a fine search (by means of maximisation of signal to noise ratio, S/N) in period and dispersion measure around the best values found in the spectral search. Pertinent information including the resulting best profile, grey scale maps of pulse profiles as a function of time and radio frequency and of signal to noise as a function of period and dispersion measure were saved to disk.

5.2.3 Suspect Scrutiny, Confirmation and Timing Observations

The final stage of analysis was human viewing. The large number of beams and the prevalence of interference signals presented considerable complications to the viewing process due to the volume of candidates produced. In previous surveys (e.g. Manchester et al. 1996) candidates of similar period occurring in multiple beams contemporaneously were generally taken as interference signals and ignored. In the case of results from this survey, the plethora of interference signals across the spectrum resulted in the misinterpretation of many pulsars as interference. It was found that this limited the applicability of this approach to the handful of periods that appeared more than ~ 250 times on any tape. All remaining candidates with signal to noise ratios greater than eight (of which there were several hundred thousand) were then scrutinised by a human viewer and promising signals scheduled for confirmation by re-observation.

Human viewing of all suspects with S/N > 8 was expected to be incomplete in its selection due to the viewing speed necessitated by the large number of candidates to be assessed. This method was used as a first pass over the data, however after all data were processed and the 30 GB result set assembled, a more complete candidate analysis scheme was employed. A custom-written graphical software package allowed for visual (and numerical) identification of the distribution of candidates in a variety of parameters. Sets of candidates could be trimmed by the graphical or command-driven selection and deletion of interference signals, and the remaining candidate list subjected to human scrutiny. A set of "macros" were developed for the deletion of dozens of commonly appearing highly coherent interference periods as well as all signals with large relative errors in dispersion measure (a characteristic of terrestrial, non-dispersed interference) and any candidate with a S/N less than 9 (or 9.5 for

$P < 20$ ms). These produced an order of magnitude reduction in the number of suspects to be viewed, and a corresponding improvement in the accuracy and completeness of scrutiny. Interference mitigation procedures employed for each tape were also recorded as macros to allow for repeatability and quantification of any selection effects imposed.

Those candidates confirmed by detection in a re-observation were added to an ongoing program of pulsar timing of new discoveries. Observations of typically 250 s were made with the centre beam of the system described above, or more recently the $2 \times 512 \times 0.5$-MHz filterbank to provide improved time resolution for short period pulsars. For most pulsars at least one timing observation was obtained at a frequency of 660 MHz to enable accurate measurement of the dispersion measure. In offline processing samples were de-dispersed and folded at the predicted topocentric pulse period. The resulting pulse profiles were fitted to a "standard" profile usually produced by adding several prior observations of high signal to noise ratio. The resulting phase offsets were used to produce barycentric times-of-arrival (TOAs) which were then used in conjunction with the TEMPO software package[1] to fit for the relevant spin, astrometric and binary parameters (see e.g. Taylor & Weisberg 1989).

5.3 Results and Discussion

5.3.1 Sky Coverage, Sensitivity and Re-Detections

The survey was deemed complete in August 1999 after the observation and successful processing of 60,852 beams in 4,702 pointings. In the first observing run an error in the telescope control system resulted in spurious rotations of the receiver feed, making the sky position corresponding to each recorded beam (except the centre beam) indeterminate and reducing sensitivity by moving off (or on!) source midway through observations. For this reason most of the region of sky surveyed under these conditions were re-observed.

Figure 5.2 shows the sky coverage achieved by the survey. One ellipse is plotted for each group of four inter-meshing pointings. Ellipses are shaded according to the number of observed and processed pointings in the group. Most groups are either medium grey (for standard once-only coverage), black (for those areas observed twice

[1] http://pulsar.princeton.edu/tempo

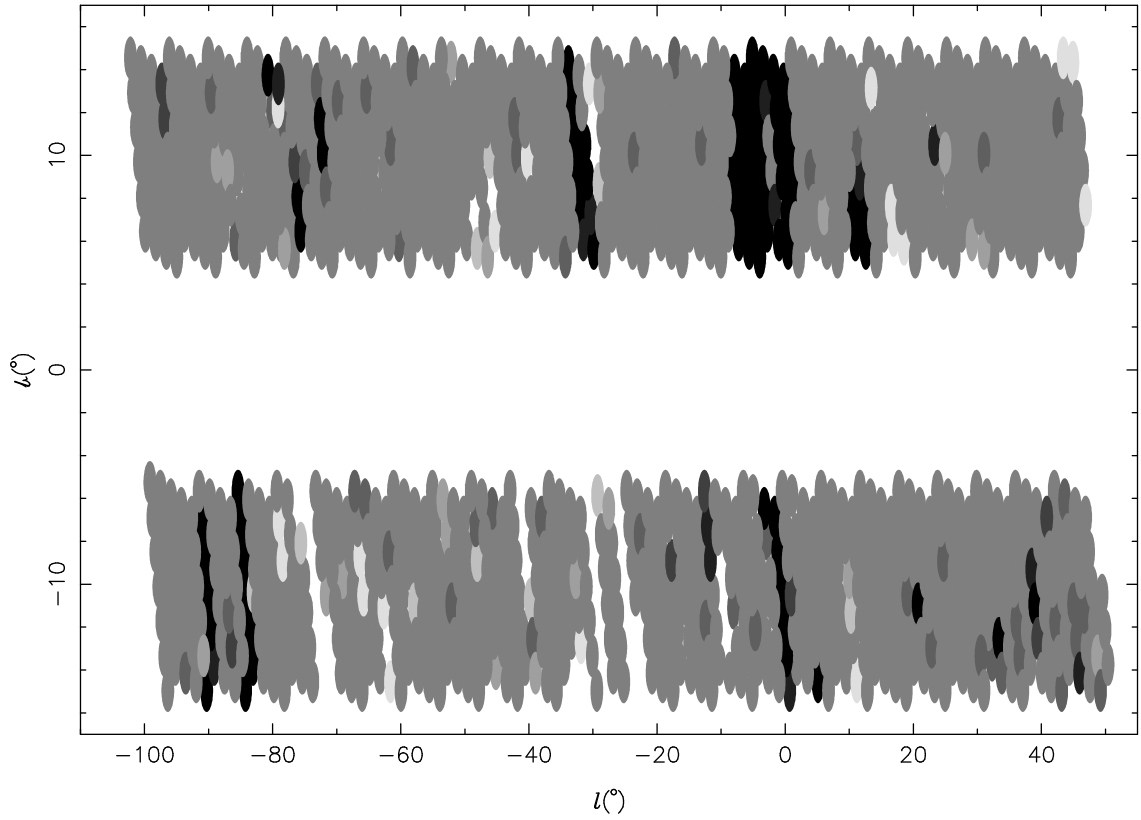

Figure 5.2: Sky coverage for the survey. Ellipses represent groups of four inter-meshed pointings. Shades of grey represent the density of coverage, from unobserved (white) to observed twice (black).

due to position uncertainty as discussed above) or white (for unobserved groups). Other shades reflect varying numbers of observed and processed beams in the group. A total of 4,465 of the proposed pointings were observed at least once, yielding a metric of completeness of 4,465/4,764 = 94 per cent.

The sensitivity of a pulsar survey is derived from the radiometer equation, altered to take into account the detection of periodic signals. It can be expressed as follows,

$$S_{\rm min} = \frac{\alpha\beta(T_{\rm rec} + T_{\rm sky})}{G(N_{\rm p}\Delta\nu t_{\rm obs})^{1/2}} \left(\frac{\delta}{1-\delta}\right)^{1/2} \tag{5.1}$$

where $S_{\rm min}$ is the minimum detectable mean flux density, α is the threshold S/N, β is a dimensionless correction factor for system losses, $T_{\rm rec}$ and $T_{\rm sky}$ are the receiver and sky noise temperatures, G is the telescope gain, $N_{\rm p}$ is the number of polarisations, $\Delta\nu$ is the observing bandwidth, $t_{\rm obs}$ is the integration time, W is the effective pulse width in time units and P is the pulse period (Dewey et al. 1985). The effective

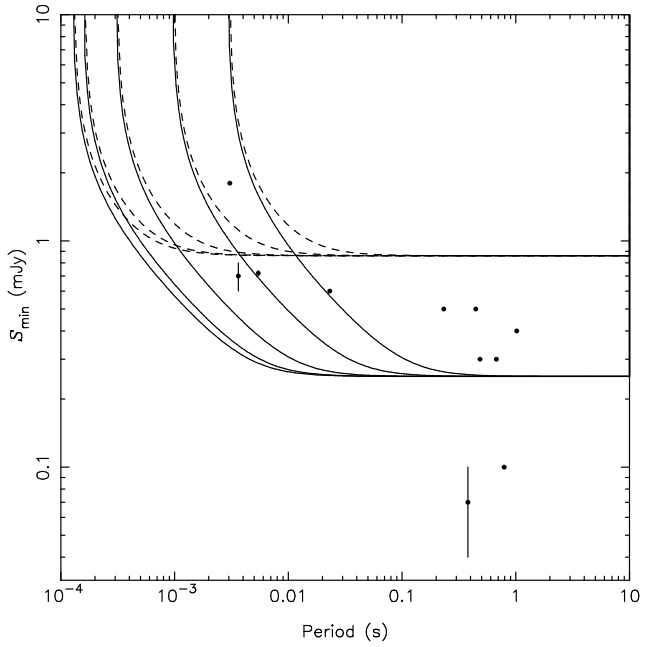

Figure 5.3: Estimated minimum detectable mean flux density ($S_{\rm min}$) as a function of pulse period for intrinsic pulse widths of 10° (solid lines) and 90° (dashed lines) at dispersion measures of 0, 10, 30, 100 and 300 cm^{-3} pc (in order of increasing $S_{\rm min}$ for a given pulse period). Points represent undetected pulsars which lie within 10′ of an observed beam, where flux density measurements have been published. Flux densities published without uncertainties are plotted without error bars and in such cases the relative uncertainty is probably around 50 per cent.

pulse width ($W = \delta P$ where δ is the observed duty cycle) is computed as the quadrature sum of the intrinsic pulse width and pulse broadening terms due to such effects as dispersion smearing, scatter-broadening and the finite sampling interval.

The system characteristics of the multibeam receiver vary from beam to beam and we use here averages of the values presented at the instrument web page[2], yielding a receiver temperature of 21 K and a gain of 0.64 K Jy^{-1}. The dimensionless parameter β embodies the loss due to one-bit digitisation ($\sqrt{\pi/2} \simeq 1.25$) and other system losses, which we treat collectively with $\beta = 1.5$. Assuming a typical sky temperature of 2 K, the calculated sensitivity as a function of pulse period is plotted in Figure 5.3 for several dispersion measures and pulse widths. Included in the effective width calculation are the dispersion smearing in filterbank channels and the sampling interval. It should be noted that the sensitivity derived is that available at the centre of the beam. The average beam response is approximately Gaussian (Manchester et al. 2001) with a half-power width of 14.3′, meaning that pulsars lying

[2]http://www.atnf.csiro.au/research/multibeam/lstavele/description.html

near the beam overlap points will be detected with half the sensitivity calculated. We calculate that the mean sensitivity within the half-power radius is 73 per cent of that at the centre of the beam, meaning that for statistical sensitivity estimates, the curves in Figure 5.3 should be raised about a tenth of a decade. The resulting basic mean sensitivity to slow pulsars is 0.3–1.1 mJy for intrinsic pulse widths of 10°–90°.

The signal-to-noise ratio used in the sensitivity equation is calculated in the time domain. We note that some pulsar surveys (e.g. Camilo, Nice & Taylor 1996; Manchester et al. 2001) have based their sensitivity analysis on the so-called "spectral" S/N, computed from the amplitudes of harmonics in the power spectrum. Our search code computes such a value for all candidates, however this is used only for the selection of signals to be subjected to a fine search in the time domain, and the threshold value used (5.0) is sufficiently low that we expect no loss of significant candidates at this stage. The (time domain) S/N threshold of 8.0 imposed in the selection of candidates for human viewing is also irrelevant for the sensitivity analysis since it found that nearly all candidates re-detected in subsequent observations had S/Ns greater than 10.0, despite attempts to re-detect large numbers of candidates with S/N between 8.0 and 10.0. We therefore use $\alpha = 10.0$ in the above analysis and in the curves plotted in Figure 5.3.

We caution that this analysis should only be taken as approximate. The variation of a pulsar's flux due to scintillation adds a considerable degree of uncertainty to its detectability, and particularly for millisecond pulsars lack of time resolution and prevalence of interference signals cause the human viewer to effectively adopt a higher threshold S/N. In particular, whilst this analysis suggests that this and similar surveys could be significantly sensitive to sub-millisecond pulsars, we would treat such a claim with skepticism. A sub-millisecond pulsar with $P = 0.8$ ms and a moderately low dispersion measure of 25 cm^{-3} pc would experience 0.25 ms of dispersion smearing, resulting in a pulse profile with a width of at least 110°. Combined with the fact that only 4 or perhaps 8 bins would be present in the pulse profile, the human viewer is forced to judge the origin of the signal essentially entirely upon the reported S/N, which itself becomes subject to significant uncertainty when the number of bins is so few. We therefore expect that the standard sensitivity analysis underestimates the minimum detectable flux density by a factor of a few for pulsars with periods shorter than a millisecond. Likewise, the minimum detectable flux density may be underestimated for very slow ($P > 5$ s) pulsars due to the rather

short time constant (0.9 s) employed in the digitiser system. The $P^{-1/2}$ duty cycle dependence of slow pulsars (e.g. Rankin 1990) aids the situation somewhat, but nevertheless it is expected that a few percent of very slow pulsars have pulse widths greater than 0.5 s, and these would experience significant S/N loss.

A total of 101 previously known pulsars were re-detected in the survey. Due to the large angular extent of each of the tessellated units of four pointings, the actual survey regions are significantly non-rectangular in l and b (see Figure 5.2) and three of these pulsars actually lie outside the nominal survey region. There were 135 previously discovered pulsars in the declared region, leaving 37 undetected in the survey. Tables 5.1 and 5.2 list the detected and undetected known pulsars, including for each pulsar the period, dispersion measure, flux density at 1400 MHz (where known), position in Galactic coordinates, angular offset from the centre of the beam in which it was detected (where known, or the nearest processed beam for undetected pulsars), and the signal to noise ratio of detections. In most cases the values for period, DM and flux density derive from the works of Taylor, Manchester & Lyne (1993), Lorimer et al. (1995) or D'Amico et al. (1998).

From the tabulated position offsets to the nearest processed beams and given the fact that the centres of adjacent beams of the grid are spaced 14 arcminutes apart on the sky, it is clear that the reason for many of the non-detections was incomplete sky coverage. Twelve undetected pulsars lay greater than 10 arcminutes from the nearest beam, leading to an alternative completeness metric of $1 - 12/135 = 91$ per cent, (or $1 - 9/135 = 93$ per cent if the loss is offset by the three known pulsars detected outside the survey region). Of the remaining 25 non-detections, 11 have published flux densities near 1400 MHz and are plotted along with the sensitivity curves of Figure 5.3. Allowing for scintillation, all are compatible with having flux densities below the sensitivity limit. We therefore expect that most of those pulsars lacking flux density measurements were also below the detection threshold at the time of observation, and conclude that the search procedure was adequate and robust in its rejection of interference without significant loss of pulsars. Possible exceptions to this statement are PSR B1556–44 which was detected at 17 times its true spin frequency (probably due to proximity in period to a persistent 256-ms interference signal), and perhaps PSR J1130–6807 which has a similar pulse period but being of unknown flux density may have simply fallen below the sensitivity limit. The discovery of PSR J1712–2715 (below) with $P = 255.4$ ms indicates that rough proximity to interference signals is not always problematic. The millisecond pulsar

Table 5.1: Detected previously known pulsars

Name	P (s)	DM (cm^{-3} pc)	S_{1400} (mJy)	l (°)	b (°)	Δ pos ($'$)	S/N
B0743–53	0.215	121.5	.....	−93.3	−14.3	7.3	85.7
B0808–47	0.547	228.3	3.00	−96.7	−8.0	.....	46.4
B0839–53	0.721	156.5	2.00	−89.2	−7.1	5.2	55.1
B0855–61	0.963	95	.....	−81.4	−10.4	4.2	20.6
B0901–63	0.660	76	.....	−79.6	−11.1	8.7	25.2
B0950–38	1.374	167	.....	−91.3	12.0	8.2	12.9
B0957–47	0.670	92.3	.....	−84.3	5.4	5.2	34.7
B1001–47	0.307	98.5	.....	−84.0	6.1	2.9	31.4
J1036–4926	0.510	136.5	.....	−78.5	7.7	5.8	10.8
J1045–4509	0.007	58.1	3.00	−79.1	12.3	0.0	37.6
J1047–6709	0.198	116.2	4.00	−68.7	−7.1	3.6	87.0
B1055–52	0.197	30.1	.....	−74.0	6.6	.....	51.0
B1110–65	0.334	249.1	.....	−66.8	−5.2	5.2	38.1
B1110–69	0.820	148.4	.....	−65.6	−8.2	5.0	18.1
B1119–54	0.536	205.1	.....	−69.9	5.9	4.2	44.7
J1123–4844	0.245	92.9	.....	−71.7	11.6	6.7	36.1
J1126–6942	0.579	55.3	.....	−64.4	−8.0	3.3	15.9
B1133–55	0.365	85.2	4.00	−67.7	5.9	5.6	100.7
J1210–5559	0.280	174.3	2.10	−62.9	6.4	7.4	33.1
B1232–55	0.638	100	1.00	−59.4	7.5	19.2	22.7
B1236–68	1.302	94.1	.....	−58.1	−5.7	11.1	32.7
B1309–53	0.728	133	.....	−54.0	8.7	2.2	20.3
B1309–55	0.849	135.1	.....	−54.0	7.5	0.8	102.4
B1317–53	0.280	97.6	.....	−52.7	8.6	4.8	43.2
B1325–49	1.479	118	.....	−50.9	13.1	6.1	17.1
J1350–5115	0.296	90.4	.....	−47.8	10.5	4.9	25.1
B1352–51	0.644	112.1	.....	−47.0	9.7	3.2	40.9
B1359–51	1.380	39	.....	−45.9	9.9	63.7	71.0
J1403–7646‡	1.306	100.6	.....	−52.9	−14.5	2.2	14.5
B1417–54	0.936	129.6	.....	−44.2	6.4	6.1	30.7
B1426–66	0.785	65.3	6.00	−47.3	−5.4	6.7	126.2
B1451–68	0.263	8.7	80.00	−46.1	−8.5	7.0	242.9
B1454–51	1.748	35.1	.....	−37.9	6.7	4.4	27.1
B1503–66	0.356	129.8	.....	−44.1	−7.3	1.9	66.5
B1504–43	0.287	48.7	.....	−32.7	12.5	4.4	107.5
B1507–44	0.944	84	.....	−32.4	11.7	.....	53.1
B1510–48	0.455	49.3	.....	−34.1	7.8	5.9	16.3
B1524–39	2.418	46.8	.....	−27.0	14.0	6.7	37.5
B1556–44	0.257	56.3	40.00	−25.5	6.4	7.0	71.3
J1557–4258	0.329	144.5	5.10	−24.7	8.0	5.6	59.5
J1603–7202	0.015	38.1	2.9(2)	−43.4	−14.5	3.6	16.1
J1614–3937	0.407	152.4	.....	−20.0	8.2	6.1	11.7
B1620–42†	0.365	295	2.20	−21.1	4.6	13.8	12.5
J1625–4048	2.355	145	.....	−19.4	5.9	8.1	16.1
B1630–59	0.529	134.9	.....	−32.3	−8.3	1.5	50.9
B1641–68	1.786	43	2.00	−38.2	−14.8	4.6	110.7
B1647–52	0.635	179.1	2.00	−25.0	−5.2	4.0	117.2
B1647–528	0.891	164	.....	−25.4	−5.5	5.8	64.1
J1648–3256	0.719	128.3	1.00	−10.4	7.7	5.5	21.0
B1649–23	1.704	68.3	1.10	−2.7	12.5	.....	38.0

† — Pulsar lies outside nominal survey region

‡ — Pulsar originally published with incorrect period; corrected period listed

Table 5.1: *continued* — **Detected previously known pulsars**

Name	P (s)	DM (cm^{-3} pc)	S_{1400} (mJy)	l (°)	b (°)	Δ pos (′)	S/N
B1700–18	0.804	48.3	0.7(2)	3.2	13.6	6.4	18.2
J1700–3312	1.358	166.8	.....	−8.9	5.5	9.1	21.5
B1702–19	0.299	22.9	8(3)	3.2	13.0	7.1	56.6
B1706–16	0.653	24.9	4(2)	5.8	13.7	6.5	231.4
B1707–53	0.899	106.1	.....	−24.3	−8.5	0.4	16.9
B1709–15	0.869	58.0	0.7(2)	7.4	14.0	4.4	15.9
B1717–16	1.566	44.9	1.1(4)	7.4	11.5	3.2	19.5
B1718–19	1.004	75.9	0.30	4.9	9.7	5.2	9.1
B1727–47	0.830	123.3	12.00	−17.4	−7.7	2.3	582.4
B1730–22	0.872	41.2	2.2(3)	4.0	5.7	5.6	64.5
J1730–2304	0.008	9.6	3.0(4)	3.1	6.0	.....	48.7
B1732–07	0.419	73.5	1.7(2)	17.3	13.3	3.5	78.4
B1738–08	2.043	74.9	1.4(4)	17.0	11.3	4.9	91.3
B1740–13	0.405	115	0.50(10)	12.7	8.2	3.9	24.0
J1744–1134	0.004	3.1	2.0(2)	14.8	9.2	3.2	24.8
B1745–12	0.394	100.0	2.0(3)	14.0	7.7	3.8	106.1
B1747–46	0.742	20.3	10.00	−15.0	−10.2	6.5	159.0
B1758–03	0.921	117.6	0.70(10)	23.6	9.3	4.1	30.3
B1802+03	0.219	79.4	.....	30.4	11.7	6.4	27.7
B1804–08	0.164	112.8	16(4)	20.1	5.6	5.2	260.9
J1808+00	0.425	141	.....	28.5	9.8	8.1	21.4
J1808–0813	0.876	151.3	2.00	20.6	5.8	7.1	34.9
B1810+02	0.794	101.6	0.30	30.7	9.7	4.7	14.6
J1811+0702	0.462	54	.....	34.7	12.1	2.2	21.0
B1813–26†	0.593	128.1	.....	5.2	−4.9	7.8	17.9
B1813–36	0.387	94.4	2.00	−3.2	−9.4	5.4	52.4
J1817–3837‡	0.384	102.8	.....	−5.3	−10.4	7.4	57.6
B1818–04†	0.598	84.4	8.0(6)	25.5	4.7	12.0	104.6
B1820–31	0.284	50.3	2.5(6)	2.1	−8.3	8.3	72.1
B1821+05	0.753	67.2	1.7(4)	35.0	8.9	3.3	111.9
B1822+00	0.779	54.4	0.40(10)	30.0	5.9	1.4	26.6
J1822–4209	0.457	72.5	1.50	−8.1	−12.8	6.3	16.2
B1839+09	0.381	49.1	1.70(10)	40.1	6.3	3.5	99.9
B1842+14	0.375	41.2	1.5(3)	45.6	8.1	5.2	30.5
B1845–19	4.308	18.3	.....	14.8	−8.3	9.3	84.6
B1848+12	1.205	71	0.50(10)	44.5	5.9	5.5	21.3
B1848+13	0.346	59.0	1.4(3)	45.0	6.3	8.1	32.1
J1848–1414	0.298	134.4	.....	19.9	−5.8	4.3	11.2
B1851–14	1.147	130.1	.....	20.5	−7.2	9.0	24.0
J1852–2610	0.336	56.8	1.40	9.5	−11.9	0.8	36.2
B1857–26	0.612	38.1	13.0(10)	10.3	−13.5	6.8	201.6
B1900–06	0.432	195.7	.....	28.5	−5.7	10.0	13.7
J1901–0906‡	1.782	72.7	3.10	26.0	−6.4	4.7	98.6
J1904–1224	0.751	118.2	.....	23.3	−8.5	2.5	14.9
B1907–03	0.505	205.7	0.80	32.3	−5.7	3.6	22.1
B1911–04	0.826	89.4	4.4(5)	31.3	−7.1	4.8	233.4
B1917+00	1.272	90.7	0.8(2)	36.5	−6.2	4.6	36.7
B1923+04	1.074	101.8	.....	41.0	−5.7	9.0	15.5
J1929+00	1.167	33	.....	37.7	−8.3	2.3	14.0
J1938+0652	1.122	70	.....	44.4	−7.1	3.8	29.2
B1942–00	1.046	58.1	0.80(10)	38.6	−12.3	6.2	21.5

† — Pulsar lies outside nominal survey region

‡ — Pulsar originally published with incorrect period; corrected period listed

Table 5.2: Undetected previously known pulsars

Name	P (s)	DM (cm^{-3} pc)	S_{1400} (mJy)	l (°)	b (°)	Δ pos ($'$)
B0923–58	0.740	57.7	.....	−81.6	−5.6	15.7
J1006–6311	0.836	196.0	.....	−74.4	−6.0	21.6
J1123–6651	0.233	111.2	0.50	−65.5	−5.4	5.4
J1130–6807	0.256	148.7	.....	−64.5	−6.4	5.8
J1137–6700	0.556	228.0	1.10	−64.2	−5.2	17.7
J1143–5158	0.676	159.0	0.30	−67.6	9.5	3.4
J1225–5556	1.018	125.8	0.40	−60.7	6.7	6.6
J1356–5521	0.507	174.2	1.50	−47.8	6.3	11.8
B1503–51	0.841	61.0	.....	−36.9	5.5	8.4
J1604–7203	0.341	54.4	.....	−43.3	−14.6	4.1
J1654–2713	0.792	92.4	0.10	−5.0	10.3	3.1
B1659–60	0.306	54	.....	−30.2	−11.4	6.3
B1700–32	1.212	109.6	6.00	−8.2	5.4	21.0
J1701–3006	0.005	115.6	.....	−6.4	7.3	6.6
J1732–1930	0.484	73.0	0.30	6.4	7.6	5.3
B1740–03	0.445	30.2	0.50	21.6	13.4	5.0
J1740–5340	0.004	71.9	.....	−21.8	−12.0	3.7
B1745–56	1.332	58	.....	−23.4	−14.3	50.1
B1802–07	0.023	186.4	0.60	20.8	6.8	7.6
J1807+07	0.464	89	.....	35.1	13.3	4.1
J1809–3547	0.860	193.8	.....	−3.5	−7.8	7.6
B1820–30A	0.005	86.8	0.72(2)	2.8	−7.9	6.6
B1820–30B	0.379	87.0	0.07(3)	2.8	−7.9	6.6
J1821+17	1.366	79	.....	45.3	14.2	8.7
B1821–24	0.003	119.8	1.80	7.8	−5.6	6.4
J1822+0705	1.363	50	.....	36.0	9.7	4.2
J1822+11	1.787	112	.....	39.9	11.6	7.4
J1823–0154	0.760	135.9	0.80	28.1	5.3	28.7
J1834+10	1.173	62	.....	40.6	8.6	8.5
J1838+06	1.122	70	.....	37.5	6.1	4.0
J1838+16	1.902	36	.....	46.7	10.3	10.2
J1859+1526	0.934	97.4	.....	47.6	5.2	76.0
J1911–1114	0.004	31.0	0.70(10)	25.1	−9.6	6.2
J1933+07	0.437	170	.....	44.8	−5.6	10.2
J1941+1026	0.905	138.9	.....	48.0	−6.2	15.9
J1947+10	1.111	149	.....	49.0	−7.3	56.5
J1950+05	0.456	71	.....	44.9	−10.6	5.5

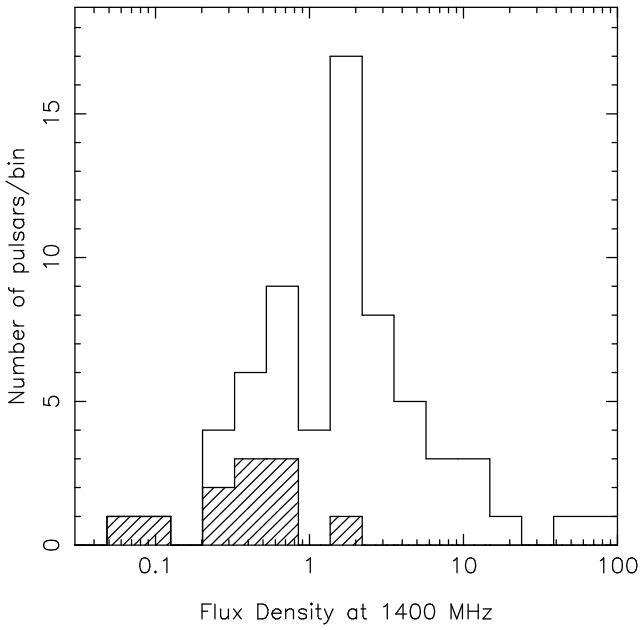

Figure 5.4: Histograms depicting distribution in flux density of all previously known pulsars with published flux density with processed beams centred less than 10′ away. The subset of such pulsars that were undetected in the survey is represented by the hatched regions.

(MSP) fraction of the undetected pulsars is high, however all except J1911–1114 (Lorimer et al. 1996) were discovered in deep directed searches of globular clusters (Lyne et al. 1987; Biggs et al. 1994; D'Amico et al. 2001a) which found mainly millisecond pulsars. Figure 5.4 shows a histogram of flux densities for previously known pulsars of published flux density with processed beams centred less than 10′ away, with the distribution of non-detections hashed. As expected from the sensitivity curves shown in Figure 5.3, the survey was sensitive to most pulsars brighter than 1 mJy, insensitive to pulsars with $S < 0.1$ mJy, and recorded a mixture of detections and non-detections in the remaining range due to scintillation and the distribution of pulse widths.

Examination of the detection parameters of previously known pulsars reveals some discrepancies with previously published results. From inspection of the position offsets of newly discovered pulsars (below, Table 5.4), we estimate a position uncertainty of 7′ for detections in this survey, consistent with the beam spacing. Of those detected pulsars with published positions greater than 10′ from the beam centre, two were not detected in pointings made closer to the published position. The (B1950) declinations reported for PSRs B1232–55 and B1359–51 of $-55°00(10)'$ and

$-51°10(15)'$ (Manchester et al. 1978) respectively are inconsistent with the B1950 declinations of $-54°40(5)'$ and $-50°06(5)'$ of the detections made in this survey. The published right ascension values have much smaller uncertainties (due to the shape of the beam of the Molonglo telescope with which they were discovered), and are consistent with our detections.

As was spectacularly illustrated with PSR J2144–3933 (Young, Manchester & Johnston 1999), pulsar surveys in the past have been prone to detecting pulsars with an apparent pulse frequency an integer multiple of the true frequency. We expect that this is due to the flattening of the power spectrum with a boxcar filter, the presence of interference signals of similar period, the dominance of odd harmonics in the pulse shape, or the exclusion of the fundamental as being below a cutoff frequency (as was the case for J2144–3933). We found that PSRs J1403–7646, J1817–3837 and J1901–0906 (Lyne et al. 1998) actually possess periods a factor of two greater than the published values. Conversely, pulsars J1036–4926, B1110–69, B1524–39, B1556–44, B1706–16, B1709–15, B1717–16, B1718–19 and B1848+12 were erroneously re-detected with shorter pulse periods. All but one of these results were made in the early stages of processing before interference rejection had been fine-tuned to avoid accidental filtering of pulsar harmonics near interference signals. After correction for such errors and with the exception of the three pulsars listed above, all other detections were made with pulse periods consistent with previously published parameters.

5.3.2 Newly Discovered Pulsars

The initial viewing of the survey results and subsequent confirmation observations resulted in the discovery of 58 new pulsars, 8 of which possess short spin periods and small period derivatives indicative of recycling and have been reported elsewhere (Edwards & Bailes 2001b; Edwards & Bailes 2001a). The final careful review of candidates produced a further 11 slow pulsars. Data from all pulsars were folded at twice and three times the discovery period to detect any errors of the kind described in the previous section. Pulsars J1055–6905, J1517–4356, J1802+0128 and J1808–3249 were all initially discovered at half the true spin period, however J1517–4356 and J1808–3249 were later detected at the correct period in subsequent survey observations, with higher signal to noise ratio. Pulse profiles for the 61 slow pulsars discovered in the survey are presented in Figure 5.5. For those pulsars with a timing

solution the profile arises from the summation of numerous good observations, whilst for others the profile from the single best observation made to date is provided. It should be noted that the baselines of some profiles are corrupted due to the response of the filterbank/digitiser low pass filter.

Timing solutions have been obtained for 48 slow pulsars. The data for each pulsar span 490–830 days, depending on when the candidate re-observation was made. Since all pulsars have been timed for well over a year, we were able to accurately measure positions and period derivatives, in addition to making improved measurements of periods and dispersion measures. We have not seen obvious timing noise in any pulsar, however it is possible that such noise is present and is absorbed by deviations from the "true" values of the fitted parameters. Dispersion measures were fitted for by the use of TOAs derived from sub-divisions of the observing band, or where available, 660 MHz observations. In the latter case the signal to noise ratio available in a reasonable integration time was poor and the use of an independent template profile was eschewed in favour of the superior 20-cm template.

Table 5.3 presents the basic parameters of the slow pulsars discovered in this survey, derived from timing measurements when available. Values in parentheses denote uncertainties in the last quoted digit and represent twice the formal uncertainty produced by TEMPO. In the case of pulsars lacking a timing solution we use twice the errors derived from the fine P-DM search, or for positions, errors corresponding to a randomly oriented offset of 7 arcminutes (i.e. $7'/\sqrt{2} \simeq 5'$ in each of α and δ). PSR J1802+0128 was timed for 493 days before it was discovered that the true spin period was twice the assumed value. Values presented for P and $\dot{P}$ are twice the values derived by this timing analysis and retain their prior relative errors. Due to the effects of the evolution of profile morphology with frequency and the use of the 20 cm as template for timing 50 cm observations, the formal errors presented for the dispersion measure may have been underestimated. Pulsar names are assigned from their equatorial coordinates in the J2000.0 equinox, with four digits of declination for those with accurate positions from timing solutions, and two digits for those without. The latter names are provisional and will be altered when accurate timing positions become available. Table 5.4 lists additional parameters for the newly discovered pulsars, including the best S/N of the discovery observation(s) and the pulsar's position offset from the centre of the beam, the width of the pulse profile at 10 and 50 per cent of peak intensity, its position in Galactic coordinates, its distance and z-displacement from the Galactic plane under

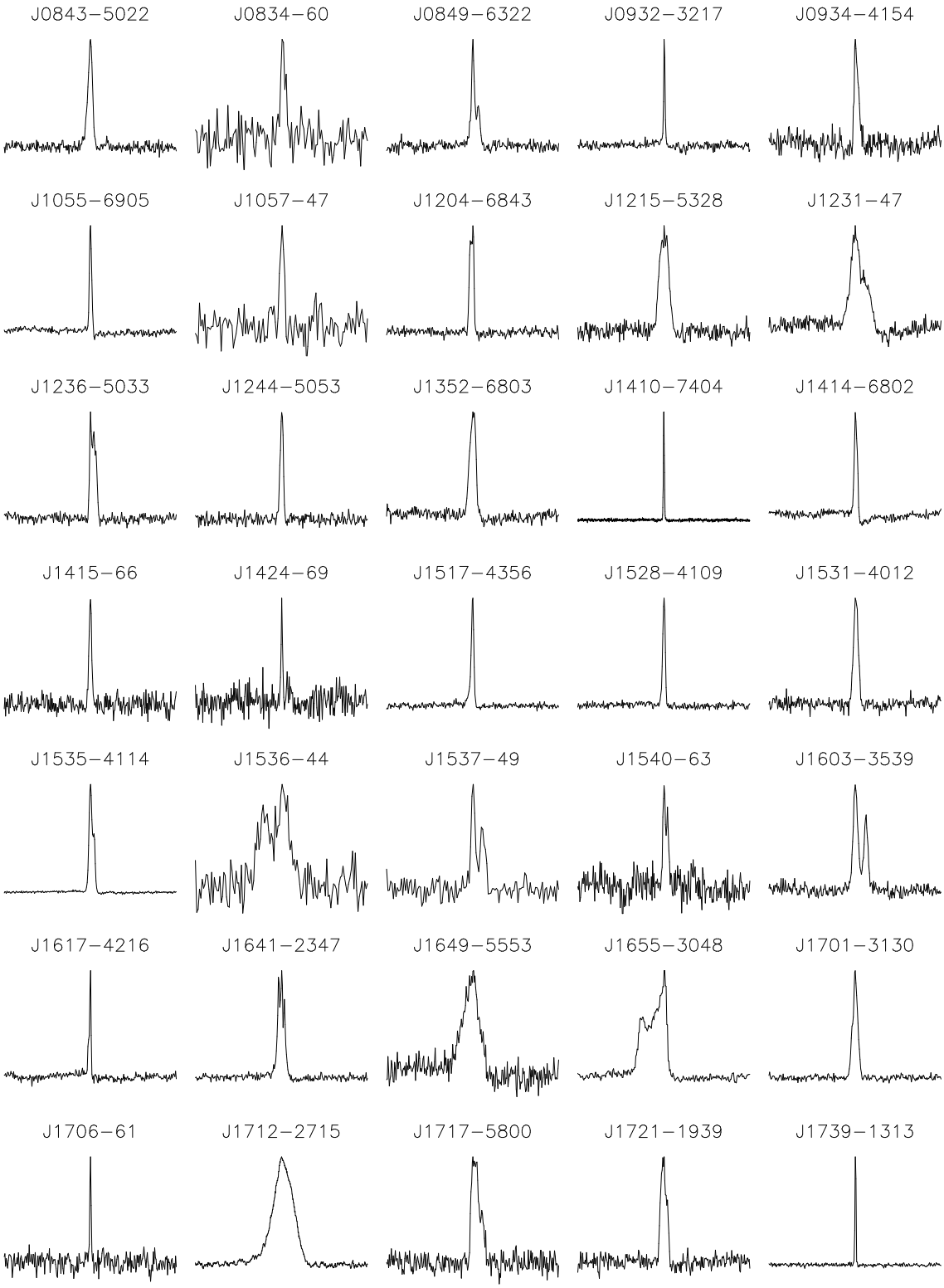

Figure 5.5: Pulse profiles for new slow pulsars

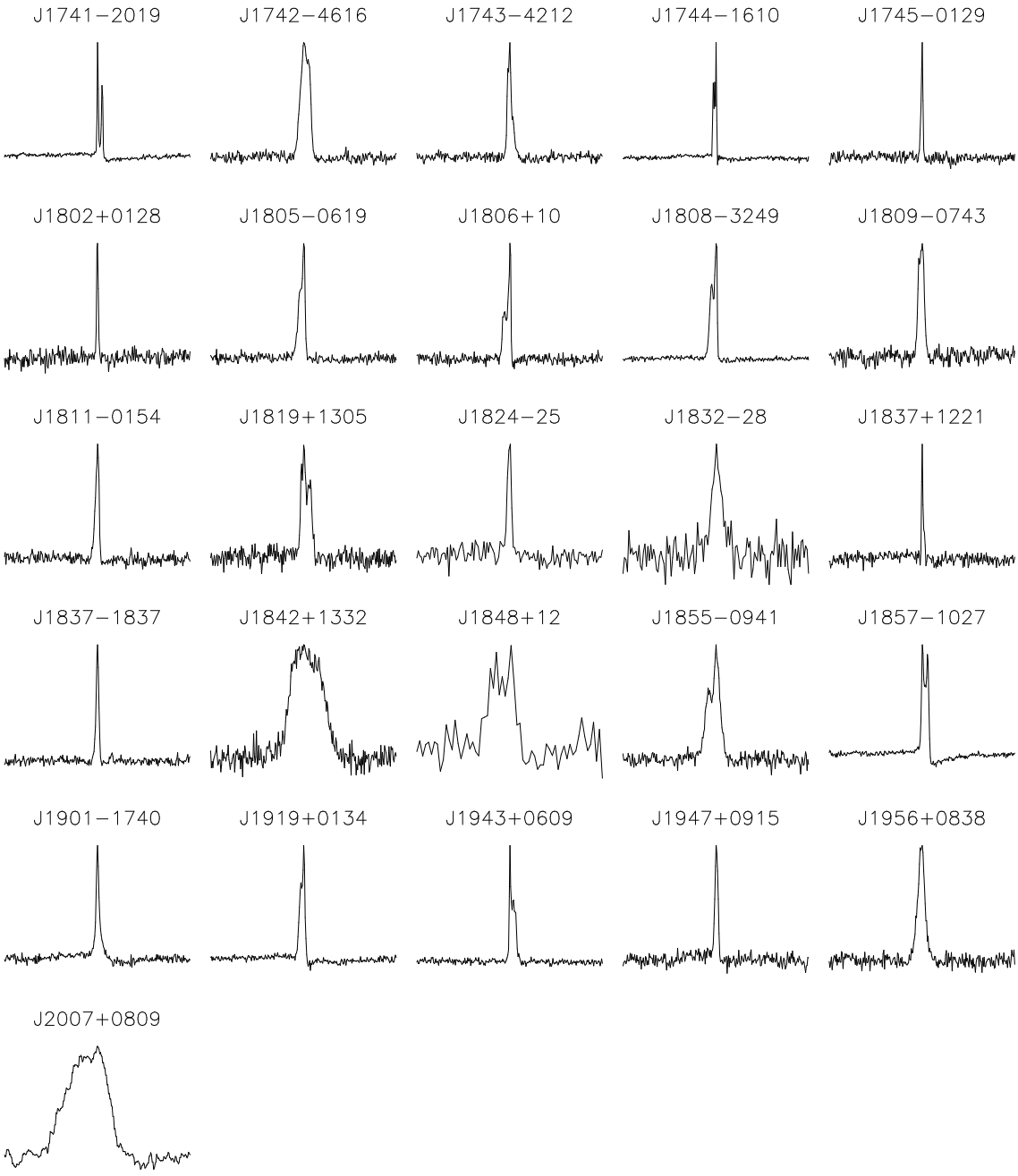

Figure 5.5: *continued* — **Pulse profiles for new slow pulsars**

Table 5.3: Dispersion measure, astrometric and spin parameters for new slow pulsars

Name	α (J2000)	δ (J2000)	P (s)	P Epoch (MJD)	$\dot{P}$ (10^{-15})	DM (cm^{-3} pc)
J0834–60	$08^{h}34^{m}50(40)$	$-60°35(5)'$	0.384645(6)	51401.1	...	20(6)
J0843–5022	$08^{h}43^{m}09\overset{s}{.}884(8)$	$-50°22'43\overset{''}{.}10(8)$	0.2089556931527(14)	51500.0	0.17238(14)	178.47(9)
J0849–6322	$08^{h}49^{m}42\overset{s}{.}59(2)$	$-63°22'35\overset{''}{.}0(1)$	0.367953256307(5)	51500.0	0.7908(5)	91.29(9)
J0932–3217	$09^{h}32^{m}39\overset{s}{.}15(6)$	$-32°17'14\overset{''}{.}2(8)$	1.93162674308(19)	51500.0	0.250(15)	102.1(8)
J0934–4154	$09^{h}34^{m}58\overset{s}{.}20(3)$	$-41°54'19\overset{''}{.}5(3)$	0.570409236430(14)	51650.0	0.269(3)	113.79(16)
J1055–6905	$10^{h}55^{m}44\overset{s}{.}71(9)$	$-69°05'11\overset{''}{.}4(4)$	2.9193969868(3)	51500.0	20.336(15)	142.8(4)
J1057–47	$10^{h}57^{m}45(30)$	$-47°57(5)'$	0.62830(3)	50989.1	...	60(8)
J1204–6843	$12^{h}04^{m}36\overset{s}{.}72(1)$	$-68°43'17\overset{''}{.}19(8)$	0.3088608620097(19)	51500.0	0.21708(19)	133.93(9)
J1215–5328	$12^{h}15^{m}00\overset{s}{.}62(7)$	$-53°28'31\overset{''}{.}6(7)$	0.63641413680(5)	51500.0	0.115(4)	163.0(5)
J1231–47	$12^{h}31^{m}40(30)$	$-47°46(5)'$	1.8732(3)	51200.8	...	31(30)
J1236–5033	$12^{h}36^{m}59\overset{s}{.}15(1)$	$-50°33'36\overset{''}{.}3(1)$	0.294759771191(4)	51500.0	0.1556(4)	105.02(11)
J1244–5053	$12^{h}44^{m}11\overset{s}{.}48(1)$	$-50°53'20\overset{''}{.}6(1)$	0.275207111323(4)	51500.0	0.9998(4)	109.95(12)
J1352–6803	$13^{h}52^{m}34\overset{s}{.}45(4)$	$-68°03'37\overset{''}{.}1(4)$	0.628902546380(16)	51650.0	1.234(3)	214.6(2)
J1410–7404	$14^{h}10^{m}07\overset{s}{.}370(5)$	$-74°04'53\overset{''}{.}32(2)$	0.2787294436271(15)	51460.0	0.00674(9)	54.24(6)
J1414–6802	$14^{h}14^{m}25\overset{s}{.}7(1)$	$-68°02'58(1)''$	4.6301880619(4)	51650.0	6.39(7)	153.5(6)
J1415–66	$14^{h}15^{m}25(50)$	$-66°19(5)'$	0.392480(10)	51396.2	...	261(6)
J1424–69	$14^{h}24^{m}15(60)$	$-69°56(5)'$	0.333415(8)	51309.7	...	123(4)
J1517–4356	$15^{h}17^{m}27\overset{s}{.}34(1)$	$-43°56'17\overset{''}{.}9(2)$	0.650836871901(6)	51500.0	0.2155(6)	87.78(12)
J1528–4109	$15^{h}28^{m}08\overset{s}{.}033(8)$	$-41°09'28\overset{''}{.}8(2)$	0.526556139140(4)	51500.0	0.3955(4)	89.50(10)
J1531–4012	$15^{h}31^{m}08\overset{s}{.}05(1)$	$-40°12'30\overset{''}{.}9(4)$	0.356849312855(6)	51500.0	0.0963(6)	106.65(12)
J1535–4114	$15^{h}35^{m}17\overset{s}{.}07(1)$	$-41°14'03\overset{''}{.}1(3)$	0.432866133845(6)	51500.0	4.0705(6)	66.28(14)
J1536–44	$15^{h}36^{m}15(30)$	$-44°16(5)'$	0.46842(6)	51063.2	...	110(30)
J1537–49	$15^{h}37^{m}30(30)$	$-49°09(5)'$	0.301313(6)	51402.3	...	65(4)
J1540–63	$15^{h}40^{m}20(40)$	$-63°24(5)'$	1.63080(16)	51307.7	...	160(20)
J1603–3539	$16^{h}03^{m}53\overset{s}{.}697(5)$	$-35°39'57\overset{''}{.}1(3)$	0.141908588964(9)	51650.0	0.12425(17)	77.5(4)
J1617–4216	$16^{h}17^{m}23\overset{s}{.}38(5)$	$-42°16'59(1)''$	3.42846630955(13)	51500.0	18.129(15)	163.6(5)
J1641–2347	$16^{h}41^{m}18\overset{s}{.}04(6)$	$-23°47'36(6)''$	1.091008429855(16)	51500.0	0.0411(15)	27.7(3)
J1649–5553	$16^{h}49^{m}31\overset{s}{.}1(1)$	$-55°53'40(2)''$	0.61357070436(7)	51650.0	1.698(16)	180.4(11)
J1655–3048	$16^{h}55^{m}24\overset{s}{.}53(2)$	$-30°48'42(1)''$	0.542935874228(9)	51500.0	0.0366(9)	154.3(3)
J1701–3130	$17^{h}01^{m}43\overset{s}{.}513(5)$	$-31°30'36\overset{''}{.}7(4)$	0.2913414710251(12)	51500.0	0.05596(12)	130.73(6)

Table 5.3: *continued* — **Dispersion measure, astrometric and spin parameters for new slow pulsars**

Name	α (J2000)	δ (J2000)	P (s)	P Epoch (MJD)	$\dot{P}$ (10^{-15})	DM (cm^{-3} pc)
J1706–61	$17^h06^m40(40)$	$-61°11(5)'$	0.361922(8)	51308.7	...	78(6)
J1712–2715	$17^h12^m11\overset{s}{.}71(1)$	$-27°15'53(2)''$	0.255359660118(3)	51500.0	1.2793(3)	92.64(13)
J1717–5800	$17^h17^m35\overset{s}{.}65(2)$	$-58°00'05\overset{''}{.}4(3)$	0.321793346869(6)	51650.0	0.1957(10)	125.22(14)
J1721–1939	$17^h21^m46\overset{s}{.}61(4)$	$-19°39'49(5)''$	0.404039751280(15)	51500.0	0.1283(15)	103(2)
J1739–1313	$17^h39^m57\overset{s}{.}821(6)$	$-13°13'18\overset{''}{.}6(4)$	1.215697613611(9)	51500.0	0.0817(9)	58.2(5)
J1741–2019	$17^h41^m06\overset{s}{.}87(3)$	$-20°19'24(5)''$	3.90450636119(13)	51500.0	16.260(13)	74.9(4)
J1742–4616	$17^h42^m26\overset{s}{.}10(2)$	$-46°16'53\overset{''}{.}5(4)$	0.412401047219(7)	51650.0	0.0338(12)	115.96(14)
J1743–4212	$17^h43^m05\overset{s}{.}223(5)$	$-42°12'02\overset{''}{.}4(2)$	0.3061669878595(16)	51650.0	0.7834(4)	131.94(5)
J1744–1610	$17^h44^m16\overset{s}{.}534(7)$	$-16°10'35\overset{''}{.}8(8)$	1.757205868816(16)	51500.0	2.3767(16)	66.67(14)
J1745–0129	$17^h45^m02\overset{s}{.}06(1)$	$-01°29'18\overset{''}{.}1(4)$	1.045406855598(18)	51650.0	0.631(4)	90.1(11)
J1802+0128	$18^h02^m27\overset{s}{.}45(2)$	$+01°28'23\overset{''}{.}7(4)$	0.554261603931(10)	51650.0	2.109(3)	97.97(12)
J1805–0619	$18^h05^m31\overset{s}{.}436(9)$	$-06°19'45\overset{''}{.}4(4)$	0.454650713078(7)	51650.0	0.9690(13)	146.22(9)
J1806+10	$18^h06^m50(20)$	$+10°24(5)'$	0.484285(15)	51259.8	...	58(6)
J1808–3249	$18^h08^m04\overset{s}{.}48(2)$	$-32°49'34(1)''$	0.364912241765(10)	51500.0	7.0494(10)	147.37(19)
J1809–0743	$18^h09^m35\overset{s}{.}92(1)$	$-07°43'01\overset{''}{.}4(5)$	0.313885674748(5)	51650.0	0.1521(9)	240.70(14)
J1811–0154	$18^h11^m19\overset{s}{.}88(3)$	$-01°54'30\overset{''}{.}9(7)$	0.92494482303(4)	51650.0	1.608(6)	148.1(3)
J1819+1305	$18^h19^m56\overset{s}{.}22(4)$	$+13°05'14\overset{''}{.}2(7)$	1.06036354400(6)	51650.0	0.373(9)	64.9(4)
J1824–25	$18^h24^m15(20)$	$-25°36(5)'$	0.223319(3)	51067.5	...	155(3)
J1832–28	$18^h32^m30(20)$	$-28°43(5)'$	0.199300(3)	51064.3	...	127(3)
J1837+1221	$18^h37^m07\overset{s}{.}12(4)$	$+12°21'54\overset{''}{.}0(6)$	1.96353198352(12)	51650.0	6.200(16)	100.6(4)
J1837–1837	$18^h37^m54\overset{s}{.}25(1)$	$-18°37'08(2)''$	0.618357697387(16)	51500.0	5.4950(12)	100.74(13)
J1842+1332	$18^h42^m29\overset{s}{.}96(6)$	$+13°32'01\overset{''}{.}5(9)$	0.47160357893(3)	51650.0	0.229(7)	102.5(7)
J1848+12	$18^h48^m30(20)$	$+12°50(5)'$	0.75473(7)	51316.7	...	139(20)
J1855–0941	$18^h55^m15\overset{s}{.}68(3)$	$-09°41'02(1)''$	0.34540115992(4)	51500.0	0.240(3)	152.2(3)
J1857–1027	$18^h57^m26\overset{s}{.}45(5)$	$-10°27'01(2)''$	3.6872190477(3)	51650.0	10.55(6)	108.9(7)
J1901–1740	$19^h01^m18\overset{s}{.}03(6)$	$-17°40'00(6)''$	1.95685759005(16)	51500.0	0.823(16)	24.4(6)
J1919+0134	$19^h19^m43\overset{s}{.}62(3)$	$+01°34'56\overset{''}{.}5(7)$	1.60398355528(6)	51650.0	0.589(11)	191.9(4)
J1943+0609	$19^h43^m29\overset{s}{.}132(5)$	$+06°09'57\overset{''}{.}6(1)$	0.446226281658(3)	51650.0	0.4659(6)	70.76(6)
J1947+0915	$19^h47^m46\overset{s}{.}22(5)$	$+09°15'08\overset{''}{.}0(8)$	1.48074382424(9)	51650.0	0.478(16)	94(4)
J1956+0838	$19^h56^m52\overset{s}{.}26(2)$	$+08°38'16\overset{''}{.}8(4)$	0.303910924347(7)	51650.0	0.2199(13)	68.2(13)
J2007+0809	$20^h07^m13\overset{s}{.}5(1)$	$+08°09'33(2)''$	0.32572436605(5)	51650.0	0.137(7)	53.9(10)

Table 5.4: Detection parameters, pulse widths and derived parameters for new slow pulsars

Name	Δ pos ($'$)	S/N	w_{50} (°)	w_{10} (°)	l (°)	b (°)	d (kpc)	$\|z\|$ (kpc)	τ_c (Myr)	B (10^{12} G)	$\dot{E}$ (10^{30} erg s^{-1})
J0834–60	...	13.9	...	...	−83.9	−11.9	0.5	0.10	...	...	...
J0843–5022	...	10.1	11.0	50.0	−91.5	−4.9	7.7	0.66	19.2	0.19	746
J0849–6322	3.9	13.2	7.0	166.3	−80.6	−12.2	> 8.4	> 1.8	7.37	0.55	627
J0932–3217	5.9	17.1	3.4	7.6	−98.7	14.1	3.8	0.93	122	0.70	1.37
J0934–4154	4.4	10.4	10.1	...	−91.6	7.4	3.2	0.41	33.5	0.40	57.3
J1055–6905	3.5	17.8	5.8	10.7	−67.1	−8.5	> 12	> 1.8	2.27	7.8	32.3
J1057–47	...	16.3	11.5	...	−76.0	10.7	3.0	0.56	...	...	...
J1204–6843	5.5	18.5	10.6	15.2	−61.3	−6.2	5.7	0.61	22.5	0.26	291
J1215–5328	8.1	12.9	22.6	...	−62.5	9.0	> 11	> 1.8	87.4	0.27	17.7
J1231–47	...	28.5	30.7	...	−60.5	15.0	1.6	0.42	...	...	...
J1236–5033	3.2	13.2	14.7	20.8	−59.4	12.2	> 8.3	> 1.8	30.0	0.22	240
J1244–5053	4.3	12.4	8.1	...	−58.2	12.0	> 8.5	> 1.8	4.36	0.53	1894
J1352–6803	3.5	32.7	16.0	188.9	−51.4	−5.9	14	1.4	8.07	0.89	196
J1410–7404	5.7	30.4	2.3	4.5	−51.7	−12.0	2.1	0.45	655	0.044	12.3
J1414–6802	2.0	27.3	7.8	14.0	−49.4	−6.4	6.6	0.74	11.5	5.5	2.54
J1415–66	...	26.3	6.5	...	−48.8	−4.8	14	1.2	...	...	...
J1424–69	...	13.0	3.6	...	−49.2	−8.5	6.3	0.94	...	...	...
J1517–4356	5.6	11.8	6.1	14.4	−31.1	11.5	4.4	0.88	47.8	0.38	30.9
J1528–4109	3.7	19.8	6.4	12.3	−27.9	12.7	6.0	1.3	21.1	0.46	107
J1531–4012	5.3	15.4	11.1	...	−26.9	13.1	> 7.8	> 1.8	58.7	0.19	83.6
J1535–4114	3.8	95.0	12.5	18.3	−26.8	11.8	2.8	0.57	1.68	1.3	1981
J1536–44	...	15.8	...	...	−28.5	9.3	5.3	0.85	...	...	...
J1537–49	...	14.5	26.3	...	−31.3	5.2	1.7	0.16	...	...	...
J1540–63	...	25.3	12.4	...	−39.4	−6.5	7.5	0.84	...	...	...
J1603–3539	4.1	13.3	30.4	...	−18.8	12.5	3.8	0.83	18.1	0.13	1716
J1617–4216	5.1	10.3	3.7	9.5	−21.5	5.9	6.3	0.65	3.00	8.0	17.8
J1641–2347	3.7	85.1	16.2	29.7	−4.2	14.7	1.3	0.34	421	0.21	1.25
J1649–5553	7.3	13.5	39.9	...	−27.9	−7.1	14	1.7	5.73	1.0	290
J1655–3048	...	32.3	57.0	72.9	−7.8	7.9	8.6	1.2	235	0.14	9.02
J1701–3130	5.9	26.8	11.6	23.5	−7.5	6.4	4.5	0.50	82.5	0.13	89.3

Table 5.4: *continued* — **Detection parameters, pulse widths and derived parameters for new slow pulsars**

Name	Δ pos (′)	S/N	w_{50} (°)	w_{10} (°)	l (°)	b (°)	d (kpc)	$\|z\|$ (kpc)	τ_c (Myr)	B (10^{12} G)	$\dot{E}$ (10^{30} erg s^{-1})
J1706–61	...	21.6	2.8	...	−30.8	−12.1	3.8	0.80	...	...	...
J1712–2715	1.1	41.7	46.5	90.2	−2.7	7.1	3.1	0.38	3.16	0.58	3033
J1717–5800	5.0	10.9	23.5	...	−27.3	−11.5	> 8.8	> 1.8	26.1	0.25	232
J1721–1939	4.6	9.7	16.9	...	4.9	9.6	4.7	0.78	49.9	0.23	76.8
J1739–1313	3.3	22.6	2.4	5.3	12.8	9.3	2.0	0.33	236	0.32	1.80
J1741–2019	6.0	59.6	11.1	13.8	6.8	5.4	2.0	0.19	3.80	8.1	10.8
J1742–4616	3.1	26.3	21.8	33.2	−15.2	−8.5	5.0	0.74	193	0.12	19.0
J1743–4212	5.2	19.6	8.6	18.8	−11.6	−6.5	4.7	0.53	6.19	0.50	1078
J1744–1610	...	12.8	7.4	10.2	10.8	6.9	2.0	0.24	11.7	2.1	17.3
J1745–0129	5.4	12.2	2.4	8.3	23.8	14.0	> 7.3	> 1.8	26.3	0.82	21.8
J1802+0128	1.9	12.5	4.1	...	28.6	11.6	> 8.8	> 1.8	4.16	1.1	489
J1805–0619	6.0	11.1	12.7	23.0	22.0	7.2	6.7	0.84	7.43	0.67	407
J1806+10	...	66.3	6.7	...	37.3	14.6	4.0	1.0	...	...	...
J1808–3249	2.1	40.8	13.8	20.7	−1.0	−6.1	5.1	0.54	0.82	1.6	5727
J1809–0743	1.3	13.0	13.8	...	21.2	5.7	> 18	> 1.8	32.7	0.22	194
J1811–0154	3.8	21.8	8.2	77.8	26.6	8.0	9.6	1.3	9.12	1.2	80.2
J1819+1305	5.1	14.3	21.4	...	41.2	12.8	4.4	0.98	45.0	0.64	12.4
J1824–25	...	15.6	9.3	...	7.1	−5.9	5.2	0.53	...	...	...
J1832–28	...	18.0	21.3	...	5.1	−8.9	6.4	1.00	...	...	...
J1837+1221	4.9	16.1	3.1	...	42.4	8.7	6.1	0.93	5.02	3.5	32.3
J1837–1837	4.8	11.0	5.8	11.6	14.8	−5.5	3.0	0.29	1.78	1.9	918
J1842+1332	3.5	33.1	72.5	...	44.1	8.1	5.9	0.83	32.6	0.33	86.2
J1848+12	...	17.8	51.0	...	44.1	6.5	7.5	0.84	...	...	...
J1855–0941	2.9	19.1	26.1	...	24.7	−5.2	4.9	0.45	22.8	0.29	230
J1857–1027	0.9	71.4	14.6	20.5	24.3	−6.1	3.6	0.38	5.54	6.3	8.31
J1901–1740	5.5	131.0	6.6	22.1	18.1	−10.1	1.3	0.22	37.7	1.3	4.34
J1919+0134	5.0	34.2	10.5	18.2	37.6	−5.6	10	0.99	43.1	0.98	5.64
J1943+0609	2.5	30.1	8.9	17.7	44.5	−8.6	3.9	0.58	15.2	0.46	207
J1947+0915	6.1	12.7	7.5	...	47.7	−8.1	5.8	0.81	49.1	0.85	5.81
J1956+0838	5.8	15.0	15.4	...	48.3	−10.3	4.3	0.77	21.9	0.26	309
J2007+0809	5.2	14.4	92.8	...	49.2	−12.8	3.4	0.76	37.7	0.21	156

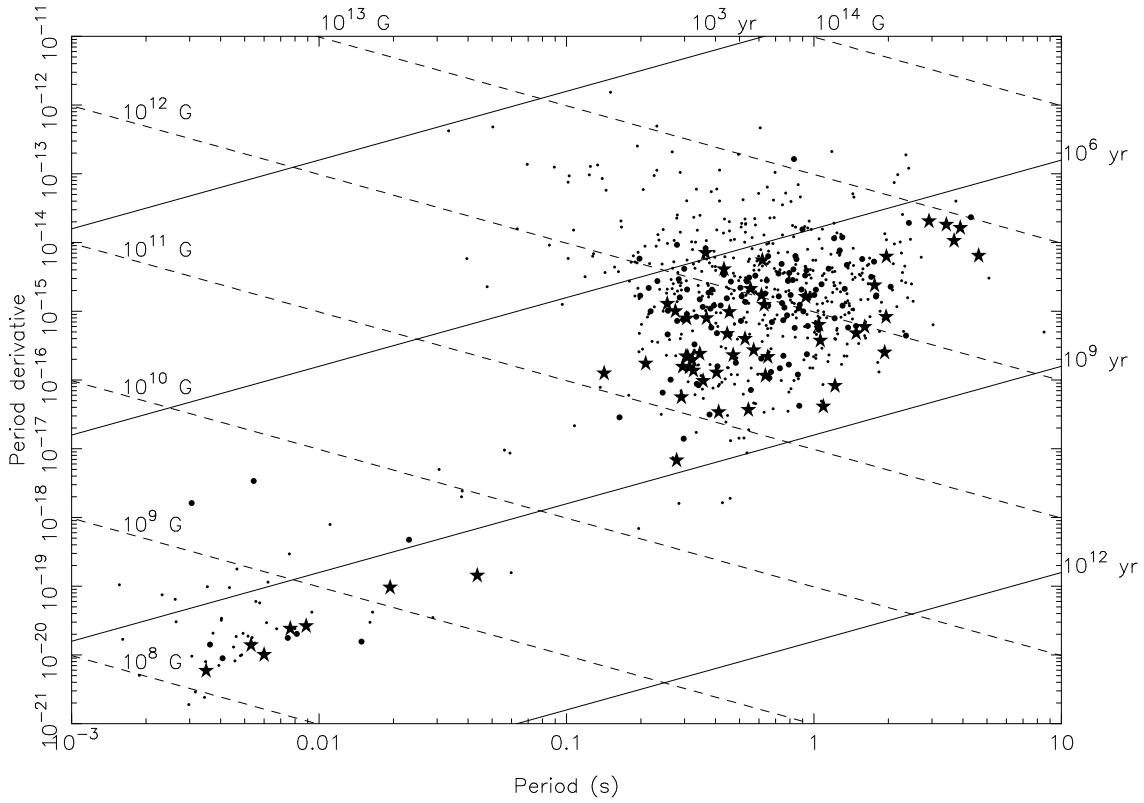

Figure 5.6: Distribution in pulse period and period derivative of new pulsars (stars),previously known pulsars in the survey region (large dots) and all other known pulsars (small dots), where such values have been measured. Also plotted are solid and dashed lines of constant characteristic age ($\tau_c \equiv P/2\dot{P}$) and inferred surface magnetic field strength ($B = 3.2 \times 10^{19}$ G s$^{-1/2}\sqrt{P\dot{P}}$) respectively.

the model of Taylor & Cordes (1993) (accurate to 30 per cent on average), and inferred parameters concerning the pulsar spin-down. These assume magnetic dipole spin-down and comprise the characteristic age ($\tau_c \equiv P/2\dot{P}$), surface magnetic field strength ($B = 3.2 \times 10^{19}$ G s$^{-1/2}\sqrt{P\dot{P}}$) and spin-down power ($\dot{E} = 4\pi^2 I \dot{P} P^{-3}$, assuming $I = 10^{45}$ g cm^2 for the moment of inertia of the neutron star). Both tables are accessible on the internet in machine-readable format at the Swinburne Pulsar Group home page[3]. For several pulsars the dispersion measure is higher than that allowed in the given direction under the model of Taylor & Cordes (1993), and the values presented are given as lower limits. Such findings are not uncommon (e.g. Camilo & Nice 1995; D'Amico et al. 1998), and indicate that the model probably underestimates the scale height of the Galactic electron distribution.

The spin parameters of the newly discovered systems are similar to those of

[3]http://www.astronomy.swin.edu.au/pulsar

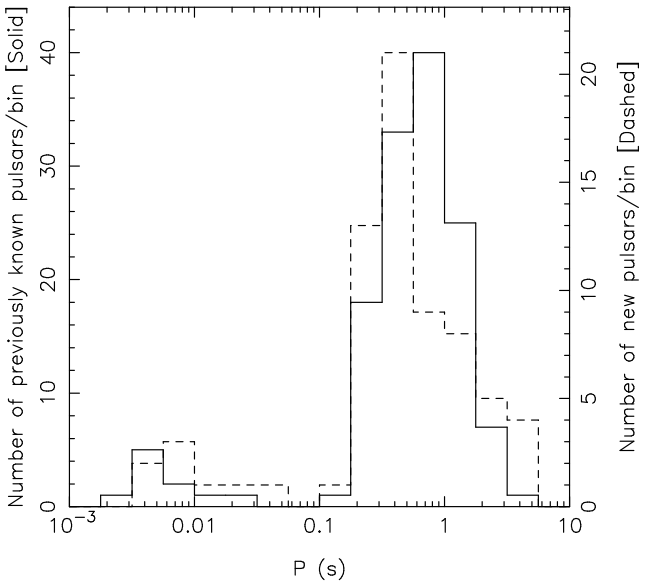

Figure 5.7: Histograms depicting distribution in pulse period of new pulsars (dashed line) and previously known pulsars in the survey region (solid line).

pulsars previously known in the search region. Figure 5.6 shows the distribution in period and period derivative of new pulsars with timing solutions and of previously known pulsars inside and outside the survey region. Both new and previously known slow pulsars in the region tend to have longer inferred characteristic ages than those outside the survey region, by simple virtue of the fact that pulsars are born near the Galactic plane and typically take several Myr to reach a z-height corresponding to $|b| > 5^\circ$ (for typical distances of several kpc). Figure 5.7 shows histograms of pulse period for the new and previously known population. It appears that this survey has uncovered a higher fraction of pulsars in the period range of 6–50 ms, however this effect is not highly significant : a Kolmogorov-Smirnov (K-S) test on the distributions for $P < 100$ ms yields a 46 per cent probability of the two samples arising from the same parent distribution. When binary evolution considerations are taken into account and the new sample restricted to the four MSPs with probable helium companions the significance rises to 91 per cent, however due to the small sample size this result must be treated with caution (Edwards & Bailes 2001a).

The discrepancy in the case of the slow pulsar population is more significant, with a K-S test indicating a different distribution at the 98 per cent level. The reason for the discrepancy, which is mainly seen as a deficit of pulsars with $P \simeq 1$ s, is not well understood. The problem remains (at 94 per cent significance) when

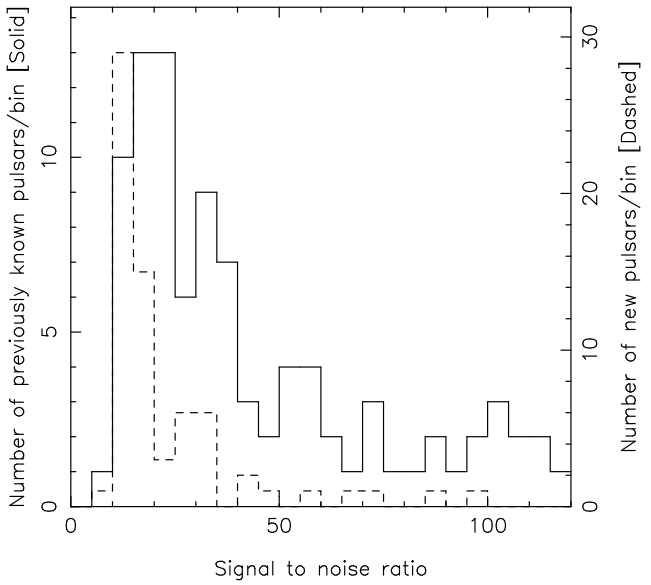

Figure 5.8: Histograms depicting distribution in maximum detected signal to noise ratio (S/N) of new pulsars (dashed line) and previously known pulsars in the survey region (solid line). One new and 8 known pulsars had S/Ns greater than 120 and are not included in this plot for clarity in low S/N bins.

the new sample is compared only to those previously known pulsars re-detected in this survey, confirming that the survey was able to detect pulsars in the period range in question. However, if there existed (by an unknown mechanism) a reduced sensitivity (or higher effective threshold signal to noise ratio) around $P \simeq 1$ s, one might expect the period distribution of the new pulsars to be more strongly affected than that of the previously known pulsars since the new population is on average of lower flux density. We note that the rejection of pulsars as mis-categorised interference signals cannot explain this result, since in this case one would expect an equal rate of rejections of new and previously known pulsars independent of signal to noise ratio or flux density. Comparison of the (yet to be measured) flux densities of new pulsars in and out of the depleted period range will help in evaluating the effective sensitivity of the survey as a function of period.

Figure 5.8 shows the distribution of signal to noise ratios in the best detections of new and previously known pulsars. As one would expect, most of the pulsars with high signal to noise ratios were detected in earlier surveys. A few of the new pulsars however were very strong and may have been missed in earlier surveys due to scintillation or due to an intrinsically flat spectrum. It is apparent from the histogram and from inspection of Tables 5.1 and 5.4 that the threshold signal

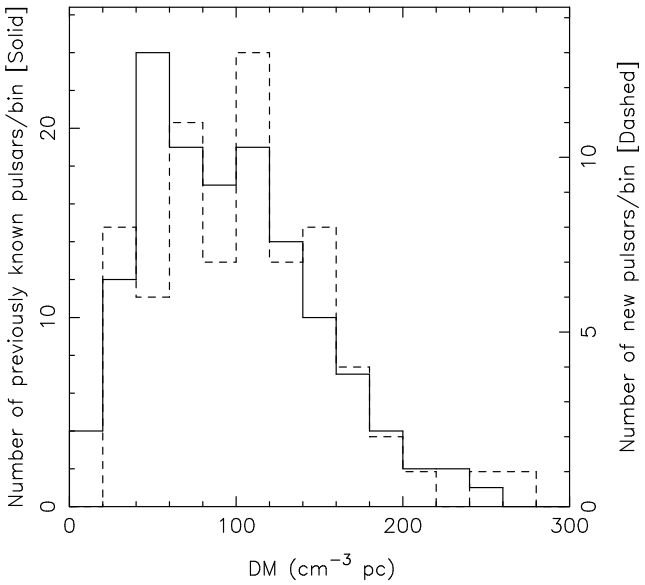

Figure 5.9: Histograms depicting distribution in dispersion measure of new pulsars (dashed line) and previously known pulsars in the survey region (solid line).

to noise ratio for this survey is approximately 10, in contrast to the value of 8.0 commonly used in previous surveys in assessing sensitivity. Numerous promising candidates with signal to noise ratios in the range of 8–10 were subjected to re-observation however only one was re-detected in such observations despite using longer integration times, probably because they actually arose from interference or by random chance (given the size and dimensionality of the search space).

As noted in the introduction, high frequency surveys are also expected to sample a different area of the pulsar spectral index distribution, compared to low frequency surveys. The sensitivity of the present work to a pulsar with a spectral index of -1.7 (typical of those discovered at 70 cm; Toscano et al. 1998) is comparable to that of the Parkes Southern Pulsar Survey (Manchester et al. 1996), the most sensitive previous 70 cm search to cover a large region of the area observed by the present study. One therefore expects the distances of the newly discovered pulsars to be comparable to the previously known population in the region, and as shown in Figure 5.9, this is indeed the case. The bulk of newly discovered pulsars had S/Ns $\lesssim$ 30, suggesting (in conjunction with their non-detection in the 70 cm survey) spectral indices of up to -0.7. Eleven newly discovered pulsars are visible from the 305-m Arecibo telescope and were presumably within the search area of previous surveys conducted there (Foster et al. 1995; Camilo et al. 1996; Ray et al. 1996;

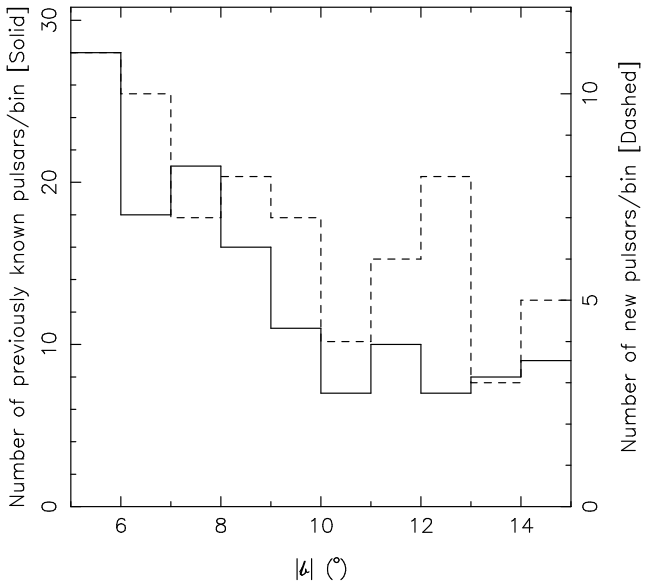

Figure 5.10: Histograms depicting distribution in angular displacement from the Galactic plane of new pulsars (dashed line) and previously known pulsars in the survey region (solid line).

Lommen et al. 2000), which were typically sensitive to ($\delta = 0.1$) pulsars brighter than $\sim$ 1 mJy at 70 cm. Their non-detection in the Arecibo surveys suggests $\alpha \gtrsim -1.1$. Several pulsars were discovered at high S/N, which could be indicative of positive spectral indices (for example, J1806+10 in Arecibo territory, yielding $\alpha \simeq 2.6$), however the non-detections may well be the result of incomplete surveys or interstellar scintillation.

Accurate characterization of the spectral indices of the newly discovered pulsars must await calibrated multi-frequency flux density measurements, however we note in passing that the detection of these pulsars at 660 MHz required significantly more integration time than expected for pulsars of average spectral index. As indicated by the lack of any enhanced preference for low Galactic latitudes in the newly detected sample compared to the previously known pulsars (Figure 5.10), reduced scatter-broadening at 20-cm in general does not appear to have been a significant factor in the discovery of the new pulsars.

5.3.3 Individual Pulsars of Interest

As previously reported (Edwards & Bailes 2001a), the pulse profile of PSR J1410–7404 is exceedingly narrow and contradicts the pulse width – period relation of

Rankin (1990). Since all major contradictions in the past have been from apparently recycled pulsars, it is conceivable that J1410–7404 is also recycled, a hypothesis supported by the small magnetic field strength inferred from timing observations. The newly discovered pulsar J1706–61 also has a measured profile width seemingly in disagreement with Rankin (1990), in this case being 70 per cent of the predicted minimum width. However, we caution that this measurement derives from a single observation of moderate signal-to-noise ratio (as visible in Figure 5.5) and that a more definite conclusion awaits the availability of an extended data set from ongoing timing observations. Should the improved profile maintain the narrow width derived here, the magnetic field strength and characteristic age derived from timing measurements will be of great utility in evaluating the recycling hypothesis for PSRs J1410–7404 and J1706–61.

As expected from the relatively old age of the sample detected here, numerous pulsars appear to exhibit noticeable pulse nulling (e.g. Ritchings 1976). Several pulsars also show drifting sub-pulses (e.g. Backer 1973) of varying degrees of regularity. Figure 5.11 depicts the instantaneous flux density of four newly discovered pulsars as a function of pulse phase and pulse number. It is apparent that the emission of PSRs J1231–47 and J1919+0134 is strongly modulated by sub-pulses showing very regular drift. PSR J1857–1027 also appears to show drifting sub-pulses in this and other observations, although as a result of the short duration of observations made for timing analysis, combined with the long pulse period ($\sim$ 3.7 s), the number of pulses recorded and hence the conspicuousness of this effect in archival observations is reduced. Detailed analysis of these pulsars will appear in a forthcoming paper (Ord et al. in preparation).

Pulse nulling appears to occur on a wide range of time scales in the detected pulsars. The data for PSR J1231–47 in Figure 5.11 were recorded in a second attempt at confirmation of this pulsar, resulting in a signal to noise ratio of 82 in an observation of 530 s. Several subsequent observations of between 900 and 4000 s succeeded in producing only one further weak detection of the pulsar. PSRs J1857–1027 and J1055–6905 appear to null on more typical timescales of $\sim$1–50 pulses, as shown in Figure 5.11. Future observations of the candidate nulling pulsars from our sample will enable analysis similar to that of Ritchings (1976), which in turn will help decide whether the observed flux density variations arise due to nulling or simply as a result of interstellar scintillation.

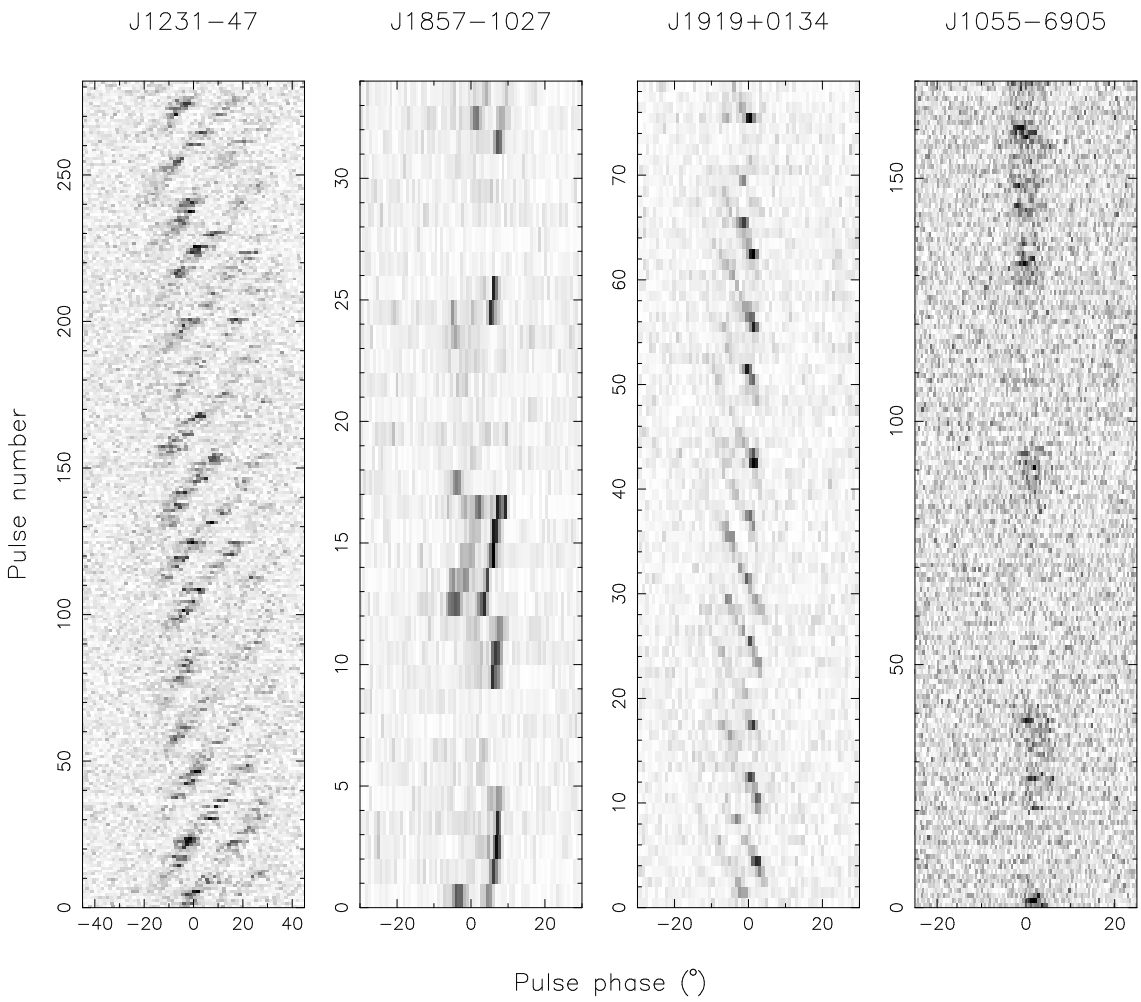

Figure 5.11: Greyscale plots of detected flux density as a function of pulse phase and pulse number for four newly discovered pulsars. Each row represents a single pulse.

5.4 Conclusions

We have conducted a survey of intermediate latitudes of the southern Galaxy for pulsars at ∼1400 MHz. The new 13-beam 21-cm receiver of the Parkes radio telescope was used to rapidly cover to moderate depth a large region of sky flanking the area of the deeper ongoing Galactic plane survey (Lyne et al. 2000a; Camilo et al. 2000b). The interference environment was formidable, however development of a comprehensive scheme for the rejection of pulsar candidates arising from interference enabled the realisation of the full expected survey sensitivity of approximately 0.5 mJy for slow and most millisecond pulsars. The survey was highly successful, detecting 170 pulsars of which 69 were previously unknown, in a relatively short observing campaign. The new discoveries are not significantly more distant than the previously known population in this region of sky, indicating that the success of the survey is attributable to its sampling of a different portion of the broad distribution of pulsar spectral indices. The detected sample, in combination with those of the Galactic plane and high-latitude surveys (when complete), will prove invaluable for population modelling due to the use of a common observing system to cover a large area of sky at high radio frequency.

Among the most interesting new objects are two recycled pulsars with massive white dwarf companions (Edwards & Bailes 2001b), four with probable low-mass He dwarf companions, two isolated millisecond pulsars, and one "slow" pulsar with a very narrow pulse profile and small period derivative, suggestive of recycling in a scenario similar to those of the known double neutron star systems (Edwards & Bailes 2001a). As expected from the large Galactic z-height of much of the survey volume, the detected population of slow pulsars was relatively old and as such exhibited a high fraction of pulsars showing nulling and sub-pulse modulation. Two pulsars show very regular drifting sub-pulses and are analysed in detail elsewhere (Ord et al. in preparation).

Chapter 6

Baseband Searching for Sub-Millisecond Pulsars

This Chapter has been submitted to The Astrophysical Journal as Edwards, van Straten, and Bailes, "A Search for Sub-Millisecond Pulsars".

Abstract

We have conducted a search of 19 southern Galactic globular clusters for sub-millisecond pulsars at 660 MHz with the Parkes 64-m radio telescope. To minimise dispersion smearing we used the CPSR baseband recorder, which samples the 20 MHz observing band at the Nyquist rate. By possessing a complete description of the signal we could synthesise an optimal filterbank in software, and in the case of globular clusters of known dispersion measure, much of the dispersion could be removed using coherent techniques. This allowed for very high time resolution (25.6 μs in most cases), making our searches in general sensitive to sub-millisecond pulsars with flux densities greater than about 3 mJy at 50 cm. No new pulsars were discovered, placing important constraints on the proportion of pulsars with very short spin periods in these clusters.

6.1 Introduction

With the discovery of the first "millisecond" pulsar, B1937+21 ($P = 1.56$ ms; Backer et al. 1982), it became clear that neutron stars can achieve very rapid rotation rates.

This period is close to but still somewhat greater than the minimum rotation period for a neutron star, below which the star becomes unstable to mass shedding at the equator (see e.g. Cook, Shapiro & Teukolsky 1994). Various equations of state have been proposed for nuclear matter and due to the differences in density under such equations, the limiting spin period of neutron stars depends on the choice of equation of state. The discovery of a pulsar with $P < 1$ ms would be of great value in eliminating potential equations of state. The distribution of periods of known pulsars cuts off quite sharply below about $P = 2$ ms, however it is not clear whether this cut-off is intrinsic to the pulsar population (see Lorimer et al. 1996). Most previous pulsar surveys had a time resolution of ~ 300 μs for nearby pulsars, resulting in a strong decline in sensitivity for periods less than a few milliseconds, indicating that the short-period cut-off may in fact be a selection effect. The only effective way to answer this question is to conduct surveys with sufficient time resolution to be well-sensitive to pulsars with $P < 1$ ms, and preferably with a flat sensitivity response to periods well below a millisecond in order to eliminate any bias towards longer pulse periods. For a traditional analogue filterbank system this would require a large number of channels with fast sampling and would involve considerable cost. An alternative is to record the raw receiver voltages at baseband and to perform all frequency decimation and detection in software for the best possible time and frequency resolution. Until recently this approach has been little used due to the formidable data storage and processing requirements, however the rapid development that has occured in these areas in the last decade means that the required hardware is now relatively affordable. We report here for the first time the use of baseband processing in a pulsar survey.

Historically approximately half of all millisecond pulsar discoveries were made in Globular clusters, with most of the remainders found in large scale surveys of the Galaxy. Since the cores of most Globular clusters are easily contained in a single telescope beam for low to intermediate observing frequencies, globular cluster searches are very efficient in their return of millisecond pulsars for observing campaigns of limited duration. Due to the large amounts of data to be processed from observations of high time and frequency resolution, globular clusters are a logical place to begin the search for sub-millisecond pulsars. We conducted several observations of each of 19 southern globular clusters with the CPSR baseband recording system (van Straten, Britton & Bailes 2000) at the Parkes radio telescope. This paper describes the searches and their results.

6.2 Observations and Analysis

In an observing run of four days from 2000 March 17–20 we conducted observations of 19 southern Galactic globular pulsars with the Parkes 64-m radio telescope. The signals from two orthogonal linear polarizations of the 50-cm receiver were mixed to baseband in a quadrature down-convertor and filtered to provide a 20 MHz band centered at a sky frequency of 660 MHz. The in-phase and quadrature components in each polarization were 2-bit sampled at a sample rate of 20 Msamples s^{-1} in accordance with the Nyquist theorem for complete description of the band-limited signal. Sampler thresholds were set at the beginning of the observation in accordance with the prescriptions of Jenet & Anderson (1998) and were held at these values for the duration of each observation. The resultant data stream had a bit-rate of 20 MB s^{-1} and was written in segments of ~ 53.7 s (corresponding to 1 GB of data) to DLT 7000 tapes. The recording system consisted of four DLT drives, a large disk array and a Sun Ultra 60 workstation and in conjunction with the down-conversion and sampling systems is known as the Caltech-Parkes-Swinburne Recorder (CPSR) (van Straten et al. , in preparation). A total of 55 observations of 30 minutes' duration each were recorded, resulting in a 1.8 TB data-set.

The observations were processed on the 64-node Swinburne workstation cluster. Each observation could be processed by one of the schemes described below in about 12 hours using 12 500 MHz Compaq EV6 processors. Tapes were unloaded to a 1-TB RAID array to facilitate the reassembly of full 30-minute contiguous data streams from the 1 GB files that were distributed across four or more tapes during recording. The statistics of samples in each file were examined and any files partially recorded before the sampler levels were correctly set were discarded.

In order to allow an efficient search in dispersion measure (DM), a filterbank was synthesised in software. The data were loaded in segments and each polarization in each segment was transformed to the Fourier domain by means of an FFT. The spectrum was then divided into 512 equal sections and each section was transformed back to the time domain with an inverse FFT to produce a number of time samples in each of 512 frequency channels. The resultant sample interval in each channel was 25.6 μs. In the case of observations of clusters with previously known pulsars, we convolved each channel with a filter matched to the inverse of the response function of the interstellar dispersion at the estimated dispersion measure to the cluster (Hankins & Rickett 1975) by multiplication while the data was still in the

Fourier domain. The squared magnitude of each sample was taken and samples were summed in polarization pairs.

The resultant data was similar in form to that recorded from orthodox analogue filterbanks, with the exception that each channel was recorded at half its Nyquist rate[1], much faster than commonly practiced with analogue filters. In addition, the use of coherent de-dispersion in clusters with known pulsars meant that the dispersion smearing induced across each channel arose only from the difference between the true and assumed dispersion measure, and was generally expected to be much shorter than the sample interval. The dispersion smearing experienced by pulsars in clusters lacking a DM estimate is given approximately by DM/22.7 pc cm^{-3} in units of samples of 25.6 μs in duration, where 22.7 pc cm^{-3} is the so-called "diagonal" DM. Unlike filterbank data where the 1-bit samples in each channel are typically made with independent thresholds, in our scheme the relative power level in each channel was known, allowing us to automatically discard data in channels contaminated by narrow-band terrestrial interference sources.

The synthesised filterbank data for each observation were partially de-dispersed with the "tree" algorithm of Taylor (1974) before being subject to a search process similar to that used for the intermediate latitude multibeam survey (Chapter 5). Data were de-dispersed and summed into time series at a range of trial dispersion measures, either about a nominal cluster DM for those with known pulsars, or up to a maximum of 732 pc cm^{-3} in 1463 steps spaced as described in Chapter 5. It is possible that the motion of a pulsar in its orbit about a close companion could induce significant change in the observed pulse period over the course of the observation, and for this reason we incorporated an acceleration search. For each trial dispersion measure we computed several time series re-binned in such a way as to compensate for the effects of a range of values of acceleration. The method used was similar to that described by (Camilo et al. 2000a). The resulting time series with trial pairs of values for dispersion measure and acceleration were then searched for periodicities and a page of diagnostic information was produced for each potentially significant candidate.

The performance of much of the signal processing in software allows for a considerable degree of flexibility. We used several different sets of parameters as appropriate depending on whether the cluster had a known pulsar and also on the available

[1]The full Nyquist rate could be achieved through the use of complex-to-real inverse transforms, however the time resolution was deemed sufficient as it stood.

Table 6.1: Observations of clusters with known pulsars

Name	Refs	DM (pc cm^{-3})	$N_{\rm obs}$	Notes
47 Tucanae	1,2	23.4–25.4	5	all FD
M4	3	61.9–63.9	3	+3×FD
NGC 6342	4	74.9–76.9	2	+2×FD
NGC 6397	5	70.8–72.8	2	+2×FD
NGC 6440	6	...	3	all SA+FD
Terzan 5	7,8	237.0-242.1	3	+3×FD
NGC 6544	5	133.0–135.0	1	+FD
NGC 6624	9	86.0–88.0	5	+4×FD
M28	10	118.8–120.8	2	+2×FD
NGC 6752	5	33.0–35.0	2	both SA+FA

References: (1) Manchester et al. 1991; (2) Camilo et al. 2000a; (3) Lyne et al. 1988; (4) Lyne et al. 1993; (5) D'Amico et al. 2001b; (6) Manchester et al. 1989; (7) Lyne et al. 1990; (8) Lyne et al. 2000b; (9) Biggs et al. 1994; (10) Lyne et al. 1987

computer time. The scheme denoted FD ("full DM search") searches the full range of dispersion measures from 0 to 732 pc cm^{-3} in 1463 steps with integrations of 1718 s. For clusters with known DM, the scheme known as FA ("full acceleration search") applied the coherent de-dispersion kernels and searched a small specified range of dispersion measures in 201 accelerations evenly spaced in the range given by $|a| \leq 30$ m s^{-2}. Due to the large computational burden of the task, the FA search only processed 859 s of data, using 2^{25}-point transforms. Finally, to maintain sensitivity to accelerated millisecond pulsars in clusters with no DM estimate, we also performed a search denoted SA ("slow acceleration search") which synthesised a filterbank of 256 channels and summed the resultant detected samples in groups of sixteen. The resultant sample rate was 204.8 μs with a diagonal DM of 90.8 pc cm^{-3}, and the full range of 0 to 2950 pc cm^{-3} was searched at 737 trial values. Again, only 859 s of data are processed, with 2^{22}-point transforms and 121 accelerations with $|a| \leq 30$ m s^{-2}.

A total of 10 clusters with previously known pulsars and 9 without were searched as indicated in Tables 1 and 2. The latter were selected from the catalogue of Harris (1996) on the basis of proximity and luminosity. Since Fruchter & Goss (2000) observed several globular clusters in radio continuum and found unidentified steep spectrum emission in NGC 6544, Liller 1, and Terzan 5, it was ensured that these clusters were included in the selection. In the case of those clusters with

Table 6.2: Observations of clusters lacking pulsars

Name	N_{obs}	Notes
NGC 2808	3	+3×FD
E3	3	+3×FD
NGC 3201	3	+3×FD
NGC 4372	4	+4×FD
NGC 4833	3	+4×FD
Ω Centaurus	4	+3×FD
Liller 1	3	+3×FD
M22	2	+2×FD
M30	2	+2×FD

previously known pulsars, most observations were searched with the FA parameters. The dispersion measure range was generally selected in such a way as to include previously published values for pulsars in the cluster and to allow for ± 1 pc cm^{-3} of variation due to gas in the cluster environment. Most observations were also searched with the FD parameters in order to detect unaccelerated pulsars with DMs outside the range of the FA search, as noted in the table. For those clusters without known pulsars, the SA search was applied and in most cases (noted in the table) FD was also used. Observations of NGC 6440 were also subjected to the SA search since the published dispersion measure value was uncertain by ± 10 pc cm^{-3}, making a search at full time resolution over the require DM range computationally complex.

6.3 Results and Discussion

6.3.1 Detections

Offline processing yielded detections of six pulsars, all of which were previously known, including PSR B1744–24A in Terzan 5 with a line-of-sight acceleration of 29 m s^{-2}. The pulsars are listed in Table 6.3 along with their pulse periods and the signal to noise ratio of detections. One promising candidate was observed in 47 Tucanae in an observation centered at MJD 51621.25740, with a topocentric period of 3.756394 ms, a dispersion measure of 24.3 pc cm^{-3} and an acceleration of 7.2 m s^{-2}. The signal-to-noise ratio of this candidate was 9.7, placing it at the threshold of credibility, and in the absence of any other detections of similar periodicities we are hesitant to label the signal a "pulsar". All other periodicities

Table 6.3: Detections

Name	Cluster	P (ms)	S/Ns
B0021–72D	47 Tucanae	5.35	34.3, 11.3
B0021–72E	47 Tucanae	3.54	15.4
B1620-26	M4	11.1	23.7,22.8,20.5
B1744-24A	Terzan 5	11.6	11.0
B1820-30A	NGC 6624	5.44	15.3
B1821-24	M28	3.05	10.4, 18.1

were consistent with random chance (due to the complexity of the search space) or persistent terrestrial interference.

The pulse profiles for the six detected pulsars are presented in Figure 6.1. Whilst the signal to noise ratios are largely poor, these profiles are of much greater time resolution than those previously published. In particular, multiple components are now resolved in the "D" and "E" pulsars of 47 Tucanae and the M4 pulsar. In the work of Camilo et al. (2000a) conducted at 20 cm, two components were observed in 47 Tuc E, and in retrospect some hint of the extra components of 47 Tuc D can also be discerned in the published profile, despite being smeared by ∼0.06 turns of phase through the use of an incoherent filterbank. The triple-component profile of the M4 pulsar was observed in all three detections, in contrast to the previously published 70-cm profile (Lyne et al. 1988) in which the outer components (if present at this frequency) were unresolved despite the nominally sufficient time resolution of ~ 0.03 turns.

6.3.2 Sensitivity

The sensitivity of pulsar observations is a function of the radiometer noise and the observed duty cycle. After Dewey et al. (1985), the minimum detectable mean flux density is

$$S_{\rm min} = \frac{\alpha\beta T_{\rm sys}}{G\sqrt{N_{\rm pol}Bt_{\rm obs}}}\sqrt{\frac{\delta}{1-\delta}} \tag{6.1}$$

where α is the threshold signal to noise ratio, β is a dimensionless loss factor,, $T_{\rm sys}$ is the system temperature, G is the telescope gain, $N_{\rm pol}$ is the number of polarizations, B is the observing bandwidth, t is the integration time and δ is the effective duty cycle. The observed pulses are broadened somewhat relative to those actually emitted

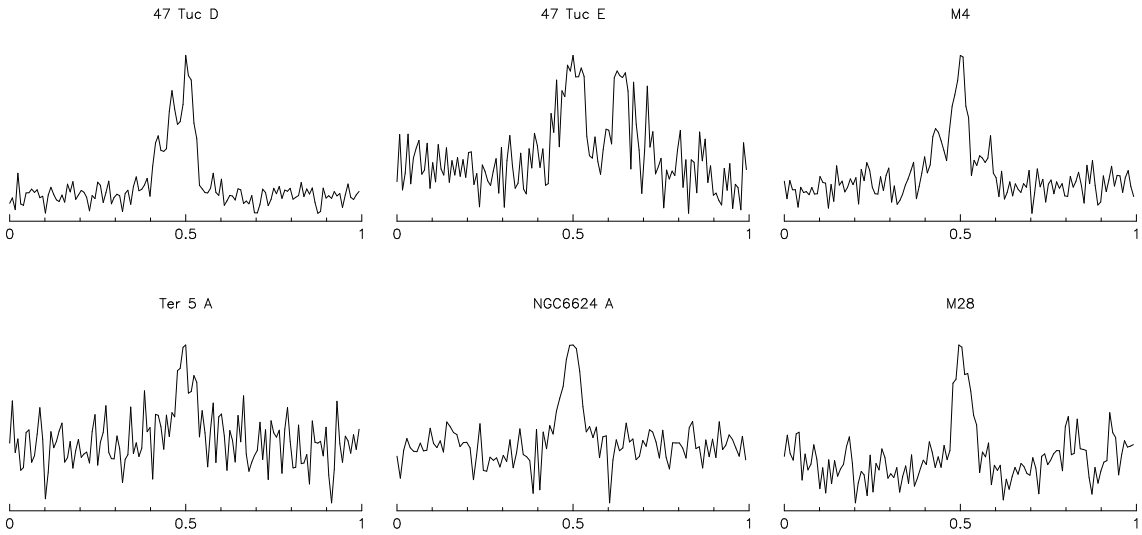

Figure 6.1: Integrated pulse profiles for the six pulsars detected. Time resolution in all cases is less than one bin. Profiles are rotated to place the maximum at phase 0.5, and normalised by the peak flux.

by the pulsar due to factors such as multi-path propagation (scatter-broadening), dispersion smearing in filterbank channels, and the finite duration of the sampling interval. These effects should be added in quadrature with the intrinsic pulse width to yield the effective pulse width. All pulsar systems incorporate a degree of sensitivity loss modeled with β, the major factor in the past being the use of 1-bit sampling which contributes $\sqrt{\pi/2} \simeq 1.25$ to this value. Most surveys in the past have assumed an extra 15 per cent loss due to other factors, giving $\beta = 1.5$. Since the present survey samples with two bits of precision, we begin with a value of 1.15 (see Jenet & Anderson 1998) and adding 15 per cent for other losses, arrive at an assumed value of $\beta = 1.3$. From the appearance of spurious signals in this search and based on the distribution of true pulsar signal to noise ratios in previous work (Chapter 5), we use a value of $\alpha = 10$ as the minimum signal to noise ratio for a pulsar candidate of firm credibility. The effective system temperature is mainly the result of contributions from thermal noise in the receiver and from Galactic synchrotron radiation. The receiver used in this work contributes approximately 60 K to the system temperature, whilst the Galactic contribution is a strong function of Galactic latitude, contributing $\sim$10 K at high Galactic latitudes and $\sim$100 K at the Galactic plane. Pulsar signals are superimposed on this noise with a gain from the 64-m collecting dish of $G \simeq 0.6$ K Jy^{-1}.

The sensitivity as a function of period for the searches described here is plotted

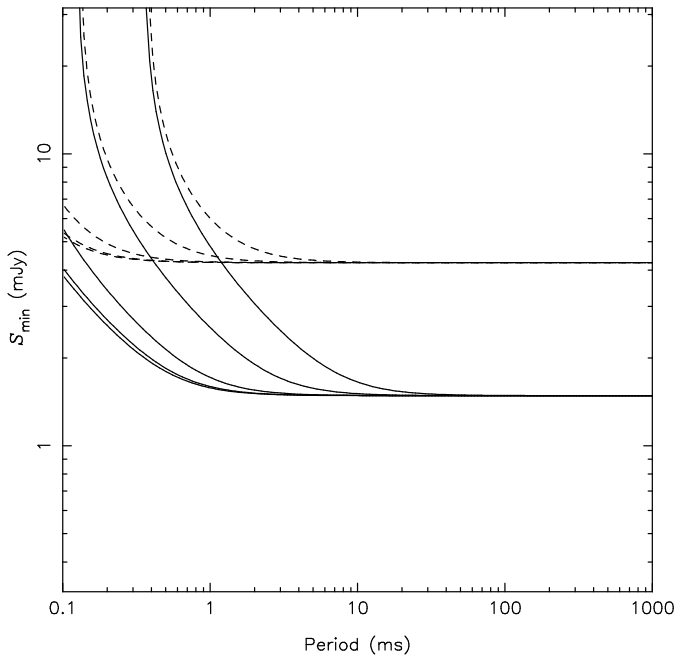

Figure 6.2: Minimum detectable mean flux density as a function of pulse period for FA search parameters. Solid and dashed lines represent pulsars with 5 and 30 per cent intrinsic duty cycles respectively. For each pulse width curves for dispersion measures of 0, 10, 30, 100 and 300 pc cm^{-3} are shown (from left to right).

in Figures 6.2 and 6.3. The values are for a cold sky of around 10 K; for clusters near the Galactic plane sensitivity drops by around a factor of 2.3. Our analysis includes the effects of the finite sample interval and dispersion smearing in filter channels, but does not attempt to model scatter-broadening due to its dependence on the composition of the intervening interstellar medium. It should be noted that sensitivity is strongly dependent on the intrinsic pulse width, a factor which has been somewhat neglected in the past. Since the majority of recycled pulsars have pulse duty cycles between 5 and 30 per cent (see e.g. Kramer et al. 1998), we show in the figures sample curves for these values, resulting in a baseline sensitivity of 1.3–4 mJy. Figure 6.2 applies to observations of 859 s in duration with 512 channels and 25.6 μs sampling, such as the FA search. The curves for FD would be of the same shape but with a slight downward shift (by a factor of $1/\sqrt{2}$ or $\sim$0.15 decades). The maximum DM range searched in the FA search was only $\pm$2.5 pc cm^{-3} and the dispersion smearing in each channel even at the edges of the range is very small due to the earlier coherent removal of a nominal cluster DM. Hence the zero-DM curves in Figure 6.2 are the most appropriate for clusters with known pulsars. For the SA search the curves in Figure 6.3 should be used. Note that the sampling

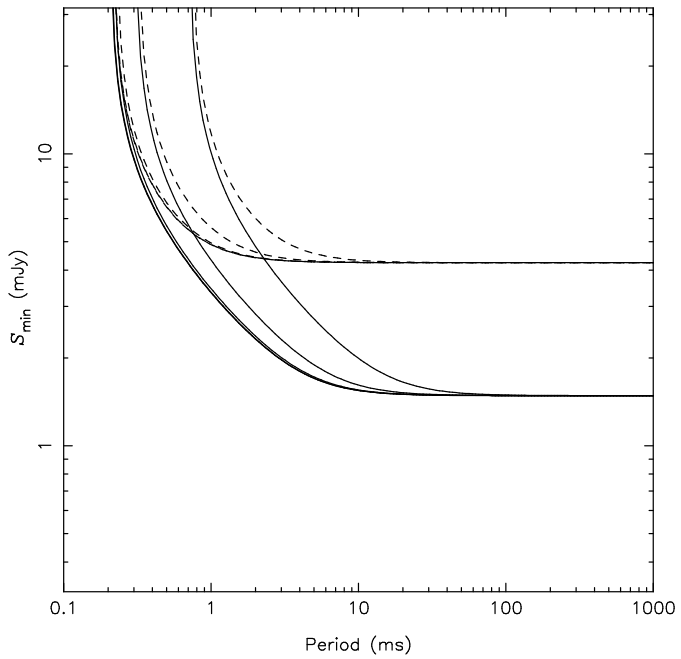

Figure 6.3: Minimum detectable mean flux density as a function of pulse period for SA search parameters. Solid and dashed lines represent pulsars with 5 and 30 per cent intrinsic duty cycles respectively. For each pulse width curves for dispersion measures of 0, 10, 30, 100 and 300 pc cm^{-3} are shown (from left to right), although the first three are in general so close as to be difficult to distinguish (c.f. Figure 6.2).

interval of this search configuration (204.8 μs) is comparable to previous searches, and the degradation of sensitivity at high dispersion measures is improved due to the small channel bandwidth (and hence the large diagonal DM of 90.8 pc cm^{-3}). Nevertheless, it is apparent from Figure 6.3 that the available sensitivity declines rapidly as periods go below 10 ms. On comparison of Figures 6.2 and 6.3 the superiority of high time resolution processing over traditional survey configurations (analogous to SA) for the detection of millisecond and sub-millisecond pulsars is clear.

6.3.3 Acceleration Effects

The preceding analysis neglects the effects of acceleration due to orbital motion. The differential Doppler shift induced over the course of the observation can result in the smearing of power across several bins of the fluctuation spectrum. Since the shift moves frequency components a by multiplicative factor (at/c), the loss of sensitivity is greatest at higher harmonics. The acceleration spacing of the FA search

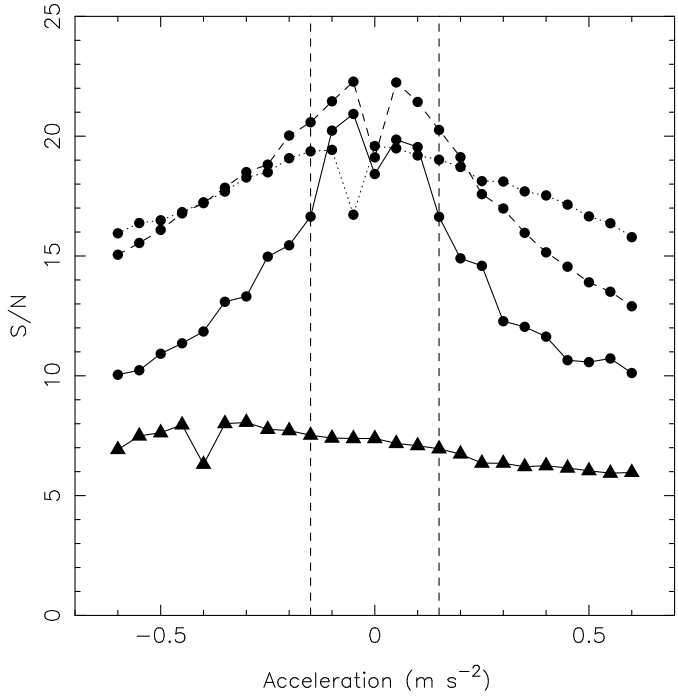

Figure 6.4: Spectral signal signal to noise ratio as a function of trial acceleration for simulated pulsar signals. Circles and triangles represent values resulting from Gaussian profiles with FWHM values of 5 and 30 per cent respectively, and are joined by solid, dashed and dotted lines for pulse periods of ∼0.43, 0.89 and 1.84 ms. All signals were simulated with zero acceleration and equal mean flux density. Vertical dashed lines are placed at ±0.15 m s^{-2} to represent displacements from zero by half the spacing used in the FA search.

is $\sim$0.3 m s^{-2}, implying a worst-case differential shift factor of 0.15 m s^{-2} × 859 s/c $\simeq$ 4.30×10^{-7} for a pulsar with an acceleration mid-way between two trial values. Since each bin of the fluctuation spectrum represents 1/859 s $\simeq$ 1.16×10^{-3} Hz, the 2500-Hz fundamental of a putative 0.4-ms sub-millisecond pulsar would experience at most $\sim$1 bin of acceleration smearing, with higher harmonics experiencing proportionately more smearing but representing a smaller fraction of the total power of the pulsar.

To examine the true sensitivity loss we processed real data from an FA search, to which we had added simulated signals from non-accelerated pulsars of various pulse widths and periods. We used a trial acceleration spacing of 0.05 m s^{-2} in the range $|a| < 6$ m s^{-2} to examine the loss of signal to noise ratio when trial accelerations do not match the true acceleration of the pulsar (in this case zero). The results are shown in Figure 6.4. Even in the worst case, a 0.4 ms signal with a pulse width of 5 per cent FWHM (that is, at the extreme lower end of observed MSP pulse widths), some 80 per cent of sensitivity was retained at the outer edges of the range

of acceleration offsets experienced in the FA search. It is clear that the impact of acceleration on sensitivity of the FA search was small for $P \gtrsim 0.4$ ms. In addition, due to scintillation it is expected that a real pulsar would experience less signal-to-noise loss than is indicated by these results. For the SA search a more modest acceleration spacing of 0.5 m s^{-2} was chosen due to the fact that the long sample interval employed itself severely limits sensitivity to sub-millisecond pulsars. In this case, any pulsar or harmonic with a period greater than 0.6 ms would experience less than one bin of acceleration-induced spectral smearing.

Of course, all of the above only applies to pulsars within the range of $|a| <$ 30 m s^{-2} searched. This range is typical of previous pulsar searches and is likely to encompass the majority of pulsar systems, however there are several known exceptions. The eclipsing binary of Terzan 5 (Lyne et al. 1990) experiences line-of-sight accelerations greater than this for approximately 30 per cent of its orbit, with a maximum value of 33.2 m s^{-2}. The eccentric double neutron star systems B2127+11C (in M15), B1534+12, B1913+16 also experience strong accelerations, exceeding 30 m s^{-2} in the line of sight for 20–50 per cent of the orbit. Such systems have relatively long pulse periods ($P \gtrsim 30$ ms) and so would be detected in the present work at accelerations up to around 40 m s^{-2}. However the acceleration in these systems exceeds even this value for a significant proportion of the time, reaching a peak in excess of 100 m s^{-2} for the highly eccentric systems B2127+11C and B1913+16. Eccentric systems with much shorter orbital periods are expected to evolve from pulsars typical of the presently known double neutron star population, and the detectability of such pulsars in this and previous globular cluster searches would be severely affected by acceleration smearing. The primary aim of this work was to detect or place limits on the existence of [sub-]millisecond pulsars (which are not expected to have neutron-star companions), and the computational load associated with high resolution baseband processing limited the feasibility of searching a broad acceleration range. However, we note that future surveys with good basic sensitivity would be well-served by searching a range of at least $\pm$100 m s^{-2}, perhaps at a reduced sample rate of $\sim$1 ms and with correspondingly fewer trial dispersion measures and accelerations.

6.3.4 The Population of Sub-Millisecond Pulsars

It is clear from inspection of Figure 6.2 and the preceding analysis that our FA search, unlike most searches in the past, had a relatively flat sensitivity function for all periods greater than ~ 0.4 ms. The FD search also provided similar characteristics for nearby (DM $\lesssim 50$ pc cm^{-3}) unaccelerated pulsars. We are therefore in a stable position to analyze the period distribution of the detected population relatively free of concerns regarding selection effects. Unfortunately the system used was only sensitive enough to detect a few pulsars, making any assertions somewhat perilous due to small number statistics. However it is clear even from this sample that the majority of recycled pulsars do have pulse periods of a few milliseconds or more. All six pulsars detected lay in the two octaves from 3–12 ms, whilst no pulsars were detected in the preceding three octave interval, 0.375–3 ms over which we had comparable sensitivity.

No new pulsars were discovered in NGC 6544, Liller 1, or Terzan 5 despite the presence of steep-spectrum emission as reported by Fruchter & Goss (2000). It is probable that several pulsars in each cluster are responsible for the emission, with each individual pulsar having a flux density below our detection limit. An exception might be the "N" source of Terzan 5 (Fruchter & Goss 2000), which was unresolved at a resolution of $2\farcs9$ (c.f. the cluster core radius of $11''$; Harris 1996). From the published spectral index and 20 cm flux, we infer a 50 cm flux density of 9 mJy. The sky temperature in this region is ~ 300 K at 70 cm (Haslam et al. 1982), implying a temperature of ~ 100 K at 50 cm (Lawson et al. 1987). The sensitivity limits are thus $160/70 \simeq 2.3$ times greater than indicated in Figure 6.2, however even so, a very broad profile and/or very short spin period would be required for the pulsar to have remained undetected at 9 mJy. It is possible that the source is a pulsar that was undetected due to scatter broadening. Up to a millisecond of scattering could be induced by the intervening interstellar medium without having hampered the detection of the presently known pulsars, with pulse periods of 11.6 and 8.4 ms (Lyne et al. 2000b). Such scattering would be catastrophic for the detection of very fast pulsars and could explain the lack of detection of the "N" source in this work. Observations made at higher radio frequency could answer this question since the time scale of scatter broadening scales as ν^{-4}. However, the lower flux density of pulsars at high frequency necessitates the use of a large bandwidth, beyond the present capabilities of baseband recording and processing systems. Analogue

filterbanks generally do not have sufficiently narrow channels to detect very fast pulsars at high dispersion measures such as that of Terzan 5. Indeed, the probable non-detection at 20 cm of the "N" source as a pulsar by Lyne et al. (2000b) must be taken with the caveat that the system used induced $\sim$200 μs of dispersion smearing, rendering it relatively insensitive to very fast pulsars. Another alternative is that the "N" source is in a binary so close (or with such a massive companion) that its line-of-sight acceleration often exceeds the bounds of our search, or that its velocity evolution is significantly non-linear on the timescale of our observations.

To strongly constrain the shape of the lower end of the millisecond pulsar period distribution, observations are needed that are not only equally sensitive all pulsars slower than $\sim$0.5 ms, but that are also sufficiently sensitive to detect a large number of pulsars. The work described here has shown that present technology is sufficient to achieve the latter requirement through baseband processing technology, however it falls short in basic sensitivity. We expect that future projects with colder receivers and larger (Nyquist-sampled) bands will achieve the necessary sensitivity to finally resolve this issue.

Chapter 7

Conclusions

In this thesis I have presented the results of two campaigns conducted at the Parkes radio telescope to search for the existence of novel pulsars in our Galaxy. The two projects employed rather dissimilar strategies but shared a common theme of the exploitation of new technology for the exploration of previously inaccessible parameter spaces. 4,000,000,000,000 bytes, 300,000 pulsar candidates, 30,000 CPU-hours, 400 telescope-hours and 69 pulsars later, our knowledge of the Galactic menagerie of stars has grown.

In terms of discoveries, the strategy used in the intermediate latitude survey (Chapters 3, 4, and 5) proved most efficacious. This was the first ever large scale high frequency survey for pulsars away from the Galactic plane. Its sample of detected and discovered pulsars will prove most useful in modelling of the Galactic population, especially when combined with the results of the ongoing surveys of low and high Galactic latitudes with the same instrument. A number of interesting individual objects were discovered, forming important pieces in the puzzle of pulsar formation and evolution.

Perhaps the most spectacular discoveries presented in this thesis were the massive white dwarf – pulsar binaries discussed in Chapter 3. The companion of PSR J1157–5112 is the latest and most convincing example of an ultramassive white dwarf. Other examples of ultramassive white dwarfs are known from optical and X-ray studies (Bergeron, Saffer & Liebert 1992; Vennes et al. 1997), however in these cases the mass is inferred from uncertain model-dependent fits to spectra. Contemporaneous with the discovery of PSR J1157–5112, van Kerkwijk & Kulkarni (1999) suggested that the companion of the eccentric binary pulsar B2303+46 was a

massive white dwarf (> 1.2 M$_\odot$) and announced the detection of a putative optical counterpart. It is ordinarily assumed that in the formation of recycled pulsars, mass transfer from the evolving progenitor of the white dwarf onto the previously-born pulsar circularises the orbit (e.g. Phinney 1992). The eccentricity of B2303+46 rules out this scenario and it was therefore suggested at first that the companion, like those of other eccentric systems such as B1913+16 and B1534+12, is a neutron star and that the eccentricity arose from the sudden mass loss of a neutron star birth event. Since the pulsar does not appear to be recycled, the assumption was that it was the second-born neutron star (Stokes, Taylor & Dewey 1985). The alternative presented by van Kerkwijk & Kulkarni (1999) is that the companion is in fact a white dwarf which managed to form *before* the neutron star by means of having an initially more massive companion, which eventually transferred sufficient matter to the pulsar progenitor to push it over the critical mass for a core collapse supernova. It was soon suggested that PSR J1141–6545 (Kaspi et al. 2000a), newly discovered in the Galactic plane multibeam survey, also arose from a similar scenario. In order to produce such a system, the initially less massive (and hence less evolved) pulsar progenitor must have accreted sufficient matter from the evolving white dwarf progenitor to result in a later core collapse event and the formation of a neutron star. Tauris & Sennels (2000) present evidence in favour of the feasibility of this model, however as with any new hypothesis, its correctness must be taken with some caution when only one or two objects to which it applies are known. The significance of the discovery of PSR J1157–5112 (Chapter 3) is that there is a strong weight of evidence from numerous other circular-orbit recycled pulsar binaries that its companion is a white dwarf, and pulsar timing results incontrovertibly show that the companion is massive (> 1.15 M$_\odot$). This proves that ultramassive white dwarfs do in fact exist as the end result of stellar evolution, lending credibility to the identifications of the optical white dwarfs and the companions of PSRs B2303+46 and J1141–6545 as examples of these stars.

A second pulsar with a massive white dwarf companion – PSR J1757–5322 – was discovered in the intermediate latitude survey and is also discussed in Chapter 3. The canonical isolated white dwarf is composed of carbon and oxygen with a mass of ~ 0.6 M$_\odot$, however such stars are relatively rare as the companions of recycled pulsars because mass transfer in main sequence – pulsar binaries usually occurs on the red giant branch, leaving the low mass helium core as a white dwarf companion. However several examples of recycled pulsars with CO companions

are now known, including PSR J1757–5322. The important difference with this pulsar, however, is its proximity to the companion. Its tight 11-h orbit results in significant energy loss due to the emission of gravitational radiation, and the system will coalesce within a Hubble time. The consequences of this dramatic event are unknown, presenting a plausible origin for pulsar planetary systems, evaporating binaries, isolated millisecond pulsars and gamma ray bursts, as discussed in detail in Chapter 3.

A total of six binary pulsars were discovered in the survey, as discussed in Chapter 4. In addition to the two already discussed, the remaining four appear to be normal low mass binary pulsars, with some possible anomalies. Most notably, the orbital period of PSR J1618–3919 appears in the middle of what previously appeared to be a "gap" in the distribution. With the discovery of this and other pulsars, the gap appears much less prominent than previously suggested, although the remaining under-density in the region appears significant. This system in combination with PSR J1745–0947 and a number of new pulsars from the Galactic plane survey (Camilo et al. 2001) with anomalously long pulse periods may in fact be examples of the products of a new channel of binary evolution recently proposed independently by Tauris, van den Heuvel & Savonije (2000) and Taam, King & Ritter (2000). However, it remains to be seen whether the scenario is capable of producing low-mass dwarfs in a high proportion of its outcomes, as is required by the low mass functions of the observed systems with anomalously long spin periods.

The survey also discovered some pulsars of interest due to their emission properties. As discussed in Chapter 4, the average pulse profile of PSR 1410–7404 is very narrow. The pulse width/period distribution of slow pulsars is well-fit by the model of Rankin (1990), especially with regard to the relation between pulse period and minimum pulse width. The average pulse of PSR 1410–7404 is far narrower than allowed by this relation and represents the only significant departure from it in an apparently slow pulsar. The pulse widths of recycled pulsars on the other hand bear no resemblance to the relation and it is expected that the recycling process results in an emission process that differs in some aspect from that of normal pulsars. The divergence of PSR J1410–7404 from the relation led me to suggest that it too may in fact be recycled, an hypothesis that received significant support from my later measurement of its period derivative, the smallest of any slow pulsar found in the survey. The pulsar may represent an example of a neutron star that was recycled in a binary later disrupted by the supernova event of its companion. Such systems are

the isolated cousins of the double neutron star systems and until now little evidence has been available to identify any pulsar with this evolutionary history.

Also of interest due to the properties of their emission are PSRs J1231–47 and J1919+0134 (Chapter 5), discovered in the intermediate latitude survey. These pulsars exhibit drifting sub-pulses of such high regularity as is only seen in perhaps two previously known pulsars. Detailed analysis of these pulsars has been conducted by my colleague at Swinburne (Ord et al. , in preparation) and adds significantly to the body of knowledge of pulsar emission.

The second project undertaken as part of this thesis was a search of Globular clusters for sub-millisecond pulsars, described in Chapter 6. The use of baseband recording technology was ambitious in terms of the computer power required to process it, and this is the first published work to use the technique for pulsar searching. Whilst previous surveys have claimed sensitivity to sub-millisecond pulsars, it became clear from the viewing of pulsar candidates in the intermediate latitude survey that the identification of a sub-millisecond pulsar candidate amongst scores of similarly sinusoidal interference signals would be difficult or impossible, even if it was bright enough to be detected despite the reduced sensitivity at such short periods. Such restrictions would also have applied to previous surveys, which shared comparable time resolution, and it is clear that the lower end of the observed millisecond pulsar period distribution is likely to be severely affected by selection effects. As evidenced by the discovery of the first pulsar, and again by the discovery of the first millisecond pulsar (see Chapter 1), it is important at all times in astronomy to push the bounds of what is thought possible in order to discover new and unexpected classes of objects. This was the philosophy behind the use of baseband recording technology in the Globular cluster search. The unprecedented time resolution (25.6 μs) provided true, full sensitivity to pulsars with periods well shorter than a millisecond, in contrast to the marginal sensitivity of previous attempts to discover sub-millisecond pulsars. Unfortunately, whilst the system was equally sensitive to sub-millisecond, millisecond and slow pulsars, it was not overly sensitive to any of them! Six pulsars were detected, all previously known and possessing millisecond periods, indicating that the population of sub-millisecond pulsars, if they exist at all, is rather smaller than that of millisecond pulsars. Stronger statements than this must await future observations of greater overall sensitivity.

The software written for these surveys effects a significant improvement in usability, flexibility and applicability to a broad range of search parameters, and should

be of use in future work. It is already seeing use in the high-latitude multibeam pulsar survey being conducted by a collaboration from Caltech and Swinburne. It is hoped that my work in the Globular cluster search will be extended (using the same software) via two possible avenues in the near future. A new Caltech-Parkes-Swinburne baseband recorder is in the planning stages, and will provide significantly greater bandwidth ($\sim$128 MHz). In combination with the 50-cm component of the new, cold, wide bandwidth coaxial receiver in construction for the Parkes telescope, this will provide an excellent system for sub-millisecond pulsar surveys. Secondly, the wide bandwidth afforded by the new recorder may be sufficient to provide good sensitivity with the centre beam of the 20-cm multibeam receiver, a system which has already proved extremely efficacious for Globular cluster searching (Camilo et al. 2000a; D'Amico et al. 2001b) but at present is limited by dispersion smearing in the analogue filterbank.

The new discoveries made in this thesis will provide material for future work for some time to come. The extended timing of the binary systems will be of particular interest if proper motion measurements become available, for this will aid in the evaluation of the proposal of Camilo et al. (2001) that the systems with anomalously long spin periods were preferentially discovered in the multibeam surveys due to a smaller scale height (and hence lower velocity distribution). Achieving phase connection over a whole orbit in the timing of PSR J1618–39 will also be of use in this regard by means of the measurement of its eccentricity, since there is some evidence that objects of rather high eccentricity tend not to be ordinary LMBPs (see § 4.5.1). A campaign of optical observations is in the planning stages and will hopefully provide data on the temperature and luminosity of some of the white dwarf companions of the newly discovered systems, aiding in the identification of the composition of their companions and providing data for white dwarf cooling models by comparison with the pulsar spin-down age. Future polarimetric studies of the recycled systems should also be of interest for theories of pulsar emission, particularly in the case of PSR J1410–7404 for which we saw some evidence of multiple components in preliminary polarimetric data, which if true would exacerbate the discrepancy with the period–width relation.

References

Ables J. G., Komesaroff M. M., Hamilton P. A., 1970, Astrophys. Lett., 6, 147

Alpar M. A., Cheng A. F., Ruderman M. A., Shaham J., 1982, Nature, 300, 728

Anderson S., Kulkarni S., Prince T., Wolszczan A., 1989a. IAU Circ. No. 4819

Anderson S., Kulkarni S., Prince T., Wolszczan A., 1989b. IAU Circ. No. 4853

Anderson S., Kulkarni S., Prince T., Wolszczan A., 1990a. IAU Circ. No. 5013

Anderson S. B., Gorham P. W., Kulkarni S. R., Prince T. A., Wolszczan A., 1990b, Nature, 346, 42

Anderson S. B., 1992, PhD thesis, California Institute of Technology

Armitage P., Livio M., 2000, ApJ, 532, 540

Arzoumanian Z., Cordes J. M., Wasserman I., 1999, ApJ, 520, 696

Arzoumanian Z., Nice D. J., Taylor J. H., Thorsett S. E., 1994, ApJ, 422, 671

Baade W., Zwicky F., 1934, Proc. Nat. Acad. Sci., 20, 254

Backer D. C., Kulkarni S. R., Heiles C., Davis M. M., Goss W. M., 1982, Nature, 300, 615

Backer D. C., 1970, Nature, 228, 42

Backer D. C., 1973, ApJ, 182, 245

Bailes M. et al., 1994, ApJ, 425, L41

Bailes M., 1989, ApJ, 342, 917

Barnes D. G. et al., 2001, MNRAS, in press

Bell J. F., Bessell M. S., Stappers B. W., Bailes M., Kaspi V. M., 1995, ApJ, 447, L117

Bergeron P., Saffer R. A., Liebert J., 1992, ApJ, 394, 228

Bhattacharya D., van den Heuvel E. P. J., 1991, Phys. Rep., 203, 1

Biggs J. D., Lyne A. G., 1992, MNRAS, 254, 257

Biggs J. D., Bailes M., Lyne A. G., Goss W. M., Fruchter A. S., 1994, MNRAS, 267, 125

Bionta R. M. et al., 1987, Phys. Rev. Lett., 58, 1494

Blandford R., Teukolsky S. A., 1976, ApJ, 205, 580

Boriakoff V., Buccheri R., Fauci F., 1983, Nature, 304, 417

Cadwell B., 1997, in American Astronomical Society Meeting 191 #113.07

Camilo F., Nice D. J., 1995, ApJ, 445, 756

Camilo F., Nice D. J., Shrauner J. A., Taylor J. H., 1996, ApJ, 469, 819

Camilo F., Lorimer D. R., Freire P., Lyne A. G., Manchester R. N., 2000a, ApJ, 535, 975

Camilo F. et al., 2000b, in Kramer M., Wex N., Wielebinski R., eds, Pulsar Astronomy - 2000 and Beyond, IAU Colloquium 177. Astronomical Society of the Pacific, San Francisco, p. 3, astro-ph/9911185

Camilo F. M., Kaspi V. M., Lyne A. G., Manchester R. N., Bell J. F., D'Amico N., McKay N. P. F., Crawford F., 2000c, ApJ, 541, 367

Camilo F. et al., 2001, ApJ, In press.

Camilo F., Nice D. J., Taylor J. H., 1996, ApJ, 461, 812

Camilo F., Thorsett S. E., Kulkarni S. R., 1994, ApJ, 421, L15

Camilo F., 1995, in Alpar A., Kiziloğlu Ü., van Paradis J., eds, The Lives of the Neutron Stars (NATO ASI Series). Kluwer, Dordrecht, p. 243

Chandrasekhar S., 1931, ApJ, 74, 81

Chen K., Ruderman M., 1993, ApJ, 408, 179

Clifton T. R., Lyne A. G., 1986, Nature, 320, 43

Clifton T. R., Lyne A. G., Jones A. W., McKenna J., Ashworth M., 1992, MNRAS, 254, 177

Cognard I., Shrauner J. A., Taylor J. H., Thorsett S. E., 1996, ApJ, 457, L81

Comella J. M., Craft H. D., Lovelace R. V. E., Sutton J. M., Tyler G. L., 1969, Nature, 221, 453

Cook G. B., Shapiro S. L., Teukolsky S. A., 1994, ApJ, 423, L117

Cordes J. M., Helfand D. J., 1980, ApJ, 239, 640

Damashek M., Backus P. R., Taylor J. H., Burkhardt R. K., 1982, ApJ, 253, L57

Damashek M., Taylor J. H., Hulse R. A., 1978, ApJ, 225, L31

D'Amico N., Bailes M., Lyne A. G., Manchester R. N., Johnston S., Fruchter A. S., Goss W. M., 1993, MNRAS, 260, L7

D'Amico N., Stappers B. W., Bailes M., Martin C. E., Bell J. F., Lyne A. G., Manchester R. N., 1998, MNRAS, 297, 28

D'Amico N., Lyne A. G., Manchester R. N., Possenti A., Camilo F., 2001a, ApJ, 548, L171

D'Amico N. D., Lyne A. G., Manchester R. N., Possenti A. an d Camilo F., 2001b, ApJ, in press, astro-ph/0010272

Davies J. G., Lyne A. G., Seiradakis J. H., 1977, MNRAS, 179, 635

Dewey R. J., Taylor J. H., Weisberg J. M., Stokes G. H., 1985, ApJ, 294, L25

Dewi J. D. M., Tauris T. M., 2000, A&A, 360, 1043

Edwards R. T., Bailes M., 2001a, ApJ, in press, astro-ph/0102026

Edwards R. T., Bailes M., 2001b, ApJ, 547, L37

Ergma E., Lundgren S. C., Cordes J. M., 1977, ApJ, 475, L29

Foster R. S., Cadwell B. J., Wolszczan A., Anderson S. B., 1995, ApJ, 454, 826

Foster R. S., Fairhead L., Backer D. C., 1991, ApJ, 378, 687

Freire P. C., Camilo F., Lorimer D. R., Lyne A. G., Manchester R. N., D'Amico N., 2001, MNRAS, in press

Fruchter A. S., Goss W. M., 2000, ApJ, 536, 865

Fruchter A. S., Gunn J. E., Lauer T. R., Dressler A., 1988, Nature, 334, 686

Fruchter A. S., Stinebring D. R., Taylor J. H., 1988, Nature, 333, 237

Fryer C., Woosley S., Herant M., Davies M., 1999, ApJ, 520, 650

García-Berro E., Ritossa C., Iben I. J., 1997, ApJ, 485, 765

Gold T., 1968, Nature, 218, 731

Goldreich P., Julian W. H., 1969, ApJ, 157, 869

Gould D. M., Lyne A. G., 1998, MNRAS, 301, 235

Hankins T. H., Rickett B. J., 1975, in Methods in Computational Physics Volume 14 — Radio Astronomy. Academic Press, New York, p. 55

Harris W. E., 1996, AJ, 112, 1487

Haslam C. G. T., Salter C. J., Stoffel H., Wilson W. E., 1982, A&AS, 47, 1

Helfand D. J., Manchester R. N., Taylor J. H., 1975, ApJ, 198, 661

Henning P. A. et al., 2000, AJ, 119, 2686

Hewish A., Bell S. J., Pilkington J. D. H., Scott P. F., Collins R. A., 1968, Nature, 217, 709

Hirata K. et al., 1987, Phys. Rev. Lett., 58, 1490

Hulse R. A., Taylor J. H., 1974, ApJ, 191, L59

Hulse R. A., Taylor J. H., 1975a, ApJ, 195, L51

Hulse R. A., Taylor J. H., 1975b, ApJ, 201, L55

Iben I., Tutukov A., 1993, ApJ, 418, 343

Iben I. J., Ritossa C., García-Berro E., 1997, ApJ, 489, 772

Jenet F. A., Anderson S. B., 1998, PASP, 110, 1467

Johnston S., Bailes M., 1991, MNRAS, 252, 277

Johnston S., Lyne A. G., Manchester R. N., Kniffen D. A., D'Amico N., Lim J., Ashworth M., 1992a, MNRAS, 255, 401

Johnston S., Manchester R. N., Lyne A. G., Bailes M., Kaspi V. M., Qiao G., D'Amico N., 1992b, ApJ, 387, L37

Johnston S. et al., 1993, Nature, 361, 613

Kaspi V. M., Lackey J. R., Mattox J., Manchester R. N., Bailes M., Pace R., 2000a, ApJ, 528, 445

Kaspi V. M. et al., 2000b, ApJ, 543, 321

Kaspi V. M., Taylor J. H., Ryba M., 1994, ApJ, 428, 713

Kopeikin S. M., 1997, Phys. Rev. D, 56, 4455

Kramer M., Xilouris K. M., Lorimer D. R., Doroshenko O., Jessner A., Wielebinski R., Wolszczan A., Camilo F., 1998, ApJ, 501, 270

Kramer M., Wex N., Wielebinski R., eds, Pulsar Astronomy - 2000 and Beyond, IAU Colloquium 177, Astronomical Society of the Pacific, San Francisco, 2000

Kulkarni S. R., 1986, ApJ, 306, L85

Lange C., Camilo F., Wex N., Kramer M., Backer D. C., Lyne A. G., Doroshenko O., 2001, MNRAS, in press

Large M. I., Vaughan A. E., Wielebinski R., 1968, Nature, 220, 753

Large M. I., Vaughan A. E., Wielebinski R., 1969a, Nature, 223, 1249

Large M. I., Vaughan A. E., Wielebinski R., 1969b, Astrophys. Lett., 3, 123

Lawson K. D., Mayer C. J., Osborne J. L., Parkinson M. L., 1987, MNRAS, 225, 307

Lommen A. N., Zepka A., Backer D. C., McLaughlin M., Cordes J. M., Arzoumanian Z., Xilouris K., 2000, ApJ, 545, 1007

Lorimer D. R., Yates J. A., Lyne A. G., Gould D. M., 1995, MNRAS, 273, 411

Lorimer D. R., Lyne A. G., Bailes M., Manchester R. N., D'Amico N., Stappers B. W., Johnston S., Camilo F., 1996, MNRAS, 283, 1383

Lyne A. G., Manchester R. N., 1988, MNRAS, 234, 477

Lyne A. G., McKenna J., 1989, Nature, 340, 367

Lyne A. G., Smith F. G., 1998, Pulsar Astronomy, 2nd ed. Cambridge University Press, Cambridge

Lyne A. G., Brinklow A., Middleditch J., Kulkarni S. R., Backer D. C., Clifton T. R., 1987, Nature, 328, 399

Lyne A. G., Biggs J. D., Brinklow A., Ashworth M., McKenna J., 1988, Nature, 332, 45

Lyne A. G. et al., 1990, Nature, 347, 650

Lyne A. G., Biggs J. D., Harrison P. A., Bailes M., 1993, Nature, 361, 47

Lyne A. G. et al., 1998, MNRAS, 295, 743

Lyne A. G. et al., 2000a, MNRAS, 312, 698

Lyne A. G., Mankelow S. H., Bell J. F., Manchester R. N., 2000b, MNRAS, 316, 491

Manchester R. N., Taylor J. H., 1977, Pulsars. Freeman, San Francisco

Manchester R. N., Lyne A. G., Taylor J. H., Durdin J. M., Large M. I., Little A. G., 1978, MNRAS, 185, 409

Manchester R. N., Newton L. M., Cooke D. J., Lyne A. G., 1980, ApJ, 236, L25

Manchester R. N., Lyne A. G., Johnston S., D'Amico N., Lim J., Kniffen D. A., Fruchter A. S., Goss W. M., 1989. IAU Circ. No. 4905

Manchester R. N., Lyne A. G., Robinson C., D'Amico N., Bailes M., Lim J., 1991, Nature, 352, 219

Manchester R. N. et al., 1996, MNRAS, 279, 1235

Manchester R. N. et al., 2000, in Kramer M., Wex N., Wielebinski R., eds, Pulsar Astronomy - 2000 and Beyond, IAU Colloquium 177. Astronomical Society of the Pacific, San Francisco, p. 49

Manchester R. N. et al., 2001, MNRAS, Submitted.

Mereghetti S., 2000, in NATO ASI "The Neutron star - Black hole Connection". in

press, astro-ph/9911252

Narayan R., Paczyński B., Piran T., 1992, ApJ, 395, L83

Nice D. J., Fruchter A. S., Taylor J. H., 1995, ApJ, 449, 156

Pacini F., 1968, Nature, 219, 145

Phinney E. S., Kulkarni S. R., 1994, Ann. Rev. Astr. Ap., 32, 591

Phinney E. S., Verbunt F., 1991, MNRAS, 248, 21P

Phinney E. S., 1991, ApJ, 380, L17

Phinney E. S., 1992, Phil. Trans. Roy. Soc. A, 341, 39

Pilkington J. D. H., Hewish A., Bell S. J., Cole T. W., 1968, Nature, 218, 126

Press W. H., Flannery B. P., Teukolsky S. A., Vetterling W. T., 1986, Numerical Recipes: The Art of Scientific Computing. Cambridge University Press, Cambridge

Pylyser E., Savonije G. J., 1988, A&A, 191, 57

Radhakrishnan V., Rankin J. M., 1990, ApJ, 352, 258

Rankin J. M., 1983a, ApJ, 274, 333

Rankin J. M., 1983b, ApJ, 274, 359

Rankin J. M., 1986, ApJ, 301, 901

Rankin J. M., 1990, ApJ, 352, 247

Ransom S. M., 2000, in Kramer M., Wex N., Wielebinski R., eds, Pulsar Astronomy - 2000 and Beyond, IAU Colloquium 177. Astronomical Society of the Pacific, San Francisco, p. 43

Ray P. S. et al., 1995, ApJ, 443, 265

Ray P. S., Thorsett S. E., Jenet F. A., van Kerkwijk M. H., Kulkarni S. R., Prince T. A., Sandhu J. S., Nice D. J., 1996, ApJ, 470, 1103

Ritchings R. T., 1976, MNRAS, 176, 249

Ritossa C., García-Berro E., Iben I. J., 1996, ApJ, 460, 489

Ritossa C., García-Berro E., Iben I. J., 1999, ApJ, 515, 381

Ryba M. F., Taylor J. H., 1991, ApJ, 371, 739

Sandhu J. S., Bailes M., Manchester R. N., Navarro J., Kulkarni S. R., Anderson S. B., 1997, ApJ, 478, L95

Segelstein D. J., Rawley L. A., Stinebring D. R., Fruchter A. S., Taylor J. H., 1986, Nature, 322, 714

Shapiro S. L., Teukolsky S. A., 1983, Black Holes, White Dwarfs and Neutron Stars. The Physics of Compact Objects. Wiley–Interscience, New York

Shapiro I. I., 1964, Phys. Rev. Lett., 13, 789

Shemar S. L., Lyne A. G., 1996, MNRAS, 282, 677

Shklovskii I. S., 1970, Sov. Astron., 13, 562

Smith F. G., 1973, MNRAS, 161, 9P

Staelin D. H., Reifenstein III E. C., 1968, Science, 162, 1481

Stairs I. H., Arzoumanian Z., Camilo F., Lyne A. G., Nice D. J., Taylor J. H., Thorsett S. E., Wolszczan A., 1998, ApJ, 505, 352

Standish E. M., 1982, A&A, 114, 297

Stappers B. W., Bessell M. S., Bailes M., 1996, ApJ, 473, L119

Stappers B. W. et al., 1996, ApJ, 465, L119

Staveley-Smith L. et al., 1996, Proc. Astr. Soc. Aust., 13, 243

Stokes G. H., Taylor J. H., Weisberg J. M., Dewey R. J., 1985, Nature, 317, 787

Stokes G. H., Segelstein D. J., Taylor J. H., Dewey R. J., 1986, ApJ, 311, 694

Stokes G. H., Taylor J., Dewey R. J., 1985, ApJ, 294, L21

Sturrock P. A., 1971, ApJ, 164, 529

Taam R. E., King A. R., Ritter H., 2000, ApJ, 541, 329

Tauris T. M., Savonije G. J., 1999, A&A, 350, 928

Tauris T. M., Sennels T., 2000, A&A, 355, 236

Tauris T. M., van den Heuvel E. P. J., Savonije G. J., 2000, ApJ, 530, L93

Tauris T. M., 1996, A&A, 315, 453

Taylor J. H., Cordes J. M., 1993, ApJ, 411, 674

Taylor J. H., Weisberg J. M., 1982, ApJ, 253, 908

Taylor J. H., Weisberg J. M., 1989, ApJ, 345, 434

Taylor J. H., Fowler L. A., McCulloch P. M., 1979, Nature, 277, 437

Taylor J. H., Manchester R. N., Lyne A. G., 1993, ApJS, 88, 529

Taylor J. H., 1974, A&AS, 15, 367

Thorsett S. E., Chakrabarty D., 1999, ApJ, 512, 288

Thorsett S. E., Deich W. T. S., Kulkarni S. R., Navarro J., Vasisht G., 1993, ApJ, 416, 182

Toscano M., Bailes M., Manchester R., Sandhu J., 1998, ApJ, 506, 863

Toscano M., Sandhu J. S., Bailes M., Manchester R. N., Britton M. C., Kulkarni S. R., Anderson S. B., Stappers B. W., 1999, MNRAS, 307, 925

Turtle A. J., Vaughan A. E., 1968, Nature, 219, 689

van den Heuvel E. P. S., Bonsema P. T. J., 1984, A&A, 139, L16

van den Heuvel E. P. J., 1984, J. Astrophys. Astr., 5, 209

van den Heuvel E. P. J., 1994, A&A, 291, L39

van Kerkwijk M., Kulkarni S. R., 1999, ApJ, 516, L25

van Straten W., Britton M., Bailes M., 2000, in Kramer M., Wex N., Wielebinski R., eds, Pulsar Astronomy - 2000 and Beyond, IAU Colloquium 177. Astronomical Society of the Pacific, San Francisco, p. 283

Vaughan A. E., Large M. I., 1970, Nature, 225, 167

Vaughan A. E., Large M. I., Wielebinski R., 1969, Nature, 222, 963

Vennes S., Thejll P. A., Galvan R. G., Dupuis J., 1997, ApJ, 480, 714

Vivekanand M., Narayan R., 1981, J. Astrophys. Astr., 2, 315

Weatherall J. C., Eilek J. A., 1997, ApJ, 474, 407

Webbink R. F., 1984, ApJ, 277, 355

Wolszczan A., Frail D. A., 1992, Nature, 355, 145

Wolszczan A., Anderson S., Kulkarni S., Prince T., 1989a. IAU Circ. No. 4880

Wolszczan A., Kulkarni S. R., Middleditch J., Backer D. C., Fruchter A. S., Dewey R. J., 1989b, Nature, 337, 531

Wolszczan A., 1991, Nature, 350, 688

Young M. D., Manchester R. N., Johnston S., 1999, Nature, 400, 848

Zhang B., Harding A. K., Muslimov A. G., 2000, ApJ, 531, L135

Appendix A

Software Reference

This appendix serves as a reference for those intending to use software developed for this thesis. For an outline of the techniques used in search software, see Chapter 2.

A.1 Major Packages

This section describes the four main programs used in search analysis, `debird`, `tree`, `minifind2` and `glean`. All are available from the Swinburne Pulsar Group CVS[1] repository, `mania.physics.swin.edu.au:/nfs/other/psr/cvsroot`, and depend on other libraries from the repository.

A.1.1 Debird: Narrow-Band Interference Rejection

For the purpose of detecting and removing filterbank channels contaminated with strong, modulated terrestrial signals, a program called `debird` was written. This program takes a file of filterbank or "treed" data and performs an FFT on each channel in turn. Strong signals in the power spectra are noted and those which exceed a given threshold and appear in less than 10% of the band are flagged for removal ("zapping"). The user can choose to have the channels zeroed and a new file saved, to have the culprit channels listed in a new file, or to display diagnostic information on the terminal only. Many command-line options are available, however a typical invocation specifies `-z` to zap channels, and limits the analysis to the first ∼20 s of data with `-t 20`. The full list of options, as produced by `-h`, is as follows:

[1] `http://www.cvshome.org`

```
-h              help
-f              parse arguments on stdin, 'find' style
-F <filename>   specifies file to analyse
-s <level>      spike threshold. Spikes larger than this
                many std deviations from the mean are
                considered as possible birdies [default: 8.0]
-z              zap birdies channels in data file
-m              always zap Multibeam red noise channels 5,6,7
-i              invert channel ordering in output beam (and header)
-l              log birdie channels to a .zap file
-n              no zapping or logging of birdies [default]
-t <seconds>    how many seconds of data to analyze [default: all]
-q              quick: process an integer power of 2 samples
                <= the number actually specified [default]
-e              process exactly the amount of data specfied
-x              don't recursively combine channels
-g <PG device>  produce a greyscale power plot of fluctuation
                frequency vs filterbank channel
-p <PG device>  produce a second greyscale plot. (use this to
                produce a postscript copy for printing)
-b              sigma value for black in plot [default: 0.5]
-w              sigma value for white in plot [default: 2.5]
-r x            use x Hz/bin for 0-100Hz fluctuation freq. greyscale
-R x            use x Hz/bin for 0-Nyq fluctuation freq. greyscale
                (rounded to nearest multiple of Hz/bin for 0-100Hz)
-T              use treed data. (if -z specified, modifies .subweights)
-S <nsub>       number of subbands in treed data
-N <ndestriped>number of samples of treed data if destriped
```

This software is found under `soft_swin/search/debird` in the Swinburne Pulsar Group CVS repository.

A.1.2 Tree: Partial De-Dispersion

The program known as `tree` performs partial de-dispersion using an algorithm similar to that of Taylor (1974). The input is either a filterbank data file, or a set of

CPSR baseband data files. The number of channels to sum into each "sub-band" is configurable, and the product of this number and the number of trial time series (at different dispersion measures, called "dmgroups") produced in each sub-band equals the number of filterbank channels used. The result of the tree algorithm is one dmgroup for each DM corresponding to a integer number of samples of differential dispersive delay across a sub-band. The range of this delay is from zero up to the number of channels that make up each sub-band, meaning that the highest DM produced corresponds to a gradient in ν–Δt space of 1, in units of samples per channel. This is called the "diagonal" DM. The `tree` program extends the approach to the "super-diagonal" DM, with a gradient of 2. The data are then summed in pairs of adjacent time samples and the range from gradient 1–2 in this data (which is, in fact, 2–4 in units of the original sample interval) is produced with the extended tree algorithm. This process is repeated up to a gradient of 32. Each repetition of the basic tree algorithm is referred to as a "fold", and a separate output file is produced for each.

In the case of baseband data, this package also performs filterbank synthesis with the specified number of channels, and optionally down-samples ("scrunches") by a given integer factor, before applying the tree algorithm. A high-order polynomial is fitted to the computed passband at the start of processing and significant departures from the fit are flagged as narrow-band interference signals, so that the corresponding channels may be zeroed after filterbank synthesis. In dual-sideband systems (such as CPSR) the baseband signal is usually high-pass filtered to produce a zero mean in the input to the sampling system. The resultant "notch" in the centre of the passband is also detected after the polynomial fitting procedure and the affected channels zeroed.

Coherent filters may be applied for the removal of dispersion to a "nominal" DM specified by the user, and samples in filterbank channels may be shifted relative to other channels to remove a "base" DM. In general these are different, the base DM being the minimum DM to be searched, and the nominal DM being approximately in the middle of the range and representing the best available estimate of the DM of any pulsars to be found in the observation. Since the base DM is removed at this stage, any DMs reported later in `minifind2` will differ from the true DM by an amount equal to the base DM: for example, pulsars with the base DM will be reported at 0.0 cm^{-3} pc, and pulsars at the nominal DM will be reported at the difference between the nominal and base DMs. In baseband mode the program

also writes out a `.subweights` file with mean power levels by sub-band number, for use in reconstructing the true signals from the output data in which each sub-band is independently sampled for optimal dynamic range. For baseband data the program also optionally writes out a `.params` file with information about the parameters used in filterbank formation and de-dispersion, and a `.gnu` command file for use with Gnuplot[2] to plot the passband data stored in the `.gnudat` file. Finally, for baseband data `tree` produces a `.hdr` file of the same format produced by the standard analogue filterbank software.

Two output formats are supported by `tree`. The first records a series of small "gulps" containing all samples in all sub-bands of all dmgroups for a given segment of the observation. This format is retained for backward compatability with earlier software which was limited to the serial file output operations available in fortran. The second, preferred format is referred to as "de-striped". In de-striped files, each dmgroup is stored in turn, with all samples in all sub-bands for a given dmgroup appearing contiguously. This facilitates efficient loading of entire dmgroups in `minifind2`, and is accomplished in `tree` through the use of `fseek()`. In both file formats, all samples in the time series for a given sub-band are written in sequence, one sub-band at a time. Samples are packed to four bits per sample. For full details on the file format the file the reader is referred to the source code of the `path_dedisp` routine of `minifind2`.

It should be remembered that the tree algorithm assumes a linear relation between dispersion delay and channel number, and hence (except for "linearised" data), the number of dmgroups produced should be limited, as described in § 2.3.

This program can optionally be run on a parallel processing system using the Message Passing Interface[3] (MPI). In this case, the first and second tasks act as masters for the sending of raw data and the reception of de-dispersed data respectively. Hence, they should reside on a machine with fast access to the storage device in use. The remaining tasks are used as processing slaves.

Whilst a program called `tree` existed for the Parkes Southern Pulsar Survey (Manchester et al. 1996), its use was limited to those survey parameters and it was decided to re-write the program from scratch. It has since been re-written again in a modular C++ design, meaning that the user may add handling of other input data formats fairly trivially by writing a new class derived from `TreeEngine`. The

[2] `http://www.gnuplot.org/`
[3] `http://www-unix.mcs.anl.gov/mpi/`

reader is referred to the source code for the existing classes for analogue filterbank (`ScampTreeEngine`) and CPSR (`BBTreeEngine`) data for two examples.

The full list of options for `tree` as produced by `-h` is as follows:

```
General options (with [defaults]):
     -s x           Produce this many sub-bands       [FB:16 CPSR:32]
     -d             De-stripe the output data          [FB:n  CPSR:y]
     -f x           Produce this many folds                       [6]
     -t {fb|cpsr}   Select input data type                    [guess]
     -o fname       Pre-extension output filename  [==1st input file]
Filterbank options:
     -g x           Produce this many samples per gulp         [6144]
CPSR options:
     -M x   Use ~x MB per slave (sets gulp size)
     -r x   Resample (scrunch) output sample rate by x                [1]
     -S x   Skip this many seconds of data at the start               [0]
     -T x   Produce this many seconds of dedispersed data          [all]
     -i     Write out a .params file with # samples produced etc      [n]
     -p     Write out gnuplot file to plot passband                   [n]
     -c x   Number of channels to use in synthesised filterbank     [512]
     -b x   "Base" DM for post-detection pre-treeing dispersion removal [0]
     -n x   "Nominal" DM for coherent removal in each FB channel      [0]
     -F x   Override header centre frequency with this value
     -B x   Override header bandwidth/sideband with this signed value
     -z x   Zap poln number x
```

This software is found under `soft_swin/search/tree` in the Swinburne Pulsar Group CVS repository.

A.2 Minifind2: Periodicity Searching

The central engine of the search software suite is `minifind2`. This program is derived from that used in the Southern Pulsar Survey (Manchester et al. 1996), and due to the complexity of the program and the legacy of fortran program structure, the organisation of the program remains complex and somewhat confusing. The software has been heavily modified and only the core routines for spectral analysis

remain essentially as they were before this thesis commenced. The consequences of major modifications have not been aesthetically pleasing, and interested readers are encouraged to attempt a complete re-write based on sound, extensible software design principles whilst maintaining identical functionality and core components of the code as they stand today.

This program takes data produced by `tree` as its input. Parameters for operation are mainly parsed from the standard input, however the user may find it more convenient to redirect the contents of a text file to the standard input of the program. Essential information provided in the input file includes the number of sub-bands in the treed data, the number of samples per gulp (or for de-striped data, the total number of de-dispersed samples), the base two logarithm of the number of samples to be used in Fourier analysis, the number of trial accelerations to use and the maximum and minimum values of acceleration (in m s^{-2}). The user can also turn on searching for single dispersed pulses ("spikes"), limit the DM range to search, and configure several options affecting memory usage, as listed below:

```
-s                  Turn on spike hunting
-d dmstart dmend    Specify DM range for search
-D                  Buffer Dmgrps on disk (not RAM)
-j naccelperjob
-t threshold        Minimum spectral S/N to record
-m nsusmax          Maximum # spectral spikes to record
-c                  Keep complex spectrum in RAM (even after forming
                    power spectrum), to form reconstructed profile
                    (This requires another 2^N floats of RAM)
-k                  Keep 0 acceleration time series in RAM (RAM:see above)
```

`Minifind2` requires, in addition to the treed data files and the standard filterbank `.hdr` file, an "accounting" file (`.accu`). The file may be produced by with `makeaccu`, which takes the same parameters as `minifind2` on its standard input.

As its output, `minifind2` produces a file for each pulsar candidate that was subjected to a find period/DM search. These are given the extension `.ph`.

For the purposes of the baseband searching project (Chapter 6), `minifind2` was modified to operate in parallel using MPI. The first process is the master and should be run on a machine with fast access to the treed data. The other tasks process jobs segmented by dmgroup and/or acceleration range. Due to the continued parsing of

parameters on the standard input, a small shell script must be written which runs `minifind2` with the desired re-direction of an input file. It is this shell script that is specified to `mpirun` as the program to be executed, and for this reason the script must specify `$*` as the first argument to `minifind2`, to pass along the MPI-specific arguments sent by `mpirun`. The following is an example of such a script:

```
#!/bin/csh
/psr/cvshome/redwards/bin/OSF1/minifind2 $* -d 0.0 5.1 -j 8 \
      < /raid/redwards/gcdata/obs/1748-2446A-51620.78137/FA/inp
```

The script could be executed with, for example `mpirun -p4pg p4pgfile mpimf` (`p4pgfile` is a user-specified cluster configuration file for the `p4` transport of MPICH[4]).

Unfortunately, as it stands at present, `minifind2` cannot operate in a stand-alone mode. Old binaries exist from before the MPI modifications were made, interested users may contact the author.

This software is found under `soft_swin/search/find2` in the Swinburne Pulsar Group CVS repository.

A.3 Glean: Suspect Scrutiny

To facilitate the scrutiny of the many thousands of pulsar suspects produced in the processing of the intermediate latitude survey (Chapter 5), a program known as `glean` was written. This program loads a specified collection of `.ph` files produced by `minifind2`, for later manipulation by the user. The program is interactive and is driven by a command-line interface. Upon loading, the user is presented with a PGPLOT[5] window (`380/xs` by default) with a scatter plot of apparent period versus signal to noise ratio.

The structure of the interactive environment is based around the maintenance of lists of suspects. Operations can be made on these lists, and the results (and the initial list of all suspects) are stored in a list of lists. Two symbolic pointers, `all` and `sel` (selection) point to elements of the list of lists and most operations work with the lists they point to, and alter them to point to the result of the operation.

A typical example would be the selection and deletion of suspects clustered around a given period corresponding to terrestrial interference. This would appear

[4] `http://www-unix.mcs.anl.gov/mpi/mpich/`
[5] `http://www.astro.caltech.edu/~tjp/pgplot/`

as a concentration of points in a vertical line in the initial plot. The user could type `id` and click the mouse with the cursor near a point in the cluster to obtain a diagnostic plot of the suspect in another PGPLOT window (`381/xs` by default). To delete the unwanted suspects, the user would first `zoom` (which allows graphical selection in the plot) into the relevant region, perhaps repeatedly to achieve the desired plot scale if the distribution of periods is narrow (as it should be if suspects in the cluster are to be deleted and the chance of deleting a pulsar is to be minimised). Once the extent of the cluster is clearly visible, the user would graphically `select` a rectangular area, which results in a new list containing only those suspects in the rectangle, and leaves `sel` pointing to this list. The user would then use the `delete` command to "delete" the suspects, which actually creates a new list consisting of those candidates that appear in the list pointed to by `all`, excluding those that also appear in `sel`. If a mistake is made, the user types `lists` to see the list of lists with the corresponding command history, and re-assigns the `all` and `sel` pointers to appropriate lists from before the mistake was made (e.g. with `all = 0` and `sel = 0`). The user can also define new symbolic pointers to list for easy reference later in the session.

A number of different parameters of each suspect are available and may be listed with the `params` command. The most useful are apparent period (`p_appar` in ms), time-domain signal to noise ratio (`sn`), dispersion measure (`dm` in cm^{-3} pc), pulse width (`width` in bins), and time of observation (`mjd` or `fracmjd` as Modified Julian Days, or the fractional part thereof). The parameters used for the x- and y-axes of the plot can be chosen with `set [xparam|yparam] <param name>`. The scales in the plot can be set to logarithmic or linear mode with `set [xlog|ylog] [y|n]`. The plot can be re-drawn to fit all points in the window with `unzoom`, and if the PGPLOT windows are re-sized for ease of use, the `reopen` command should be used to allow the program to adjust to the new dimensions.

The intermediate latitude survey suspects were viewed in sets corresponding to one tape of raw data at a time. There were numerous common interference periods, making the manual selection process described above overly tedious and prone to error. To alleviate this, `glean` has built-in macro support. If `glean` sees a command it does not recognise, it looks for a file of the same name in a sub-directory `glean` off the user's home directory. If the file exists, the contents are parsed line by line as if they had been entered at the command-line interface. Macros may also call other macros recursively.

For the intermediate latitude survey I made a number of macros which deleted sets of interference periods that occurred frequently. For each use of the `select` command, the program displays a boolean expression defining the selected region in terms of the parameters corresponding to each plot axis. This same string (or another of the same syntax) may be used as the argument to the `cond` command, for conditional selection of suspects. Hence a macro may delete a set of interference signals by means of `cond` and `delete` commands. The `cond` command can also be used for broad exclusions on the basis of such parameters as signal to noise ratio. Since I had found that suspects of S/N less than 9 were rarely if ever convincing enough to warrant re-observation, I used a global `cond sn < 9` to select these candidates for subsequent deletion. For millisecond pulsars this constraint was made more severe due to the prevalence of spurious signals up to signal to noise ratios of 9.5. I therefore used `cond sn < 9.5 && p_appar < 20` to select all suspects with periods less than 20 ms and S/N less than 9.5 for removal in a subsequent `delete`. To facilitate reproducibility in my suspect scrutiny, for each tape I made a macro file containing the list of commands applied in the gleaning.

The final step in suspect scrutiny is the viewing of diagnostic plots for the remaining suspects. I generally preceeded this with `sort p_appar` to sort the suspects in ascending order of apparent pulse period. This was useful since different criteria are generally employed in the evaluation of short-period pulsars compared to long-period pulsars. Following this step, the `view` command presents the viewer with diagnostic plots in the second window, which may be paged through in forward or reverse. Hard-copies or "soft-copies" (postscript files) may be produced by pressing `h` or `s` in the PGPLOT window.

To reduce the memory requirements for `glean`, a minimum S/N may be specified on the command line. Suspects not meeting this minimum will not be loaded into the initial list. The user may also specify a command to be executed automatically when the program starts, and may provide a directory to search, or a file containing the list of `.ph` files, as alternatives to listing all files on the command line (or as a shell-expanded wildcard), since this approach often fails due to the limitation placed on argument list sizes by the shell ("`arg list too long`"). The command-line options for `glean` are:

```
-g <path>      Globs all .ph files from <path>
-f <listfile>  Load all files listed in listfile
```

```
-c <command>    Execute a command on startup
-t <S/N>        Minimum S/N of loaded files [def: 8.0]
-l              Assume little-endian files [def: no]
-h              Prints this help message
```

A.4 Processing Strategies

This section outlines the steps used in processing observations for the intermediate latitude survey and the baseband globular cluster searches. A number of ancillary programs are mentioned which may be of use to future users. They are available on request from the author.

A.4.1 Intermediate Latitude Survey

Data were recorded on DLT 7000 tapes by the PMDAQ online software at the Parkes radio telescope, at a rate of approximately two tapes per 16-hour observing day. These were returned to Swinburne for processing on the Swinburne supercluster. The scripts `dumptape` and `sc_master` handled the automation of the tape robots and the unloading of observations in one beam per file to disk. The kernel of this translation process was the program `sc_td`[6], part of the standard Parkes pulsar software suite. It was run in "linearization mode" to effect the channel expansion described in § 2.3.

The remaining processing was automated by an MPI program (`mpimaster`) to distribute the load across the cluster of workstations. This program is quite complex and specific to the intermediate latitude survey, so may not be of use to other users.

The automation software (`mpimaster`) noticed data from each beam of each pointing as they appear on disk. A slave was then asked to run `debird` and `birdie_hunter` on the file. The latter program checked for the appearance of broad-band interference in the file and logged such signals in a `.s.` file. Once all beams from a group of six pointings had been processed in this way, occurrences of similar periods in numerous beams were analysed by `birdie_summary` and recorded as in § 2.6.2. Slaves were then asked to search the beams, which meant running `tree` and `minifind2`.

[6]Available from the ATNF Pulsar Group CVS repository,
`attila.atnf.csiro.au:/psr/cvsroot`, under `soft_atnf/search/sc_td`

Throughout the processing of multibeam data, result and log files were produced and kept in a location pointed to by the environment variable `$book_disk_find`. Since these frequently filled the available disk space on any given supercluster node, many such directories were made on some of the 64 workstations. With the availability of a 1 TB space with the supercluster upgrade, these book-keeping directories were consolidated and re-organised into sub-directories for each tape. Other directories used by the software (mainly as remnants from old fortran code) are `$masterbook` and `$FIND_STD_BIRDFILE`.

A.4.2 Baseband Search

Data were recorded in 1-GB ($\sim$53.7 s) segments to DLT drives by the CPSR system. Since four tape drives were in operation at once to keep up with the recording rate, processing long observations as a continuous data stream involved unloading data from at least four tapes to disk. This was automated with the `cpsr_dumprobot` script, which co-ordinated the tape robot and drive, left CPSR files in sub-directories for each tape, and consulted the log file of the Caltech Fast Pulsar Timing Machine (which was used simultaneously with CPSR, mainly for the scheduled telescope driving capabilities of its associated software) to determine the telescope position at the time of recording of each file. A sub-directory for each observation was also made, with symbolic links leading to the files in the tape-by-tape sub-directories.

When a complete observation was available in its sub-directory, the sampling statistics were examined for quality control with a program called `vetstats`. This program plotted the variance values for each of the four sampled channels of the dual-polarization, quadrature-sampled CPSR data, with one data point per file. In this way, bad data recorded at the start of the observation (before the level-setting procedure had been completed) could be discarded by deletion of the offending file(s). The `gcsetup` script was then used to create two sub-directories (for the FD and FA and/or SA searches, as described in Chapter 6) with symbolic links to the CPSR files in each. For each round of processing of each observation, a script was produced by `gcmkscript`, which examined the CPSR files and organised them into contiguous groups of the desired integration time. This script then called one of the family of `gcsearch.50.*` scripts, which in turn ran `tree` and `minifind2` in MPI mode, with parameters appropriate for the particular strategy being employed.